Dynamical performance of optical amplifiers for long-haul/ultra long-haul transmission systems

Lee, S.C.J.

Award date:
2005

TU/e technische universiteit eindhoven

DYNAMICAL PERFORMANCE OF OPTICAL AMPLIFIERS FOR LONG-HAUL/ULTRA LONG-HAUL TRANSMISSION SYSTEMS

by S.C.J. Lee

/faculteit elektrotechniek

Eindhoven University of Technology
Faculty of Electrical Engineering
Division of Telecommunication Technology and Electromagnetics
Electro-optical Communication (ECO) Group

DYNAMICAL PERFORMANCE OF OPTICAL AMPLIFIERS FOR LONG-HAUL/ULTRA LONG-HAUL TRANSMISSION SYSTEMS

by S.C.J. Lee

Master of Science Thesis
carried out from 11-01-2004 to 11-01-2005

Supervisors:
Dr. Claudio Zuccaro (Siemens AG)
Dr. Huug de Waardt (TU/e)

Graduation professor:
Prof. ir. A.M.J. Koonen

Preface

This Master's thesis covers the work of my graduation project as a student of the Telecommunications and Electromagnetism Group (TTE) at the University of Technology in Eindhoven. This work was done at Siemens Information and Communication Networks in Munich (Germany) and consisted of research in the dynamic behaviour of erbium-doped fiber amplifiers in long-haul optical transmission links. Because of the level of confidentiality and competition regarding this area of research, it may happen that some results and figures in this thesis are not described and explained in full details. I hereby beg for understanding from the reader regarding these issues.

I would like to thank Siemens and Dr. Claudio Zuccaro for giving me the opportunity to carry out my Master's thesis project at the company, where I could work in not only an innovative but also business-driven environment. This has proved to be a great and educational experience which will no doubt be useful for my personal development. Also, I would like to thank Dr. Zuccaro for his devoted support and guidance as my supervisor at Siemens as well as many fruitful discussions and advice.

Special thanks also goes to Prof. Khoe and Dr. De Waardt for being respectively my professor and my supervisor at the university. They have been supervising and guiding me well during the last stages of my study. I am very grateful to them for the trust, freedom, and independence I've received to be able to do my graduation project well.

Furthermore, I would also like to recognize and thank the following individuals for their support and help in making my work at Siemens successful: Kuno Zhuber-Okrog, Wolfgang Langer, Lutz Rapp, Anton Schex, Erhard Waretzi, Biljana Bacovic, Anand Chittawadgi and all other colleagues.

Last but not least, I want to thank my family and friends for their constant support all along. Without them, I would not have come so far in completing my graduation project and study.

Abstract

Erbium-doped fiber amplifiers (EDFA), featuring high gain over a large wavelength range, low intrinsic losses and long fluorescence times, have emerged as key enabling components in optical WDM networks. However, when used in WDM networks where channels are added or removed abruptly, power transients occur in the remaining channels. Especially in a link of cascaded EDFAs, these power transients can add up to several dBs in as fast as a few microseconds. These can lead to equipment damage and degradation of optical signal-to-noise ratios (OSNR) and bit-error rates (BER) in transmission links. This thesis investigates and explains the occurrence of such power transients and discusses different methods used so far to control the transients.

So far, simulation models based on either simplified EDFA models or simple control system models are used to study power transients in optical EDFA systems and to optimize new gain control designs. However, real-case EDFA systems consists of different levels of complex control mechanisms working together, which lead to large discrepancies. This thesis presents a novel complex and precise simulation model combining an accurate dynamic EDFA model with different levels of detailed complex control, based on a realistic and state of the art optical amplifier used in practice. It shows that it is possible to simulate the effects of all levels of control behaviour in a complex system and their exact effects on power transients fast and accurately, so that the results reflect those obtained from measurements.

Furthermore, the results are not only accurate for one single amplifier, but also on an entire transmission link system with 7 fiber spans. Because of the accuracy, the simulation model can be used for accurate analysis of transient behaviour in optical amplifier designs. Also, systematic and time-consuming measurements can be replaced by simulations, thereby saving a lot of time and money.

Contents

Contents iii

List of Figures vi

List of Tables xii

List of Abbreviations xiii

1 Introduction 1

2 The evolution of optical networks 3
2.1 Progress of optical transmission systems 3
2.2 Realisation of all-optical networks 4

3 An Erbium-doped fiber amplifier 8
3.1 Introduction to an EDFA 8
3.2 Mathematical model of an EDFA 11
3.3 Simulation model of an EDFA 13

4 Power transients in optical networks 15
4.1 A WDM transmission link 15
4.2 Dynamics of erbium-doped fiber amplifiers 16
4.3 Causes and negative effects of transients 20
4.3.1 Causes of transients 20
4.3.2 Negative effects of transients 20
4.4 Behaviour of transients 22

5 Different methods to control an EDFA 26
5.1 Gain control by adjustment of the pump power 27
5.1.1 Forward control 27
5.1.2 Electronic feedback control loop 28
5.2 Gain clamping by all optical feedback (lasing) 30
5.2.1 Using Bragg reflector 30
5.2.2 Using ring laser structure 31

5.3 Link control by an extra compensating channel 32
5.4 Best method to control an EDFA 33

6 A multilevel gain controlled optical amplifier 35
6.1 Structure of a complex optical amplifier 36
6.1.1 Variable optical attenuator 36
6.1.2 Gain flattening filter 37
6.1.3 Dispersion compensating fiber 39
6.2 Different levels of control 39
6.2.1 Gain tilt control 40
6.2.2 Electronic gain and transient control 44
6.2.3 ASE correction 47
6.2.4 OSNR and power preemphasis 48
6.2.5 Time constants of different control levels 50

7 Simulation model of optical amplifier 51
7.1 Structure of simulation model 51
7.2 Implementation of model in Matlab 55
7.2.1 Gain tilt control with VOA 55
7.2.2 ASE correction 56
7.2.3 OSNR and power preemphasis 56
7.3 Implementation of model in Simulink 57
7.3.1 Optical path 57
7.3.2 Electronic gain and transient control 58
7.4 Total simulation model with Matlab and Simulink 62

8 Simulation and measurement results 64
8.1 Results for a single optical amplifier 64
8.1.1 Measurement setup 64
8.1.2 Static results 66
8.1.3 Dynamic results 68
8.2 Results for an optical transmission link 72
8.2.1 Measurement setup 72
8.2.2 Static results 74
8.2.3 Dynamic results 78
8.3 Discussion 83

9 Analysis of transients based on simulations 85
9.1 Surviving channel configurations 86
9.2 SRS effects and tilt 88
9.3 Gain ripple 91
9.4 ASE correction 93

10 Conclusion 94

Bibliography **96**

A Spectral Hole Burning **100**

List of Figures

2.1 *Evolution of transmission capacity throughout the past 25 years.* 4
2.2 *From optical transport to optical networking: evolution of optical transmission networks.* 5
2.3 *An optical add/drop multiplexer (OADM).* 6
2.4 *Three functions of an OXC:* (a)*fiber switching* (b)*wavelength switching* (c)*wavelength conversion.* 6
2.5 *Block diagram of an OXC.* 7
2.6 *Example of a transparent optical network with wavelength routing.* 7

3.1 *Emission spectrum of an erbium-doped silicon fiber.* 8
3.2 *Simple setup of an erbium-doped fiber amplifier.* 9
3.3 *Simplified energy levels scheme of erbium ions.* 9
3.4 *A three-level energy system for erbium ions in an EDFA.* 10
3.5 *A simplified two-level energy system for erbium ions in an EDFA.* 11
3.6 *Dividing the wavelength range into discrete intervals with finite width.* . . 14

4.1 *Structure of a typical WDM transmission link.* 15
4.2 *Lifetime of erbium ions.* 17
4.3 *Power excursion of 3.68 dB in remaining channel number 4 when seven out of eight channels are dropped in a WDM transmission system* [16]. . . 17
4.4 *Results by Srivastava et al* [9]. (a)*Oscilloscope trace showing the time dependence of the surviving channel power* P_{SS} *along with the dropped channel power* P_{SD}. (b)*Changes in the surviving channel power as a function of time for the loss of one, four, and seven out of eight WDM channels.* 18
4.5 *Results by Zyskind et al* [5]. (a)*Measured output power as a function of time after 2, 4, 6, 8, 10, and 12 EDFAs. At t = 0, 4 out of 8 signal channels are dropped.* (b)*same as (a), but smaller time scale* (c)*Delay, and reciprocal of the delay, after dropping 4 out of 8 channels for surviving channel power excursion of 1dB, as a function of length of the amplifier chain.* 19
4.6 *Changes in BER and OSNR as a function of added/dropped channels for* (a)*system that is OSNR limited and* (b)*system that is limited by nonlinear impairments* [7]. 21

4.7 *Transient behaviour of the BER for cases of* (a)*add and* (b)*drop of different number of channels out of 40. Initial BER level for the case of dropping of 25 channels is chosen higher to accomodate the BER behaviour* [7]. 21
4.8 *Plot of the time-resolved BER during a channel-add/drop event when transient control is off* [8]. 22
4.9 *Transient response of total optical power and single channel power for different percentages of total channels dropped* [33]. (a)*10 channels total before drop.* (b)*20 channels total before drop.* 23
4.10 *Transient response of single channel power measured after every second EDFA in a link with 10 EDFAs where 50% of the total channels are dropped* [33]. (a)*10 channels total before drop.* (b)*20 channels total before drop.* 24
4.11 (a)*Rise time of transient to a level of 2dB as a function of the number of EDFAs.* (b)*same as in (a), but the reciprocal rise time is plotted to show inverse proportional relation* [33]. 25
4.12 *Influence of speed of the drop T_s on the shape and speed of the transient channel power rise* [33]. 25

5.1 *Experimental setup for forward pump power control* [11]. *A: Voltage-controlled attenuator; C1: Coupler for supervisory wavelength; C2: Coupler for 5% tap; C3: Coupler for pump wavelength; F: Filter for ASE suppression; I: Isolator.* 27
5.2 *Surviving channel power transients when seven out of eight channels are added or dropped in a forward pump control* [11]. 28
5.3 *Schematic view of a gain block with electronic feedback control* [12]. 29
5.4 *Transient response of surviving channel power of automatic gain control by Suzuki et al* [14]*;* (a)*for 1 to 32 channels addition* (b)*for 32 to 1 channels drop.* 30
5.5 *Gain clamped amplifier with Farby Perot laser structure using fiber grating reflectors. EDF: erbium-doped fibre, WSC: wavelength selective coupler.* . 30
5.6 *Surviving channel power transients when seven out of eight channels are* (a)*dropped* (b)*added* [20]. 31
5.7 *Gain-clamped amplifier scheme in a ring laser structure. WSC: wavelength selective coupler.* 31
5.8 *Results obtained by Desurvire et al* [22] *using the ring laser structure of optical gain clamping.* 32
5.9 *Link control for surviving channel protection in optical networks by using a control channel* [25]. 32
5.10 *Power excursions due to cross saturation of an EDFA cascade for a surviving channel. Five of seven WDM channels are switched on /off at 1 kHz* [25]. 33

6.1 *Schematic view of a state of the art optical amplifier.* 35

6.2 *Gain coefficients of EDFs with population inversion rate as a parameter.* . 36
6.3 *Tilt control with a VOA* 37
6.4 *Spectral attenuation of standard single mode fiber. It can clearly be seen that the attenuation curve is tilted.* 38
6.5 *Function of an optical gain flattening filter.* 38
6.6 *Influence of gain ripple on gain control.* 39
6.7 *Broadening and attenuation of two adjacent pulses as they travel along a fiber.* 40
6.8 *Raman gain spectrum for SSMF at a pump wavelength $\lambda_p = 1$ μm. The Raman gain scales inversely with λ_p.* 41
6.9 *The effect of SRS crosstalk on signals transmitted through a fiber span* [27]. (a)*Fiber input spectrum.* (b)*Fiber output spectrum after 100-km of fiber.* 43
6.10 *Compensation of spectral tilt resulting from transmission fiber with and without gain tilt control (GTC).* 44
6.11 *Schematic view of optical amplifier with electronic gain control* 45
6.12 *A combined proportional integral feedback with feed-forward control.* 46
6.13 *Output powers after 840-km transmission using equal input powers* [29]. *Solid curve denotes amplified spontaneous emission in 0.2-nm optical bandwidth. Triangles denote signal powers. S/N denotes optical signal-to-noise ratios.* (a)*Results of OSNR preemphasis after five iterations of algorithm.* (b)*Results of power preemphasis after second iteration of algorithm.* 50

7.1 *Structure of simulation model with Matlab and Simulink.* 52
7.2 *Schematic view of the simulation model containing the different Matlab programs and their functions. White function blocks are values that are defined already and gray function blocks involves calculation and processing.* 54
7.3 *Simulink model of the optical path in the amplifier.* 57
7.4 *Simulink model of optical amplifier with optical path and electronic gain control.* 59
7.5 *Example of non-linear distortions in the optical output power of a laser diode as a function of its drive current* 60
7.6 *Total simulation model of optical amplifier with fiber span and DCF given in Simulink.* 62
7.7 *Simulation model of a transmission link with 7 fiber spans and 8 amplifiers.* 62

8.1 *Measurement setup for static and transient measurement of the single optical amplifier.* 65
8.2 *Simulation and measurement results of output power spectrum for one single amplifier with manual gain setting.* (a)*Type A amplifier.* (b)*Type B amplifier.* 67
8.3 *Simulation and measurement results of output power spectrum for one single amplifier with automatic gain setting.* (a)*Type A amplifier.* (b)*Type B amplifier.* 68

8.4 *Dynamic simulation and measurement results of relative surviving channel power change for one single amplifier with manual gain setting when 19 of 20 channels are dropped.* (a)*Results after control group A for surviving channel frequency 194.3 THz and Type A amplifier.* (b)*Same as (a), but for a Type B amplifier.* 69
8.5 *Dynamic simulation and measurement results of surviving channel power change for one single amplifier with manual gain setting when 19 of 20 channels are dropped.* (a)*Results at output of optical amplifier for surviving channel frequency 194.3 THz and 196.1 THz alternately and Type A amplifier.* (b)*Same as (a), but for a Type B amplifier.* 70
8.6 *Measurement of ASE power in an optical amplifier before and after a 16 to 1 channel drop. The effects of SHB can clearly be seen.* 71
8.7 *Dynamic simulation and measurement results of surviving channel power change for one single amplifier with automatic gain setting when 19 of 20 channels are dropped.* (a)*Results at output of optical amplifier for surviving channel frequency 194.3 THz and 196.1 THz alternately and Type A amplifier.* (b)*Same as (a), but for a Type B amplifier.* 72
8.8 *Measurement setup for static and transient measurements of a transmission link with 7 spans.* 73
8.9 *Simulation and measurement results of pre-amplifier output power spectrum at the end of a transmission link with 7 fiber spans of 15 dB loss each.* (a)*Static results prior to a drop where the blue channels survive.* (b)*Static results prior to a drop where the red channels survive.* 75
8.10 *Simulation and measurement results of pre-amplifier output power spectrum at the end of a transmission link with 7 fiber spans of 25 dB loss each.* (a)*Static results prior to a drop where the blue channels survive.* (b)*Static results prior to a drop where the red channels survive.* 77
8.11 *Simulated power spectra of WDM channels along the transmission link after the 1st, 3rd, 5th, and 8th (last) amplifier.* 77
8.12 *Relative power change for surviving channel at 196.1 THz as well as the total power. Results are at the end of a transmission link with 7 spans of 15 dB loss each in case of a 76 to 5 channels drop with blue surviving channels. Dark lines represent simulation results and gray lines represent measurement results.* 79
8.13 *Relative power change for surviving channel at 195.6 THz along the transmission link. Results are for a 76 to 5 channels drop with blue surviving channels and a link consisting of 7 spans with 15 dB loss each. Dark lines represent simulation and gray lines represent measurement results.* 80
8.14 *Relative power change for surviving channel at 191.7 THz as well as the total power. Results are at the end of a transmission link with 7 spans of 15 dB loss each in case of a 76 to 5 channels drop with red surviving channels. Dark lines represent simulation results and gray lines represent measurement results.* 81

8.15 *Relative power change for surviving channel at 196.1 THz as well as the total power. Results are at the end of a transmission link with 7 spans of 25 dB loss each in case of a 76 to 5 channels drop with blue surviving channels. Dark lines represent simulation results and gray lines represent measurement results.* 82
8.16 *Relative power change for surviving channel at 191.7 THz as well as the total power. Results are at the end of a transmission link with 7 spans of 25 dB loss each in case of a 76 to 5 channels drop with red surviving channels. Dark lines represent simulation results and gray lines represent measurement results.* 83

9.1 *Simulation results of the channel powers at the end of a transmission link for a 76 to 5 channels drop. Results are plotted for every present WDM channel as a function of the time. Surviving channels are blue at 196.1, 196.0, 195.7, 195.6, and 195.5 THz.* 86
9.2 *Same as in figure 9.1, but for red surviving channels at 192.1, 192.0, 191.9, 191.8, and 191.7 THz.* 87
9.3 *Same as in figure 9.1, but for mixed surviving channels at 196.1, 194.25, 193.45, 192.75, and 191.7 THz.* 87
9.4 *Same as in figure 9.1, but for separated surviving channels at 196.1, 196.0, 191.9, 191.8, and 191.7 THz.* 88
9.5 *Power transients of the 196.1 THz channel after a cascade of* n_{casc} *EDFAs* [35]. (a)*Effects of SRS after a drop of 30 out of 45 channels without fast tilt control. The arrow indicates the ultrafast SRS contribution to the transient behavior.* (b)*Same results when very fast SRS tilt control is implemented with a reaction time of 500 ns.* 89
9.6 *Dynamic simulation of channel powers (normalized) at the end of a transmission link during a 76 to 5 channels drop. Realistic fiber span models which cause SRS effects are used in the simulation. Large changes in channel powers can be observed for the surviving channels.* 90
9.7 *Dynamic simulation of channel powers (normalized) at the end of a transmission link during a 76 to 5 channels drop. Simple attenuation blocks are used to simulate the loss by fiber spans yielding no SRS effects in the simulation. Smaller changes in channel powers can be observed for the surviving channels.* 90
9.8 *The surviving channel power transients of figures 9.6 and 9.7 are given again and compared to each other in dB. The difference between the results with and without SRS effects can clearly be observed.* 91
9.9 *Simulated power spectrum at the end of a transmission link consisting of 8 optical amplifiers and 20 WDM signal channels. Results are shown for a link with and without gain ripples in the optical amplifiers.* 92
9.10 *Simulated power transients in surviving channel (1533.5 nm) of a 20 to 1 channel drop with and without gain ripple.* 92

A.1 *A demonstration of spectral hole burning. A laser at 1064 nm saturates the gain around 1064 nm more than the gain at other wavelengths. For comparison, the unsaturated gain (without laser power) is shown as a dotted curve.* 100
A.2 *ASE spectra with saturating laser tuned to 1532 and 1552 nm (top), and the subtracted spectrum (bottom). Spectra were recorded with 0.5 nm resolution* [41]. 101
A.3 *SHB results obtained by Srivastava et al* [38]. (a) *Dependence of spectral hole-burning on amplifier compression for saturation at 1551 nm.* (b)*Spectral hole widths for saturation at different wavelengths.* 101
A.4 *Gain reduction divided by gain, caused by SHB for one channel* [42]. . . . 102

List of Tables

6.1 *Different levels of control with their time constants* 50

8.1 *Channels used for single optical amplifier measurements* 65
8.2 *Operating conditions for manual gain setting results in figure 8.2* 66
8.3 *Operating conditions for automatic gain setting results in figure 8.3* 67
8.4 *Operating conditions for results in figures 8.4 and 8.5* 69
8.5 *Parameters for simulations in figure 8.7* 72
8.6 *Surviving channels for two different cases of 76 to 5 channels drop* 74
8.7 *Parameters for simulations in figure 8.9* 75
8.8 *Parameters for simulations in figure 8.10* 76
8.9 *Parameters for simulations in figures 8.12, 8.13 and 8.14* 78
8.10 *Parameters for simulations in figures 8.15 and 8.16* 82

List of Abbreviations

AGC	Automatic gain control
ASE	Amplified spontaneous emission
ATM	Asynchronous transfer mode
BER	Bit-error rate
CW	Continuous-wave
DBR	Distributed Bragg reflector
DCF	Dispersion compensating fiber
DSP	Digital signal processor
DWDM	Dense wavelength division multiplexing
EDF	Erbium-doped fiber
EDFA	Erbium-doped fiber amplifier
FR	Frame relay
FWM	Four wave mixing
GFF	Gain flattening filter
GTC	Gain tilt control
IP	Internet protocol
LAN	Local area network
LD	Laser diode
OADM	Optical add/drop multiplexer
OSNR	Optical signal-to-noise ratio
OXC	Optical cross-connect
SDH	Synchronous digital hierarchy
SHB	Spectral hole burning
SOA	Semiconductor optical amplifier
SPM	Self phase modulation
SRS	Stimulated Raman scattering
SSMF	Standard single mode fiber
VOA	Variable optical attenuator
WDM	Wavelength division multiplexing
XPM	Cross phase modulation

Chapter 1

Introduction

With the need for more and more transmission capacity, wavelength division multiplexed (WDM) transmission systems are playing an ever increasing role in today's high-bandwidth networks. These WDM networks can achieve significant enhancement in flexibility, efficiency and throughput by enabling wavelength selective switching, that is, add-drop multiplexing of channels.

Erbium-doped fiber amplifiers (EDFA), featuring high gain over a large wavelength range, low intrinsic losses and long fluorescence times, have emerged as a key enabling component in these optical WDM networks. In particular, owing to their long fluorescence time, EDFAs in high-speed WDM links was thought not to suffer from the effect of cross-gain modulation. However, when EDFAs are used in WDM networks where channels are added or removed abruptly, the situation becomes very different.

Such sudden channel addition or removal, caused either by unintentional failures or by deliberate network reconfigurations, will lead to changes in the gain of an EDFA. This, in turn, will result in dynamic excursions of the optical power in the remaining channels. Moreover, these power transients can add up to several dBs when EDFAs are cascaded, thereby damaging optical components or degrading system performance, such as the optical signal-to-noise ratio (OSNR) and bit-error rate (BER) of the channels.

In order to stabilize the EDFA behaviour and reduce power transients, EDFAs with controllable gain and output power are necessary. Because the response time of these transients will increase when optical amplifiers are cascaded in a transmission link, fast gain control is needed in order to counter these problems. Up till now, several different gain control schemes have been proposed. Among these, fast electronic feedback pump control is thought to be one of the most effective and promising ways to control EDFAs.

This thesis starts with a study and explanation on the occurrence of such power transients and presents different ways to control the transients. Because of so much different control schemes, it is often difficult to decide which to use when designing an optical amplifier with EDFAs. Also, because the behaviour of transients is so complex,

several different levels of control are often used in an optical amplifier. It is therefore important to do simulations for a better understanding of transient behaviour in optical amplifiers and their design considerations.

Up till now, simulation models are based on either simplified EDFA models or simple control system models. These are then used to predict and analyze the effects of different design parameters and novel techniques on power transients in real-case complex optical EDFA systems. However, when measurements are done, the results don't correspond quantitatively with those from the simulations because many different levels of complex control methods are working together in a real-case optical EDFA system, producing unexpected discrepancies.

In this thesis, a real-case optical amplifier with a fast electronic control scheme will be introduced, followed by the presentation of a novel complex and precise simulation model, combining an accurate dynamic EDFA model with different levels of detailed complex control based on the realistic and state-of-the-art amplifier used in practice. Details regarding the implementation of these controls into the simulation model will also be discussed. Moreover, it is questioned whether such a complex simulation model can be implemented to simulate realistic results and how much these simulations can compare to measurement results.

Continued by simulation and measurement results, the thesis shows that it is possible to simulate the effects of all levels of control behaviour in a complex system and their exact effects on power transients accurately, so that simulation data reflect those from measurements. Furthermore, the proposed simulation model is shown to not only produce accurate results for one single optical amplifier, but also for an entire transmission link system consisting of 7 spans and 8 optical amplifiers.

Finally, it is shown that the simulation model can also be used for deeper and accurate analysis on the behaviour of these power transients in the optical amplifier. Therefore, the performance and transient behaviour of novel untested optical amplifier designs can be simulated too, thereby saving large amounts of time- and money-consuming measurements in the labs.

Chapter 2

The evolution of optical networks

2.1 Progress of optical transmission systems

With the successful development of lasers in the 1960s, fiber-optics became the technology of the future for telecommunications. But problems relating to the two most important elements, the light source and the transmission medium, meant that practical applications remained elusive. By 1970, however, a laser diode capable of continuously lasing at room temperature and an optical fiber with a transmission loss of 20 dB/km at last provided the levels of performance required. In a little over 10 years, fiber-optic communications underwent remarkable growth, substituting traditional copperline transmission systems.

At the end of the 1980s, typical transmission losses of 0.2 dB/km were achieved for optical fibers, enabling distances of over 100 km to be transmitted without any regeneration or amplification. Along with the development of erbium-doped fiber amplifiers (EDFA) in 1989 [1], transatlantic transmission distances of more than 10000 km could be covered without the use of regenerators. However, because of high optical powers, nonlinear effects play a major role in limiting system performances.

With increasing performances of optical transmission systems, the speed with which data was transmitted could also be increased. In the early 1990s, signals were transmitted with a speed of 1 to 2.5 Gb/s per transmission channel. In 1991, a laboratory experiment showed that data transmission over 21000 km at 2.5 Gb/s was possible [4]. By employing wavelength division multiplexed (WDM) transmission technologies, where various channels are transmitted simultaneously through a single optical fiber, transmission rates could be enhanced even more.

The first deployment of WDM was broadband WDM. In 1994, by using fused biconic tapered couplers, two signals could be combined on the same fiber. Because of limitations in the technology, the signal frequencies had to be widely separated, and systems typically used 1310 nm and 1550 nm signals, providing bit rates of 5 Gb/s on a single fiber. Although the performance did not compare to today's technologies, the

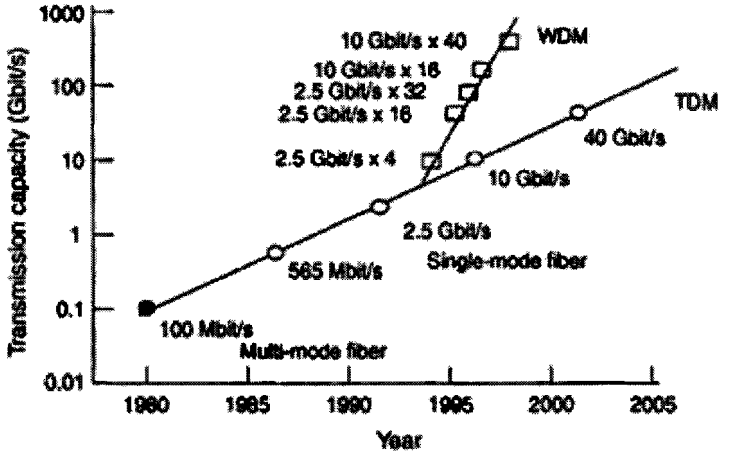

Figure 2.1: *Evolution of transmission capacity throughout the past 25 years.*

couplers provided twice the bandwidth out of the same fiber, which was a large cost savings compared to installing a new fiber.

As optical filters and laser technology improved, the ability to combine more than two signal wavelengths on a fiber became a reality. Dense wavelength division multiplexing (DWDM) combines multiple signals on the same fiber, ranging up to 40 or 80 channels with spacings of 50 to 100 GHz. By implementing DWDM systems and optical amplifiers, networks can provide a variety of bit rates and a multitude of channels over a single fiber. The wavelengths used are all in the range where optical amplifiers perform optimally, typically from about 1530 nm to 1565 nm. Nowadays, commercial optical systems can serve bit rates of up to 40 Gbit/s per channel. By employing DWDM transmission technologies, transmission rates of more than several Tbit/s can be achieved in an optical point-to-point link. Figure 2.1 shows the evolution of transmission capacity throughout the past 25 years.

2.2 Realisation of all-optical networks

With the emergence of DWDM transmission technologies, the capacity with which data is transmitted can be expanded over existing fibers, resulting in lower costs. Fiber-congested, point-to-point transmission links of long-distance networks were therefore one of the first applications for DWDM. Nowadays, 80-channel dense WDM terminals are widely deployed to enhance the bandwidth capacity of the long-haul network backbone.

Aside from the enormous capacity gained, DWDM offers more advantages to optical networks. By employing DWDM, signals with different transmission rates and formats like Synchronous Digital Hierarchy (SDH) and Asynchronous Transfer Mode (ATM) can be transmitted together in the same optical fiber using different wavelength channels.

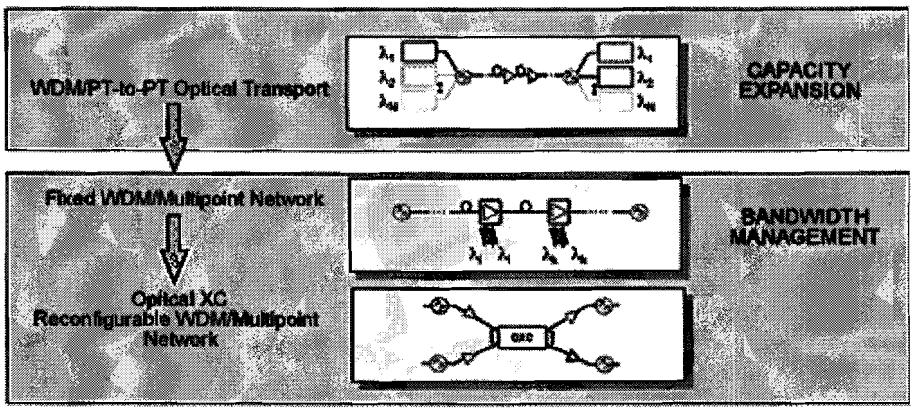

Figure 2.2: *From optical transport to optical networking: evolution of optical transmission networks.*

Together with the use of EDFAs, which are also bit-rate and format independent, the so-called transparent networks can be realized.

With the increasing speed, amount and complexity of data that is being transmitted, electronic switching and routing forms a limitation in these opaque optical networks. In every network node, optical signals has to undergo an optoelectronic conversion in order to retrieve routing information and to regenerate the signals. After this, the electrical signals are then converted back to optical powers again to be transmitted further in the network.

This limitation can be overcome by the introduction of optical add/drop multiplexers (OADM) and optical cross-connects (OXC), allowing the switching and routing functionality of networks to be done fully optically. With this, optical networks have started the migration from transport-only networks, where point-to-point optical transport plays the major role, to all-optical networks where full optical bandwidth management is the ultimate goal (see figure 2.2).

In figure 2.3, a model of an OADM is given. An OADM can efficiently drop and add various wavelengths at intermediate sites along the network, resolving a significant challenge for existing DWDM networks. It is now possible for ATM, frame relay (FR), native local area networks (LANs), high-bandwidth Internet protocol (IP), and others to connect directly to the network via a wavelength in the optical layer. Instead of point-to-point networks, multipoint networks with different services running on the same physical optical infrastructure are made possible.

Together with the OADM, the OXC will offer the ability to create a flexible, high-capacity, efficient all-optical network with full optical bandwidth management. An OXC is a network element that can accept various wavelengths on input ports and route them to appropriate output ports in the network. In order to accomplish this, it needs 3

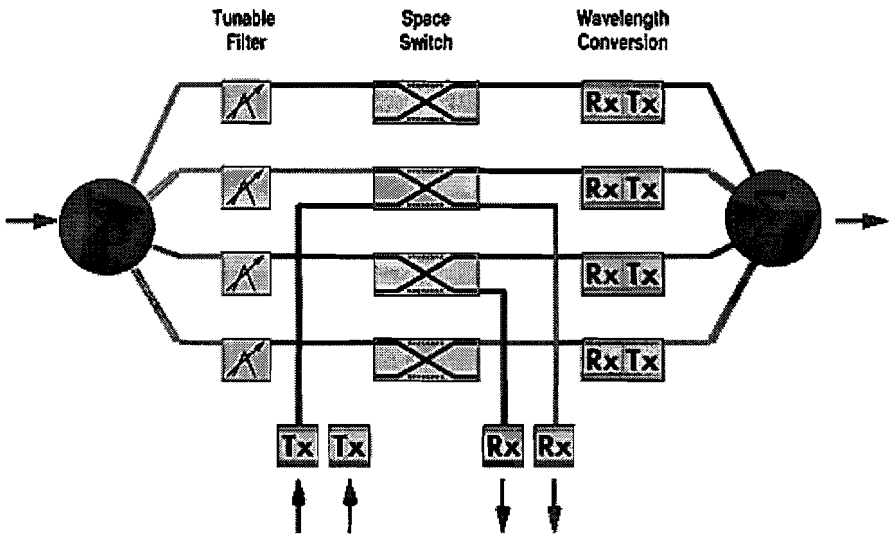

Figure 2.3: *An optical add/drop multiplexer (OADM).*

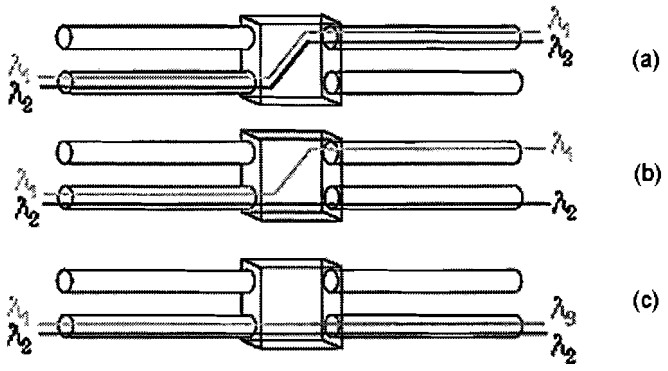

Figure 2.4: *Three functions of an OXC:* (a)*fiber switching* (b)*wavelength switching* (c)*wavelength conversion.*

functions: 1) fiber switching, 2) wavelength switching, and 3) wavelength conversion. Figure 2.4 illustrates these functions in detail. The implementation of an OXC is given as a block diagram in figure 2.5.

In today's optical networks, the realization of all-optical networks has already begun. Figure 2.6 shows an example of a transparent optical network as it can be found nowadays. The optical nodes in the long haul network represent OXCs and the gateways/routers connecting the metro to the long haul network represent OADMs. Between the optical nodes, optical amplifiers like EDFAs are used to amplify the signals so that long distances can be overcome without regeneration. The arrows show an example of dynamic wavelength routing. It can be seen that the same wavelengths (λ_5) can be reused in different paths of a network.

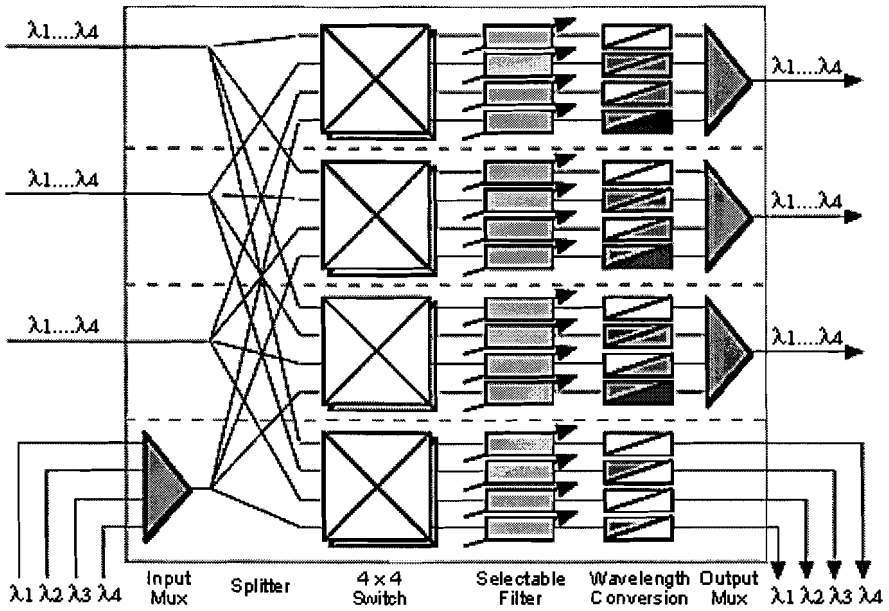

Figure 2.5: *Block diagram of an OXC.*

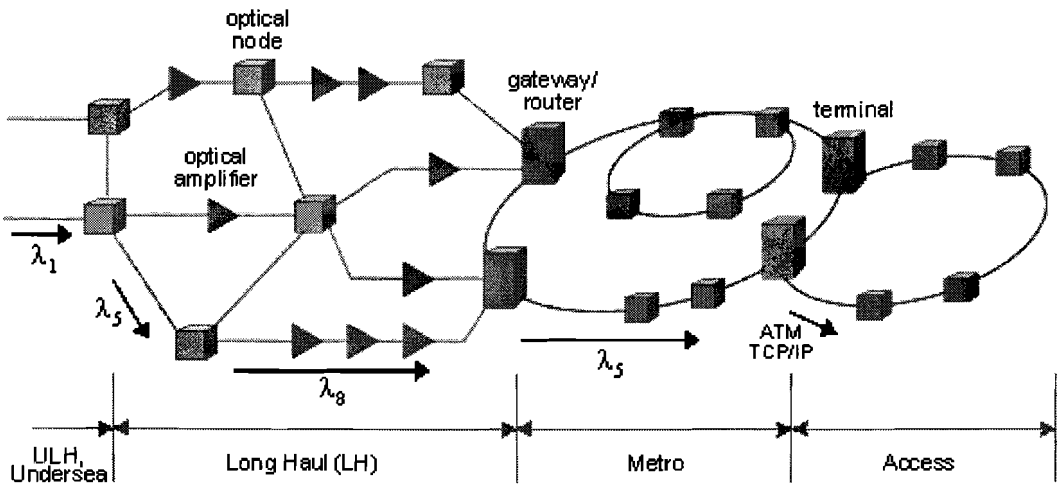

Figure 2.6: *Example of a transparent optical network with wavelength routing.*

Chapter 3

An Erbium-doped fiber amplifier

3.1 Introduction to an EDFA

During the years, erbium-doped fiber amplifiers (EDFA) have emerged as key enabling components in optical WDM networks. The key of their success is the broad absorption and emission spectrum of erbium-doped fibers in the wavelength range of 1500-1600 nm. Because of the low loss in silica fibers, a lot of optical components work at this wavelength range. This makes EDFAs ideal as amplifiers in optical transmission systems. Figure 3.1 shows the emission spectrum for an erbium-doped silicon fiber. The broad spectrum of the fiber can be seen.

Also, because of the high absorption in the range of 950-1000 nm, EDFs can easily be pumped with existing lasers so that amplification at 1500-1600 nm can be realized. These characteristics explain why EDFAs are widely used nowadays as optical amplifiers

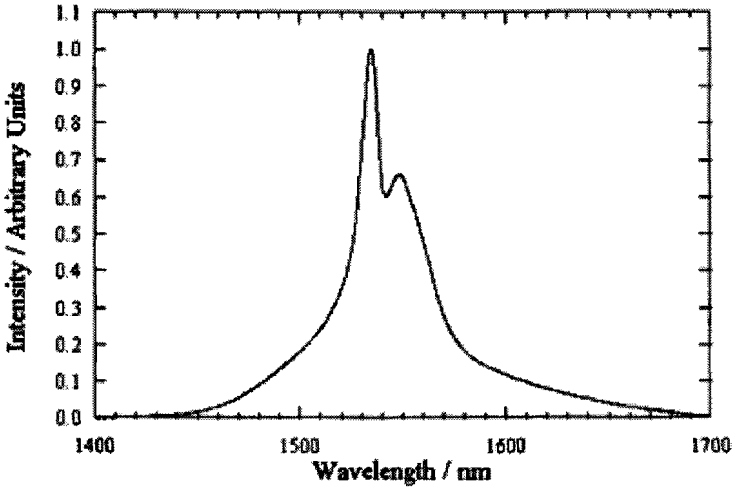

Figure 3.1: *Emission spectrum of an erbium-doped silicon fiber.*

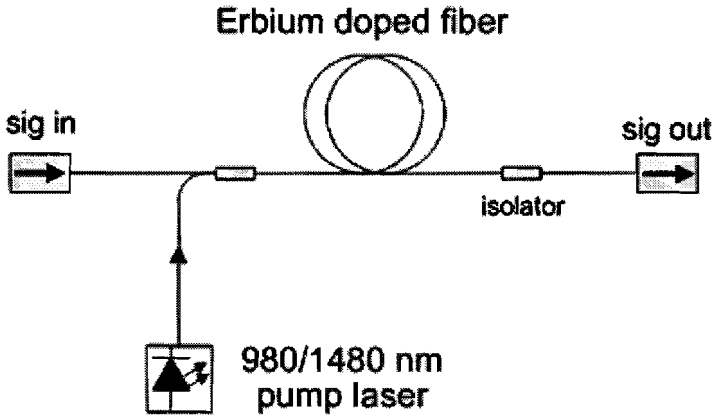

Figure 3.2: *Simple setup of an erbium-doped fiber amplifier.*

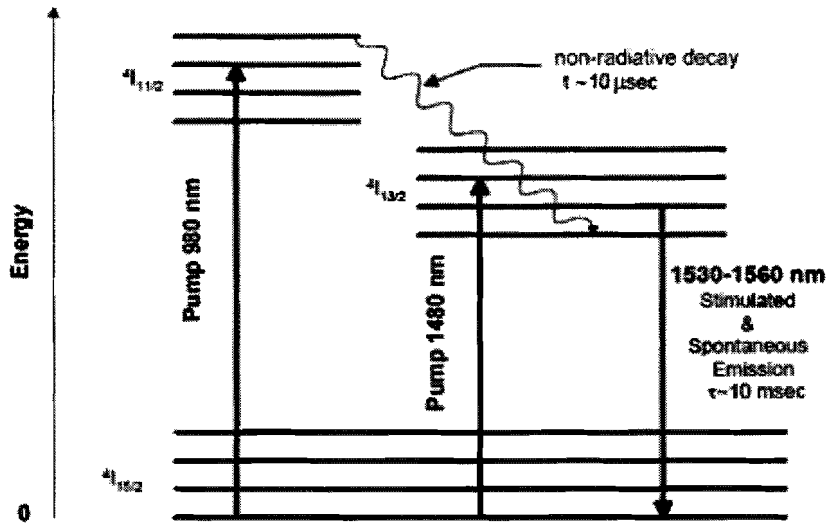

Figure 3.3: *Simplified energy levels scheme of erbium ions.*

in transmission links. Figure 3.2 shows a simple setup of an EDFA.

For better understanding of how an EDFA works, the energy scheme of erbium ions (Er^{3+}) in an EDF should be explained. From figure 3.3, it can be seen that by pumping the EDF with a laser of 980 nm, the erbium ions are brought from the ground state ($^4I_{15/2}$) into an excited state with a higher energy level ($^4I_{11/2}$). When the ions are at this energy level, non-radiative decay occurs so that the ions relax to a lower energy level ($^4I_{13/2}$).

When the erbium ions reach this energy level of $^4I_{13/2}$, they remain at this level for a

time of about 10 ms. This is much longer than the 10 μs of the non-radiative decay from $^4I_{11/2}$ to $^4I_{13/2}$, where no photon emission occurs. After the time of 10 ms, the excited erbium ions at the $^4I_{13/2}$ level will return back to their ground state ($^4I_{15/2}$), thereby emitting light of wavelengths between 1530 and 1560 nm. This can happen in the form of stimulated or spontaneous emission of light.

For stimulated emission, light of a particular wavelength between 1530 and 1560 nm is sent through the pumped EDF. This light will "trigger" the excited erbium ions at the $^4I_{13/2}$ level to return to its ground state, thereby emitting light of the same wavelength. This way, amplification of light entering the pumped EDF is achieved and an EDFA is realized.

In addition, spontaneous emission can also happen. In this case, the excited ions are not "triggered" by light entering the EDF, but fall back to the ground energy state spontaneously. Light is also emitted when this happens. This spontaneous emission of light is an unwanted but inevitable process, where an extra amount of light is spontaneously emitted next to the desired amplified light signals. Because of the amplifying character of the EDFA, this spontaneous noise will also be further amplified when travelling through the pumped EDF. This causes an amplified amount of noise at the output of the EDFA, which degrades the performance of the amplifier. This noise is commonly referred to as amplified spontaneous emission (ASE) noise.

In figure 3.3, it can also be seen that instead of pumping the EDF with a 980 nm laser, a laser with a wavelength of 1480 nm can be used to pump the erbium ions into excited state.

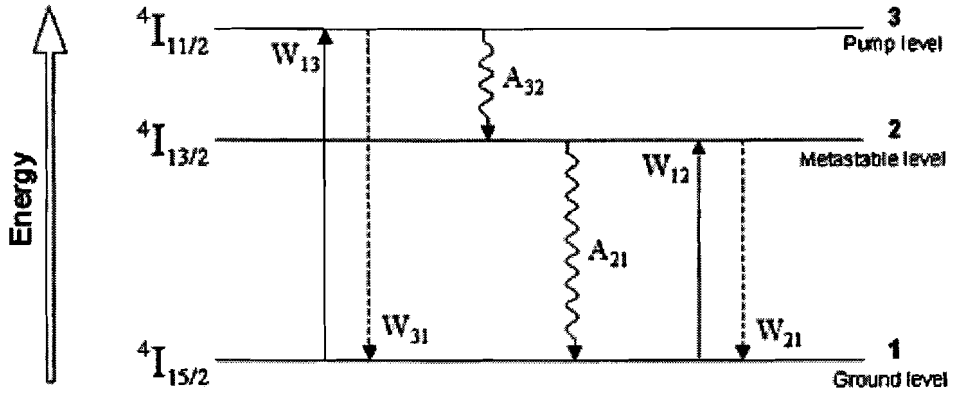

Figure 3.4: *A three-level energy system for erbium ions in an EDFA.*

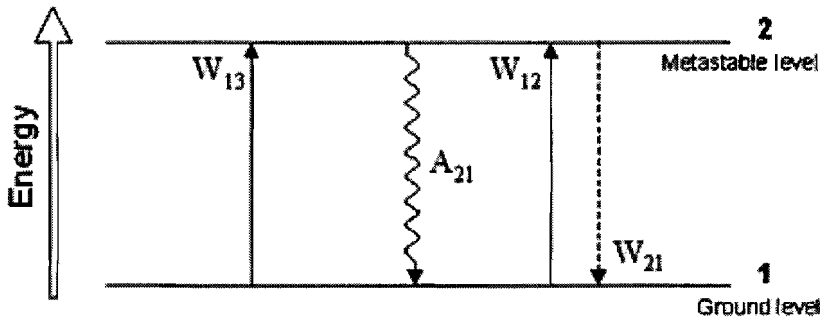

Figure 3.5: *A simplified two-level energy system for erbium ions in an EDFA.*

3.2 Mathematical model of an EDFA

In order to derive the mathematical model of an EDFA, it is common to start with a three-level energy system. Figure 3.4 shows a schematic diagram of such a three-level system for an EDFA. All possible transitions between the three energy levels are given in the figure. These transition rates are given in numbers per time and volume unit. Stimulated transition rates from energy level i to j are given by W_{ij} and spontaneous transition rates by A_{ij}.

It can be seen from the figure that W_{13} represents the pumping rate of the 980 nm pump laser and W_{31} the stimulated emission rate from the 980 nm pump level to the ground level. A_{32} represents the spontaneous fast non-radiative decay rate from the 980 nm pump level to the metastable level and A_{21} the spontaneous emission rate from metastable level to ground level. Finally, W_{12} represents the stimulated absorption rate from ground to metastable level and W_{21} the stimulated emission rate from metastable level to ground level.

Because of the fast non-radiative decay A_{32} from level 3 to 2, this transition dominates over all other transitions from level 3 to all lower levels. Therefore, the transition rate W_{31} from level 3 to 1 is so small that it can be neglected. Also, because the transition A_{32} is non-radiative and much faster than all other transitions, it can be assumed that all erbium ions that are pumped to level 3 will fall back to the metastable level 2 instantaneously without emitting any light. With this assumption, the three-level energy system can be simplified to a two-level system.

Figure 3.5 gives this simplified two-level energy system. With this two-level system, the rate equations can be derived for the erbium ion population densities n_1 and n_2 at the ground and metastable energy levels:

$$\frac{\partial n_2(z,t)}{\partial t} = -\frac{\partial n_1(z,t)}{\partial t} \tag{3.1a}$$

$$= W_{12}(z,t) + W_{13}(z,t) - W_{21}(z,t) - A_{21}(z,t) \tag{3.1b}$$

$$= n_1(z,t) \int_{-\infty}^{\infty} \frac{1}{h\nu} \left[\sigma_{12}(\nu) + \sigma_{13}(\nu)\right] \frac{S_f(z,t,\nu) + S_b(z,t,\nu)}{A(\nu)} d\nu \tag{3.1c}$$

$$-n_2(z,t) \int_{-\infty}^{\infty} \frac{1}{h\nu} \sigma_{21}(\nu) \frac{S_f(z,t,\nu) + S_b(z,t,\nu)}{A(\nu)} d\nu$$

$$-\frac{n_2(z,t)}{\tau_{21}}$$

In the previous equations, σ_{ij} are the appropriate emission/absorption cross sections, h is the Planck's constant, $S_f(z,t,\nu)$, $S_b(z,t,\nu)$ the forward and backward propagating powers at frequency ν in a frequency interval $d\nu$ and at a distance z in the fiber, A the core area, and τ_{21} the lifetime for spontaneous emission.

Because of a two-level system, the total density of the erbium ions in the EDF $\rho_{Er^{3+}}(z)$ is equal to the sum of the erbium ion population densities n_1 and n_2 at the ground and metastable energy levels: $n_1(z,t) + n_2(z,t) = \rho_{Er^{3+}}(z)$. Therefore, a change in $n_2(z,t)$ will lead to a similar but opposite change in $n_1(z,t)$, leading to $\frac{\partial n_2(z,t)}{\partial t} = -\frac{\partial n_1(z,t)}{\partial t}$, which was given already in equation 3.1a.

For the forward propagating optical powers $S_f(z,t,\nu)$ in the fiber, the following equation is used:

$$\frac{\partial S_f(z,t,\nu)}{\partial z} = \Gamma(\nu) S_f(z,t,\nu) \left\{n_2(z,t)\sigma_{21}(\nu) - n_1(z,t)\left[\sigma_{12}(\nu) + \sigma_{13}(\nu)\right]\right\} \tag{3.2}$$

$$+\frac{1}{2} m_t \Gamma(\nu) n_2(z,t) \sigma_{12}(\nu) h\nu$$

where $\Gamma(\nu)$ is the overlap integral between the mode intensity distribution and the doped fiber core and m_t the number of transverse modes that exist. For single mode fibers, where 2 orthogonal modes are possible, $m_t = 2$.

For the backward propagating optical powers $S_b(z,t,\nu)$, the same equation as in 3.2 is used, but a minus sign has to be added to the terms, yielding:

$$\frac{\partial S_b(z,t,\nu)}{\partial z} = -\Gamma(\nu) S_b(z,t,\nu) \left\{n_2(z,t)\sigma_{21}(\nu) - n_1(z,t)\left[\sigma_{12}(\nu) + \sigma_{13}(\nu)\right]\right\} \tag{3.3}$$

$$-\frac{1}{2} m_t \Gamma(\nu) n_2(z,t) \sigma_{12}(\nu) h\nu$$

By using the following definitions,

$$\sigma_a(\nu) = \sigma_{12}(\nu) + \sigma_{13}(\nu) \tag{3.4}$$
$$\sigma_e(\nu) = \sigma_{21}(\nu) \tag{3.5}$$
$$\tau = \tau_{21} \tag{3.6}$$

where σ_a is the absorption cross section, σ_e the emission cross section, and τ the spontaneous emission lifetime, equations 3.1 to 3.3 can be rewritten as:

$$\frac{\partial n_2(z,t)}{\partial t} = \int_{-\infty}^{\infty} \frac{1}{h\nu} \left[n_1(z,t)\sigma_a(\nu) - n_2(z,t)\sigma_e(\nu)\right] \frac{S_f(z,t,\nu) + S_b(z,t,\nu)}{A(\nu)} d\nu - \frac{n_2(z,t)}{\tau} \tag{3.7}$$

and

$$\frac{\partial S_{f,b}(z,t,\nu)}{\partial z} = \pm\Gamma(\nu) S_{f,b}(z,t,\nu) \left\{n_2(z,t)\sigma_e(\nu) - n_1(z,t)\sigma_a(\nu)\right\} \mp \frac{1}{2} m_t \Gamma(\nu) n_2(z,t)\sigma_e(\nu) h\nu \tag{3.8}$$

3.3 Simulation model of an EDFA

The EDFA simulation model makes use of the coupled differential equations given in 3.7 and 3.8. These coupled equations have then to be solved numerically. In order to be able to do this, the continuous equations will have to be discretized first.

This has to be done for the frequency spectrum, so that the entire wavelength range of the EDFA is divided into N intervals with wavelengths at λ_k and widths of $\Delta\lambda_k$. The power for every wavelength will be

$$P_k = \int_{c_0/\lambda_{k1}}^{c_0/\lambda_{k2}} 2S_{f,b}(z,\nu) d\nu \tag{3.9}$$

where $S_{f,b}(z,\nu)$ is the optical power propagating in the forward or backward direction. This discretization of the wavelength range is shown in figure 3.6.

With equation 3.9, the coupled equations 3.7 and 3.8 can be written in discrete form, yielding

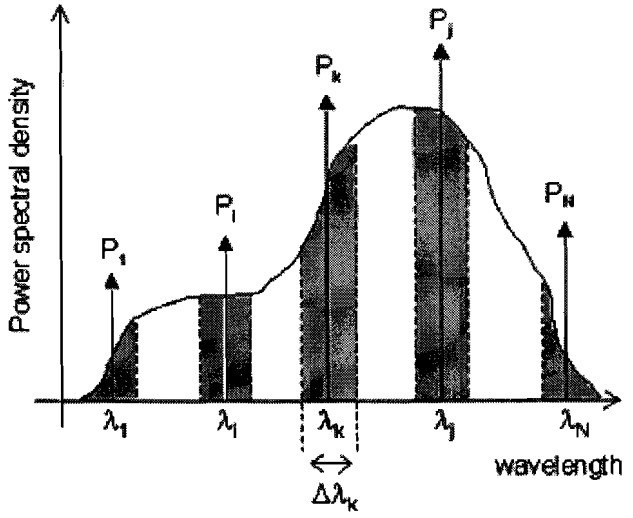

Figure 3.6: *Dividing the wavelength range into discrete intervals with finite width.*

$$\frac{\partial N_2(z,t)}{\partial t} = -\sum_{k=1}^{2N} \left[(\sigma_k^a + \sigma_k^e)N_2 - \sigma_k^a\right] \frac{p_k}{A_k} - \frac{N_2}{\tau} \tag{3.10}$$

and

$$\frac{\partial p_k(z,t)}{\partial z} = \pm\rho_{dot}\Gamma_k \left\{\left[(\sigma_k^a + \sigma_k^e)N_2 - \sigma_k^a\right] p_k + \sigma_k^e m_t N_2 \Delta\nu_k\right\} \tag{3.11}$$

In the static case, equation 3.10 doesn't depend on the time, so that

$$\frac{\partial N_2(z,t)}{\partial t} = -\sum_{k=1}^{2N} \left[(\sigma_k^a + \sigma_k^e)N_2 - \sigma_k^a\right] \frac{p_k}{A_k} - \frac{N_2}{\tau} = 0 \tag{3.12}$$

working this equation out yields

$$N_2(z) = \frac{\sum_{k=1}^{2N} \frac{\sigma_k^a}{A_k} p_k}{\frac{1}{\tau} + \sum_{k=1}^{2N} \frac{\sigma_k^a + \sigma_k^e}{A_k} p_k} \tag{3.13}$$

With equations 3.13 and 3.11, the power spectra in the EDFA can be numerically calculated for the static case. For dynamic simulations, the atomic populations are assumed to remain constant during a time step of dt. The simulation is seperated in two steps: a spatial integration with population densities fixed during dt, followed by a time integration.

Chapter 4

Power transients in optical networks

4.1 A WDM transmission link

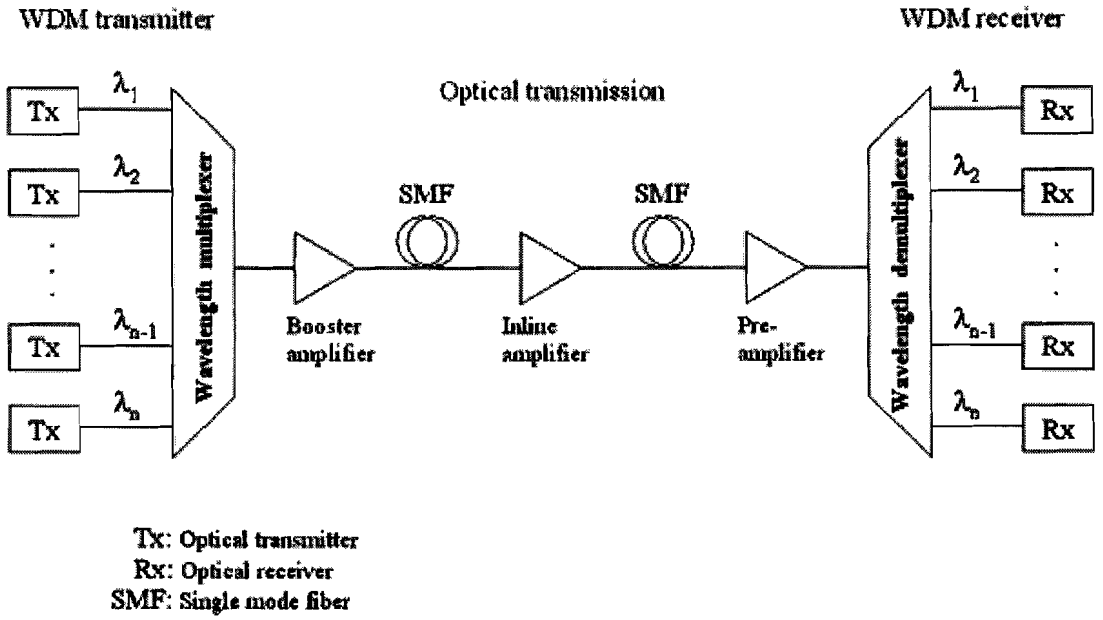

Figure 4.1: *Structure of a typical WDM transmission link.*

In figure 4.1, the structure of a typical amplified WDM transmission link, along with the key components, is given. Such a link can be found either in point-to-point transmission, or between two optical nodes of a network. In the latter case, the WDM transmitter and receivers should be replaced by OXCs or OADMs.

It can be seen that by using WDM, different signals with different wavelength channels from the transmitters are multiplexed onto a single optical fiber and transmitted. Nowadays, 40 to 80 channels in the C-band (1528-1563 nm) and another 40 to 80 channels in the L-band (1565-1610 nm) are typically used for signal transmission. A single mode fiber (SMF) is used to carry these signals over distances of more than 1000 km.

Because the powers of these signals decrease as a result of attenuation in the optical fiber, optical amplifiers are needed to amplify the signals so that long distances through the fiber can be overcome. Three different types of optical amplifiers can be distinguished:

1. *Booster amplifier*

   Used at the starting point of a link, meant to amplify the signals coming out of the multiplexer to an appropriate level suitable for transmission over the fiber.

2. *Inline amplifier*

   Used for long distance transmission in the middle of a link, meant to compensate the loss caused by long fiber spans.

3. *Pre-amplifier*

   Used at the end of a link, meant to amplify the signals coming from the last fiber span to an appropriate level so that the signals can easily be detected by the receivers after demultiplexing.

Commonly, EDFAs are used as optical amplifiers in transmission links. Because of their high gain over a large wavelength range, low intrinsic losses and long fluorescence times, EDFAs are the key enabling components in high capacity optical WDM links. In particular, owing to their long fluorescence time, EDFAs suffer little to no crosstalk at bit level, which is a serious drawback with semiconductor optical amplifiers (SOA). This is why EDFAs are widely used as optical amplifiers in WDM transmission networks.

4.2 Dynamics of erbium-doped fiber amplifiers

As mentioned in the previous section, erbium-doped fiber amplifiers (EDFAs) do not suffer from crosstalk at bit level because of their long fluorescence times. The fluorescence time of an EDFA is in principle the same as the intrinsic time constant of erbium for spontaneous emission, τ_{21}. This is in the order of 1 to 10 ms (see figure 4.2). This means that if the powers of signals change with frequencies higher than 10 kHz, the gain of the EDFA will not be influenced. In optical communications, data is modulated with a frequency in the order of GHz onto optical signals, which is much higher than 10 kHz. Light modulated at these high bit rates will therefore appear as constant light power for the amplifier, making EDFAs immune to bit-by-bit crosstalk [1]-[3].

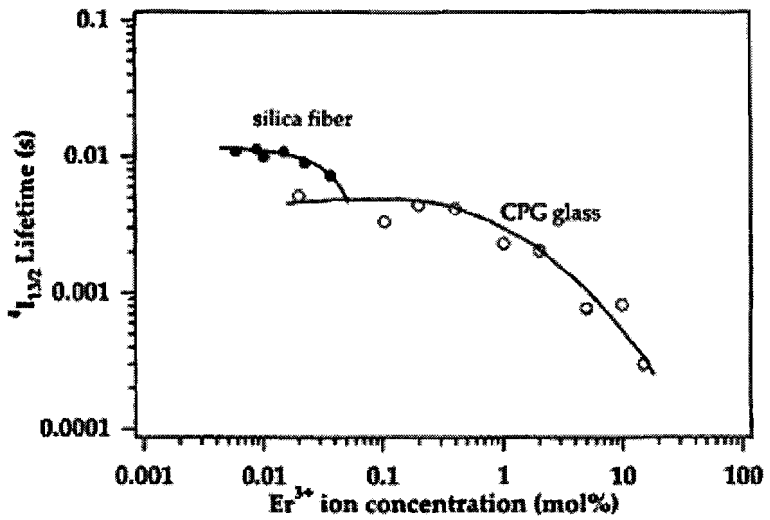

Figure 4.2: *Lifetime of erbium ions.*

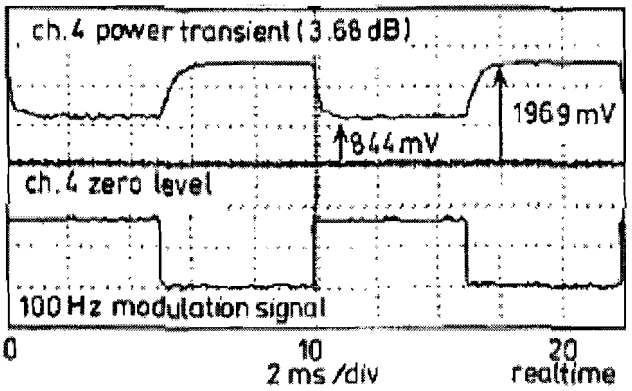

Figure 4.3: *Power excursion of 3.68 dB in remaining channel number 4 when seven out of eight channels are dropped in a WDM transmission system* [16].

However, when EDFAs are used in add/drop networks or cross-connect networks, the situation becomes very different. When channels are routed in these networks, channels may be switched on and off in the ms range. In this case, the gain in an EDFA changes in response to the input power variation, which will result in changes of the optical power and in dynamic power excursions of the remaining channels (see figure 4.3). These in turn will lead to degradation of the optical signal to noise ratio (OSNR) and bit error rate (BER) of the channels. Moreover, the gain spectrum of conventional EDFAs is dependent on the absolute gain at a particular wavelength. As the gain of an EDFA changes there is a change of the slope of the gain spectrum too. This dynamic gain tilt results in undesirable variation not only in the gain of signals but also in the gain difference between the WDM channels.

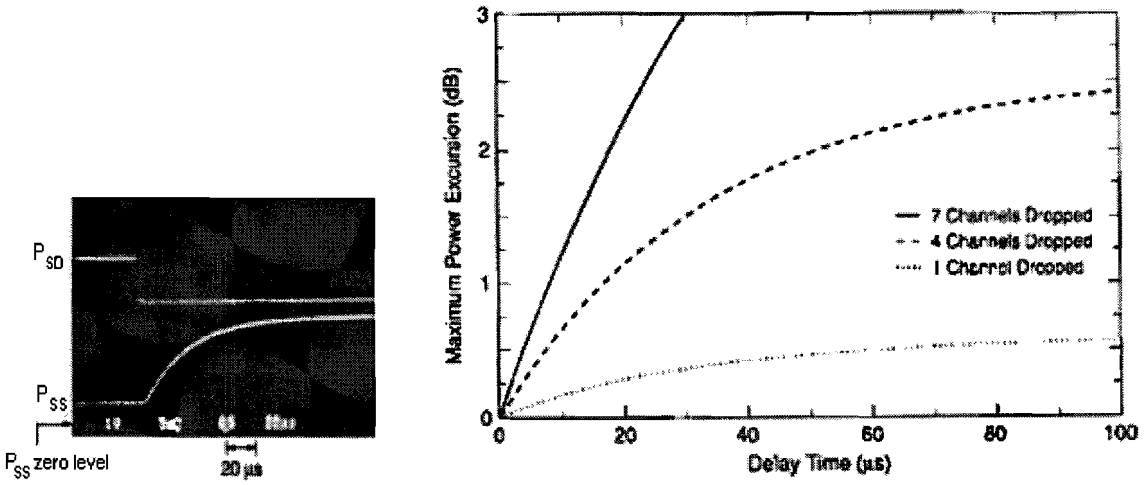

(a) (b)

Figure 4.4: *Results by Srivastava et al* [9]. (a) *Oscilloscope trace showing the time dependence of the surviving channel power PSS along with the dropped channel power PSD.* (b) *Changes in the surviving channel power as a function of time for the loss of one, four, and seven out of eight WDM channels.*

The situation becomes even worse when it is taken into consideration that in most cases, amplifiers are operated at nearly full power. This means that the amplifiers are working in saturation region, shortening the time constant of an EDFA to about 10 to 40 μs [9]. This effect is shown in figure 4.4, where the power excursion of the surviving channel is plotted against the time with different numbers of channels dropped. It can be seen that when 7 out of 8 channels are dropped, the power excursion of the surviving channel reaches 1 dB already in about 10 μs.

Detailed simulations and experiments by Zyskind et al [5] showed even worse results when EDFAs are cascaded in a link. Their results showed that power excursions of the surviving channels become faster and worse if the number of EDFAs was increased. This is shown in figures 4.5(a) and 4.5(b). At the end of a chain of ten EDFAs, the power transients already reached 1 dB in less than 2 μs. The peak values of these transients even total up to almost 4 dB. Figure 4.5(c) shows the time it takes for a transient in the surviving channel power to reach 1 dB, for an increasing number of EDFAs in a link. It can be seen that the relation between the time constant and the number of EDFAs is inversely proportional. This means that for a chain of N amplifiers, the time constant of the transients is 1/N times that for a single amplifier [5], [6].

Finally, the time constant for an EDFA in saturation can be given by the following equation:

$$\tau_{sat} = \frac{\tau_{21}}{1 + \sum_i P_i^{out}/P_i^S}, \tag{4.1}$$

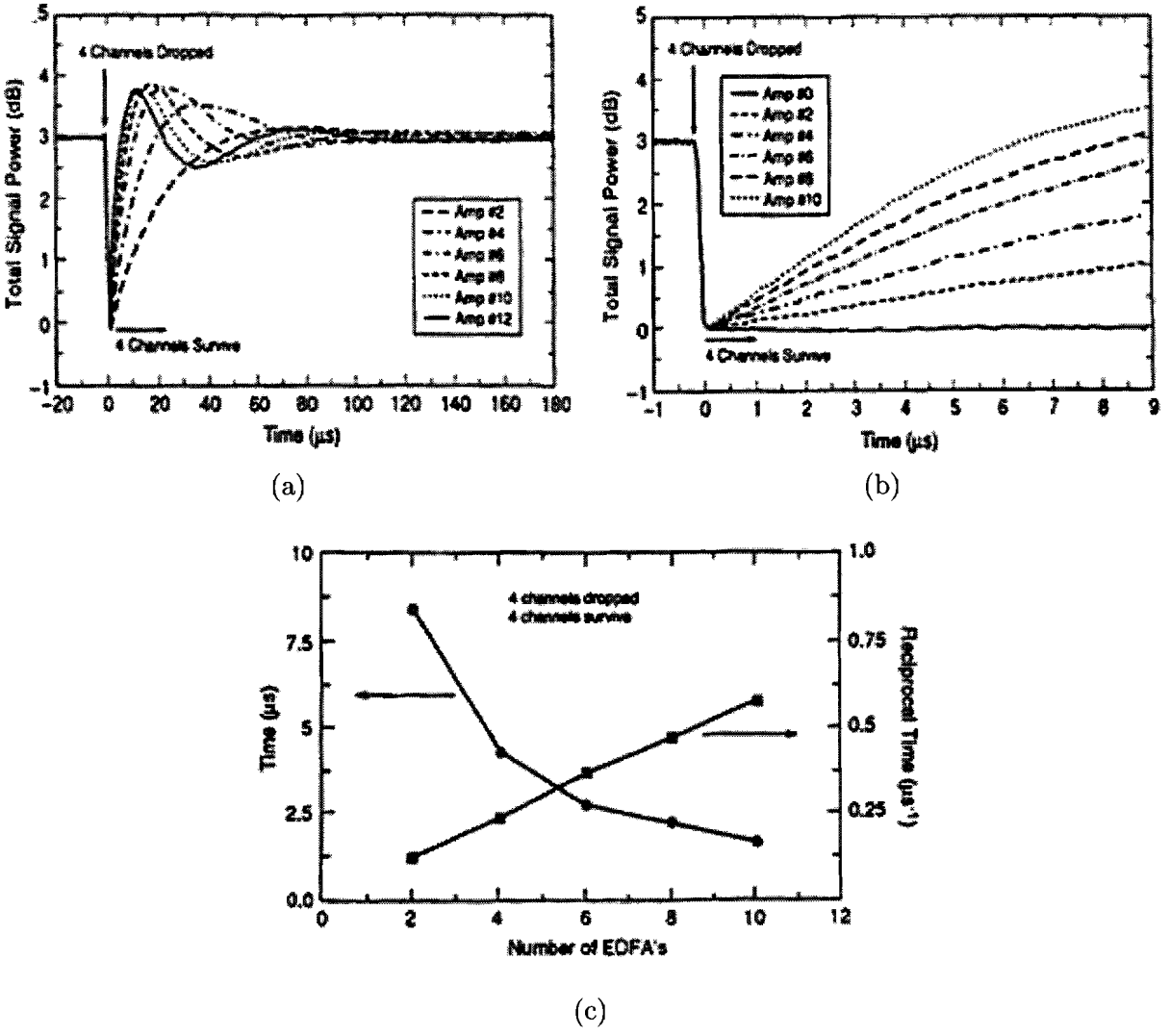

Figure 4.5: *Results by Zyskind et al* [5]. (a)*Measured output power as a function of time after 2, 4, 6, 8, 10, and 12 EDFAs. At t = 0, 4 out of 8 signal channels are dropped.* (b)*same as (a), but smaller time scale* (c)*Delay, and reciprocal of the delay, after dropping 4 out of 8 channels for surviving channel power excursion of 1dB, as a function of length of the amplifier chain.*

where τ_{21} is the intrinsic lifetime of an erbium ion, P_i^{out} is the output power of the ith frequency channel, and P_i^S is the saturation power of the ith frequency channel. This equation shows that the time constant of an EDFA will decrease when it operates with more channels at higher power. And when there is a cascade of N EDFAs, the time constant will be $1/N$ times smaller, yielding $\tau_{sat}^N = \tau_{sat}/N$.

4.3 Causes and negative effects of transients

4.3.1 Causes of transients

In all cases, variations in the input power of an EDFA lead to power transients at the output. There are several causes for these variations in input power:

1. *network routing and switching*

   With wavelength routing and switching, channels can be added or dropped out of a link. Therefore, the number of used channels in a fiber will change randomly. With the evolution of all-optical networks, the next step might be to introduce optical burst and packet switching, so that even the power of a single channel will no longer be constant but changing on a time scale corresponding to the length of the bursts and the gaps between the bursts. This will cause even more drastic variations in the power.

2. *network reconfiguration*

   Network reconfigurations can occur because of maintenance or upgrades in the network. In this case, the number and power of channels can vary because of system configurations.

3. *unintentional failures*

   Example of unintentional failures are equipment failures and mechanical failures such as fiber break or bending. These failures can either be caused by human error (digging damage) or natural disasters (earthquake). In most cases, these failures will lead to a sudden loss of many channels, resulting in a significant decrease of the input power almost instantaneously.

4.3.2 Negative effects of transients

After looking at the causes of transients, negative effects resulting from these transients should also be investigated. It is clear that fluctuations in optical power cause power transients at the output of EDFAs. In most cases, a drop in optical power will cause upward power transients (overshoot), and adding optical power will cause downward power transients (undershoot).

When power transients jump upwards, these increased optical powers can damage optical components and equipment in the communication link. Also, these high optical powers can cause non-linear effects such as Brillouin and Raman scattering, self phase modulation (SPM), cross phase modulation (XPM), and four wave mixing (FWM), thereby degrading system performances such as optical signal-to-noise ratios (OSNR) and bit-error rates (BER).

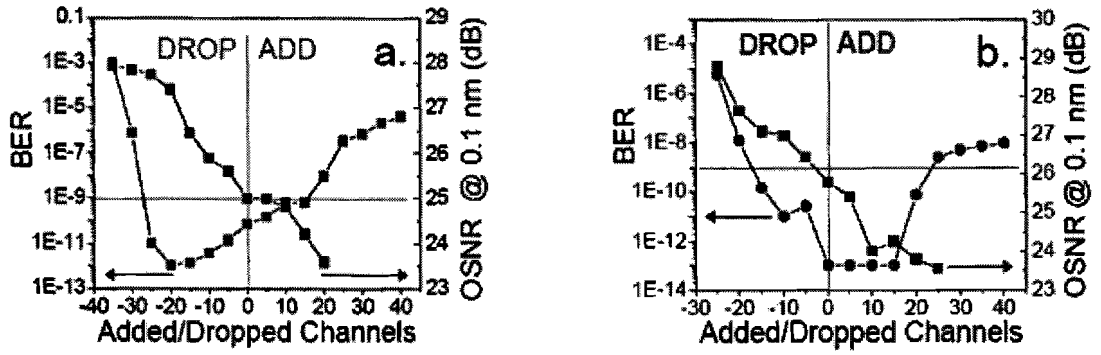

Figure 4.6: *Changes in BER and OSNR as a function of added/dropped channels for* (a)*system that is OSNR limited and* (b)*system that is limited by nonlinear impairments* [7].

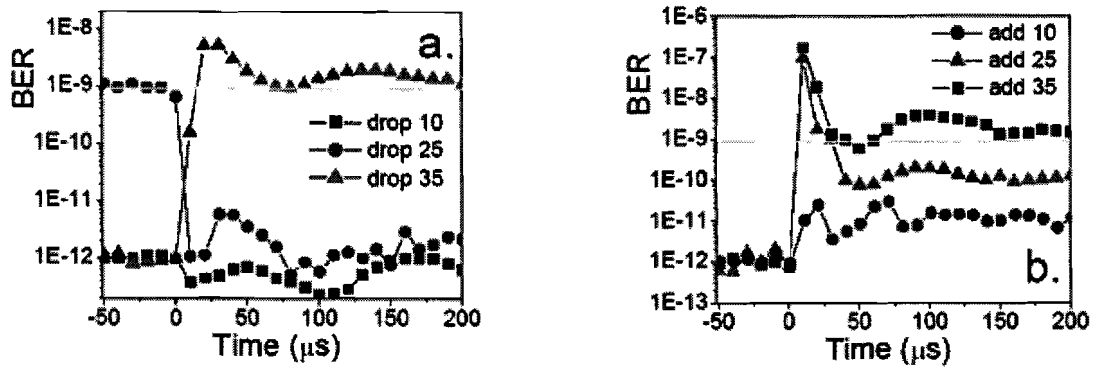

Figure 4.7: *Transient behaviour of the BER for cases of* (a)*add and* (b)*drop of different number of channels out of 40. Initial BER level for the case of dropping of 25 channels is chosen higher to accomodate the BER behaviour* [7].

In the other case, when power transients jump downwards, the optical powers at the receiver decrease, leading to eye closure. If the optical channel power is further reduced such that it falls below the sensitivity of the receiver, severe bit errors result. In addition, the decrease in channel power leads to degradation in OSNR since the path-averaged power of the channels becomes lower.

Figures 4.6 and 4.7 show OSNR and BER measurement results by Turukhin et al regarding adding and dropping of channels in a realistic transmission link with 40 WDM channels [7]. In figure 4.6, it can be seen that adding more channels leads to lower optical power, resulting in a lower OSNR. The OSNR increases again when more channels are dropped, as a result of higher optical power. However, it can also be seen that when channels are either dropped or added, more bit errors occur.

It is interesting to see that in figure 4.6(a), the BER decreases when more channels are dropped (better system performance). This is because of the increase in optical

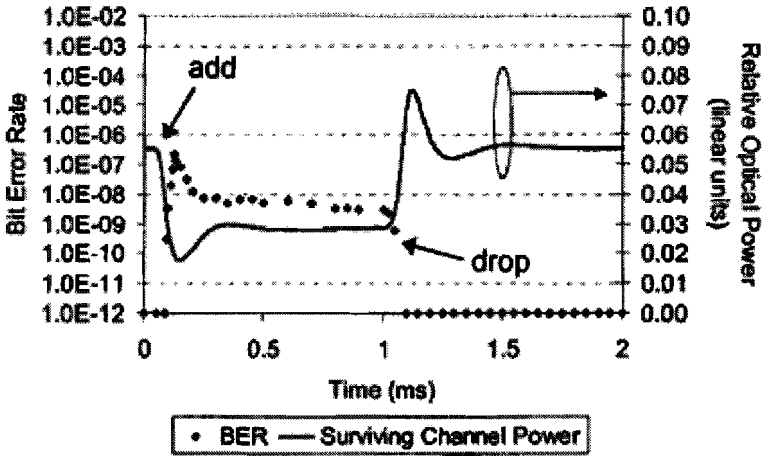

Figure 4.8: *Plot of the time-resolved BER during a channel-add/drop event when transient control is off* [8].

power as a result of power transients jumping upwards. This leads to a better OSNR which in turn leads to less bit errors. However, when more than 20 channels are dropped, the optical channel power jumps so high that nonlinear effects take over and worsen the BER. One must therefore be aware of the fact that even though the OSNR is increasing, more bit errors can occur in the event of channel drops.

In figure 4.7, the transient behaviour of the BER as a result of power transients is showed for different add/drop cases. Just like power transients, BERs can instantaneously jump to levels a lot higher than steady state values.

The results shown in figure 4.8, obtained by Wong et al [8], are comparable to those of Turukhin. In this figure, the BER is given together with the surviving channel optical power in the case of add/drops. This shows the relation between the surviving optical power and the BER very nicely. When seeing all these negative effects, it is apparent that transient control is necessary in EDFAs.

4.4 Behaviour of transients

Before trying to control power transients in EDFAs, it is important to understand their behaviour. Therefore, several simulation results obtained by Schilling [33] are shown in this section for better understanding of transient behaviour of optical powers in different operating conditions.

In figure 4.9, power transients for the total optical power and single surviving channel optical power is shown for different percentages of total channels dropped. In figure 4.9(a), there are a total of 10 channels before the drop, and in figure 4.9(b), there are

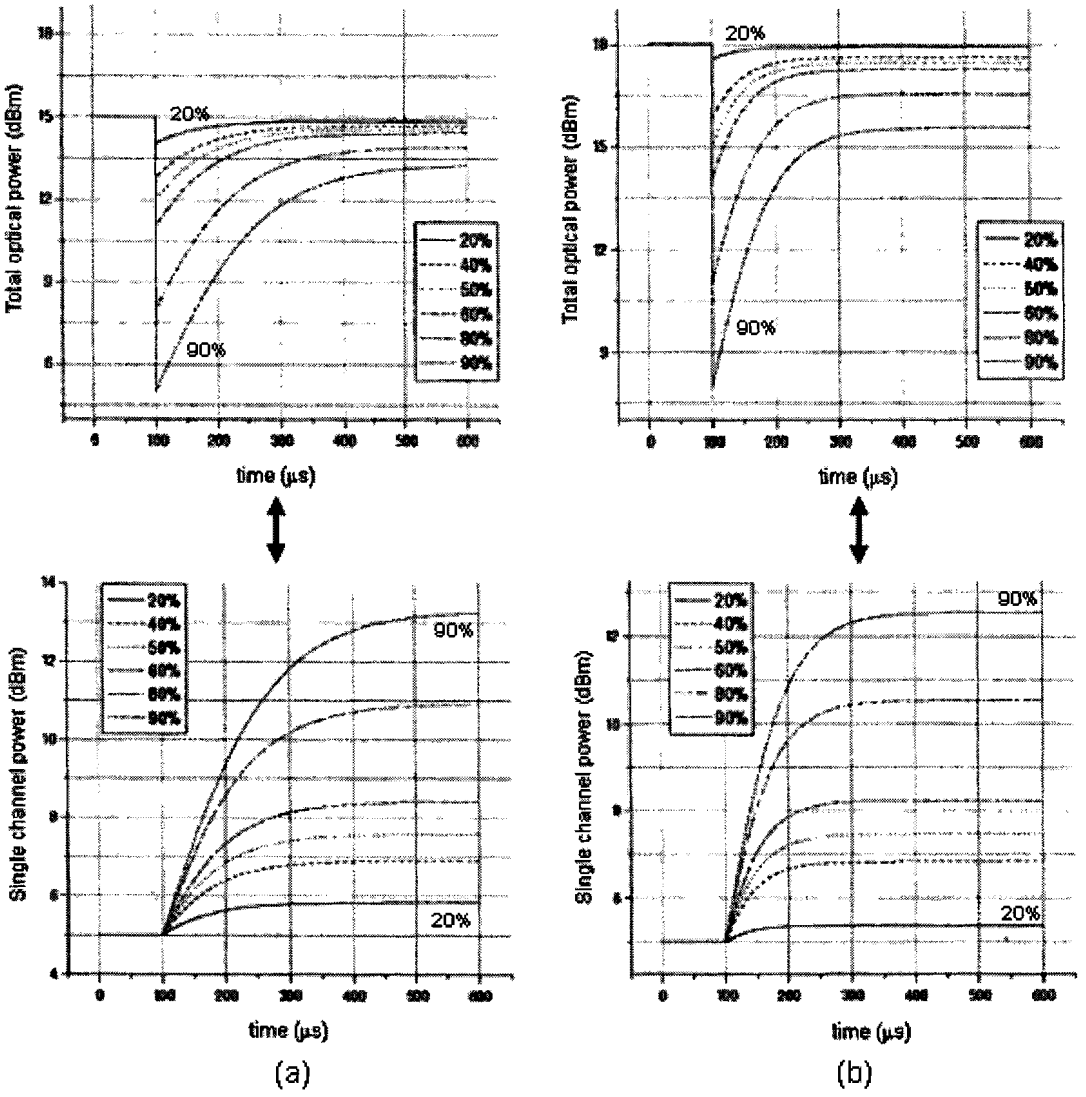

Figure 4.9: *Transient response of total optical power and single channel power for different percentages of total channels dropped* [33]. (a)*10 channels total before drop.* (b)*20 channels total before drop.*

20 channels before the drop. The results are for a single EDFA, with a channel distance of 100 GHz (C-band), input power of -10 dBm per channel, and a gain of 15 dB. The channels are dropped with an instantaneous step and the pump power is kept constant.

It can be seen that the total optical power at the output of the EDFA decreases instantaneously with the drop. But directly after this, the total power rises back again to a value close to the one before the drop. The values before and after the drop differ because of amplified spontaneous emission (ASE). Also, it can be seen that the single channel power jumps up when channels are dropped. This is because the level of inversion

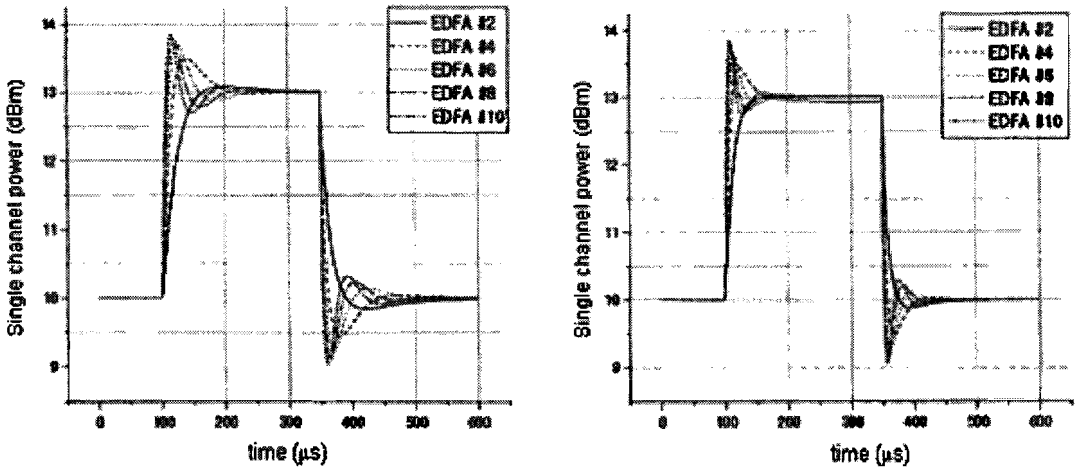

Figure 4.10: *Transient response of single channel power measured after every second EDFA in a link with 10 EDFAs where 50% of the total channels are dropped* [33]. (a)*10 channels total before drop.* (b)*20 channels total before drop.*

in the EDFA remains the same so that the remaining channels increase in power. This can also be derived from the following equation for the saturated gain:

$$\gamma(\nu) = \frac{1}{I_v} \cdot \frac{dI_\nu}{dz} = \frac{\left(I_p^* - 1\right)\sigma_{SE} N}{1 + 2I_\nu^* + I_p^*}, \tag{4.2}$$

where I_v is the power of the signal at frequency ν, I_p is the pump power, N is the atomic density of the medium, σ_{SE} is the stimulated emission cross-section, $I_\nu^* = I_v/I_s$, and $I_p^* = I_p/I_{ps}$. I_s is the signal saturation power and I_{ps} is the pump saturation power.

When more channels are dropped, the height and speed of the power transients increase. Finally, the number of used channels in the EDFA also plays a role. When more channels are used, transient speed becomes faster.

Figure 4.10 shows the transient response of the single channel power after an increasing number of EDFAs. It can be seen that the overshoots of the transients become worse and the rise time increases with the number of EDFAs. The total number of WDM channels also influences the transient speed, making it faster when more channels are used (compare figure 4.10(a) to (b)). By the way, these results compare well to the results obtained by Zyskind et al [5] shown in figure 4.5. This also applies to figure 4.11, where the inverse proportional relation between the rise time and the number of EDFAs in cascade is shown.

Finally, the influence of the speed of the drop T_S on the power transients is investigated and given in figure 4.12. If channels are dropped slowly (in the order of 1 ms)

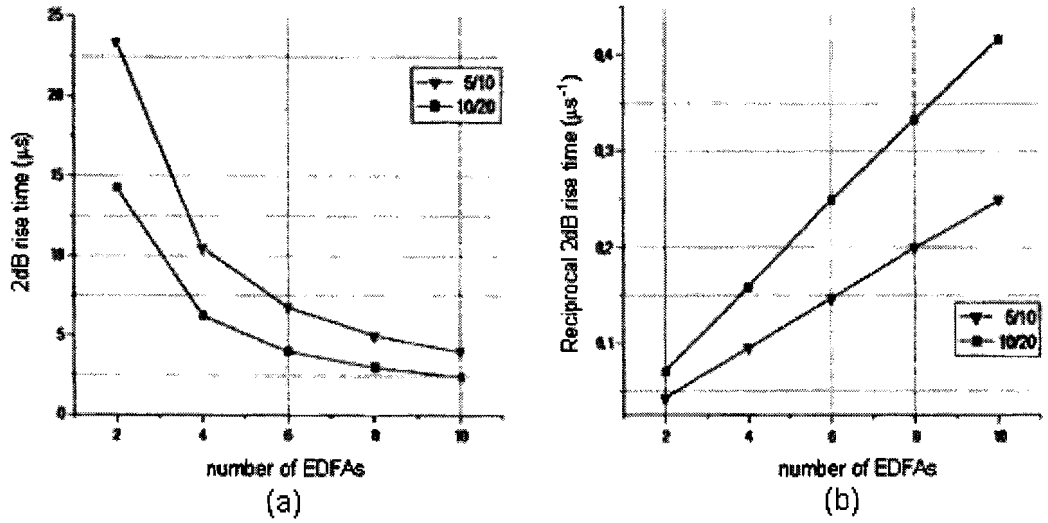

Figure 4.11: (a)*Rise time of transient to a level of 2dB as a function of the number of EDFAs.* (b)*same as in (a), but the reciprocal rise time is plotted to show inverse proportional relation* [33].

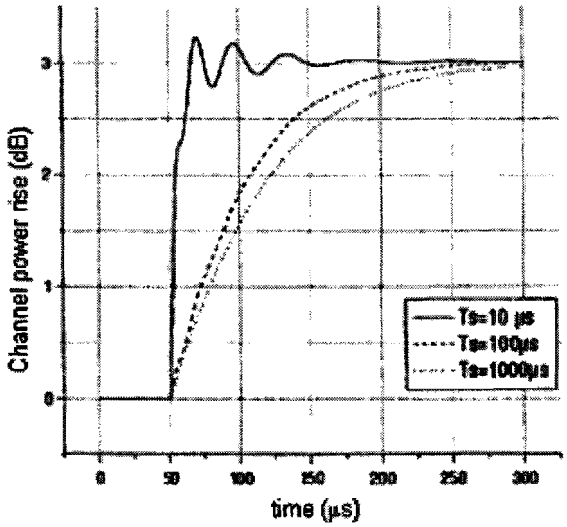

Figure 4.12: *Influence of speed of the drop Ts on the shape and speed of the transient channel power rise* [33].

and not instantaneously, transient effects in the channel power are less. The speed and height of the overshoot in the channel power decrease significantly.

Chapter 5

Different methods to control an EDFA

As previously discussed, power transients can lead to a lot of negative effects, thereby endangering the reliability and quality of service of optical networks. Therefore, it is very important to stabilize the behaviour of EDFAs and to reduce these power transients. This can be done by controlling the gain of the EDFAs. Throughout the years, different methods have been developed to do this. These methods can basically be grouped into three different methods.

The first method is to control the amplifier gain, by adjusting the pump power (*pump control*). This can be done either using a control feedback loop or by forward control. In the latter case, one simply measures the input power changes and changes the pump power according to the characteristics of the amplifier. In the feedback control loop case the gain or some parameter proportional to it is continuously measured and the pump power is adjusted to give the preset gain value.

The second method is to inject an additional optical signal inside the gain bandwidth into the EDFA, in order to control the level of saturation and thereby adjusting the gain (*lasing*). Again, adjusting the power in the additional channel can be done by using a feedback control loop or by forward control, setting the extra channel power in response to input power changes.

In the first two methods, the main purpose is to keep the gain of an EDFA constant (*gain clamping*) by means of automatic gain control (AGC). This is done for every optical amplifier in a transmission link. However, in the third method, a continuous-wave (CW) channel is used to compensate for the power variations at the beginning of a transmission link, thereby stabilizing all the amplifiers in the entire link (*link control*). The focus is laid on controlling the whole link, rather than individual amplifiers.

In further sections, several of these different control methods are briefly discussed and the results of these methods obtained by other researchers are shown.

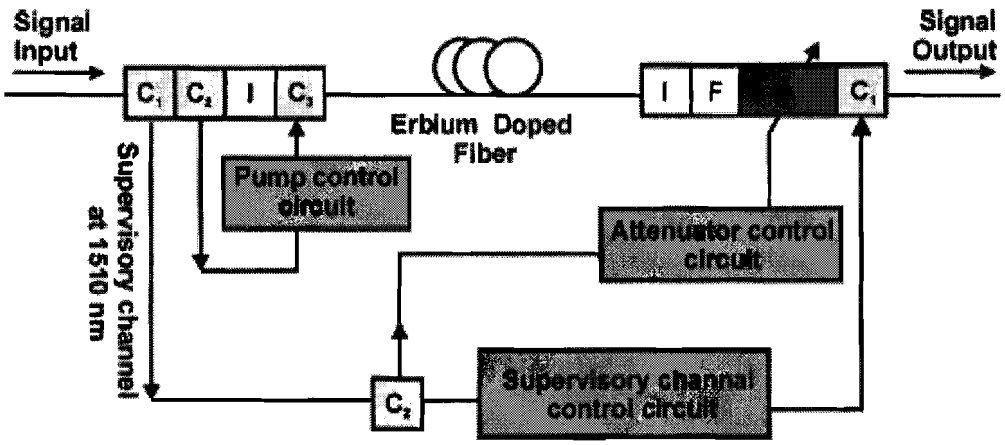

Figure 5.1: *Experimental setup for forward pump power control* [11]. *A: Voltage-controlled attenuator; C1: Coupler for supervisory wavelength; C2: Coupler for 5% tap; C3: Coupler for pump wavelength; F: Filter for ASE suppression; I: Isolator.*

5.1 Gain control by adjustment of the pump power

To achieve constant gain for EDFAs, the pump power is adjusted using an electronic feedback control loop or forward control.

5.1.1 Forward control

A feed-forward compensation with a low-frequency (100 kHz) control of the pump power was proposed and analyzed theoretically and experimentally by Giles et al [10]. The pump power is automatically adjusted in response to the total input power, resulting in a constant amplifier gain. For an eight channel WDM transmission system a similar control scheme has been demonstrated experimentally by Park et al [11]. Figure 5.1 shows the proposed configuration of the EDFA.

The EDFA is codirectionally pumped by a 980 nm laser diode (LD) with power up to 80 mW. The EDFA is has two control circuits. The first low speed one compensates for changes in span losses with an attenuator control circuit, the second high speed one keeps the amplifier gain constant with a pump control circuit. In the experiment, the input signal consisted of eight signal channel from 1541 nm to 1559 nm, seven of them could be switched on and off, and a supervisory channel at 1510 nm. The variation of span losses were simulated, by attenuating the whole input signal.

The supervising channel is dropped at C1. Changes in span losses can be measured as power variations of the supervisory channel at the attenuator control circuit, which adjusts the attenuator A. The response time of the attenuator is 9 ms. Additionally the supervisory channel is processed at the supervisory channel control circuit and a new supervisory channel is added to the amplifier output signal.

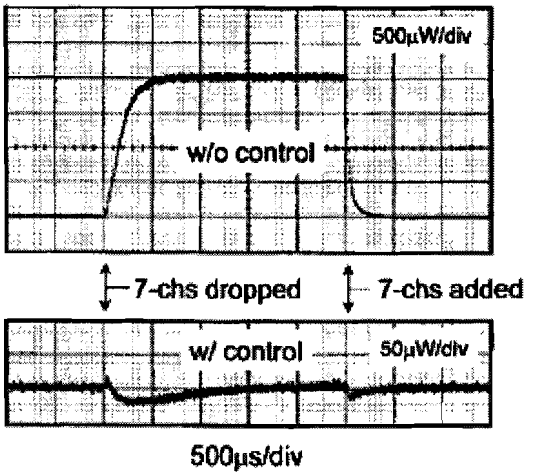

Figure 5.2: *Surviving channel power transients when seven out of eight channels are added or dropped in a forward pump control* [11].

For fast gain control of the EDFA, a small part (5 %) of the power of the signal channels is tapped before the EDFA and measured by the pump power control circuit, which adjusts the pump so that the gain stays constant. The response time of the pump power control circuit is 650 ns. The power excursion of the surviving channel was reduced to 1 % of that without control circuits, which corresponds to 0.17 dB power excursion, when seven out of eight channels were added or dropped (see figure 5.2).

In the discussed experiments the input power is measured and the pump power is adjusted for constant gain, relying on characteristics of the amplifier, which has to be determined before. This is in contrast to feedback control, where the gain is measured continuously and adjusted to the desired value by a feedback control loop.

5.1.2 Electronic feedback control loop

Examples for gain control using electronic feedback loops have been presented in publications by Jolley et al [12], Drake et al [13] and Suzuki et al [14].

Jolley et al [12] address mainly the problem that the spectral slope of the gain changes, if the gain changes. The spectral equalization of gain can only be achieved for a specific gain. The authors propose a two stage amplifier consisting of two electronically gain controlled gain blocks and an adjustable attenuator in between. The attenuator and not the gain blocks are used to adjust the output power of amplifier if necessary.

A schematic view of a gain block is shown in figure 5.3. It consists of a 980-nm pumped EDFA with a probe laser that is injected into the input of the gain block and measured at the output. The probe laser was at 1572 nm outside the flat gain

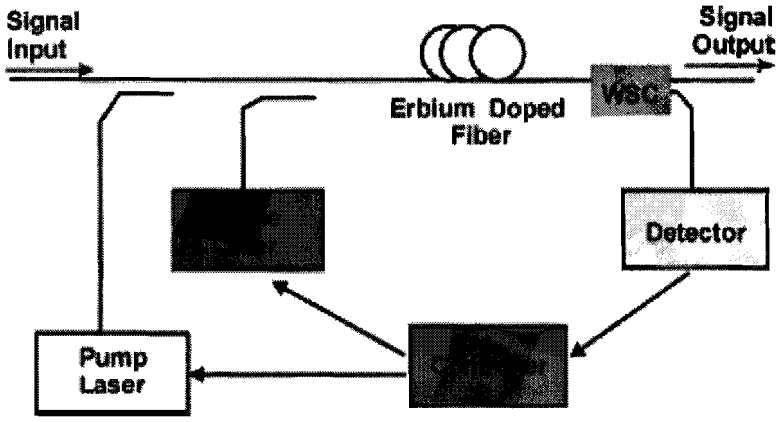

Figure 5.3: *Schematic view of a gain block with electronic feedback control* [12].

window used for WDM transmission in this experiment. The control circuit uses negative feedback to the pump current to maintain the EDFA gain constant at the probe laser wavelength. Results are only given for the reduction of gain tilt, but not for the achieved dynamic response.

The electronic feedback control has some advantages compared to optical gain clamping. The gain of the gain block can easily be changed electronically if required. The feedback signal can be filtered electronically to optimize the dynamic response of the control loop and to avoid the oscillations occurring in the all optical feedback loop.

Drake et al [13] compared two schemes of electronic feedback control loops. In the first design instead of the gain, the pump absorption was measured and kept constant. In the second design the gain at a probe wavelength was measured, like in the experiment of Jolley et al., but the probe signal was injected counter directionally in this experiment. The design with measurement of the pump absorption is simpler, whilst the more complex probe technique provides greater accuracy.

Suzuki et al [14] implemented a three stage optical amplifier, where each stage (gain block) had an automatic gain control circuit (AGC), adjusting the pump power. The first stage served as low noise pre-amplifier, the second compensated for losses due to dispersion compensation and a power control variable attenuator and the third stage provided high output power.

The AGC of the each gain block was realized by a feedback control loop that monitored the input and output total powers to keep the gain and the gain profile constant. The time constant of the circuit was designed to be less than 10 μs. The maximum transient power fluctuation of the surviving channel was measured to be less than 0.45 dB when signals (32ch-1ch) were added or dropped. These results are shown in figure 5.4.

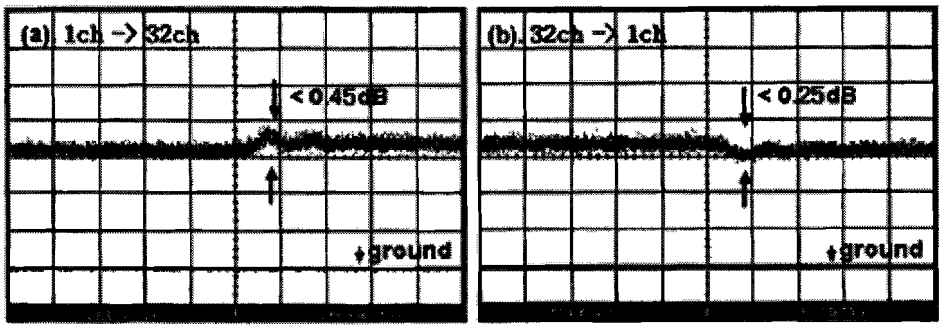

Figure 5.4: *Transient response of surviving channel power of automatic gain control by Suzuki et al* [14]; (a)*for 1 to 32 channels addition* (b)*for 32 to 1 channels drop.*

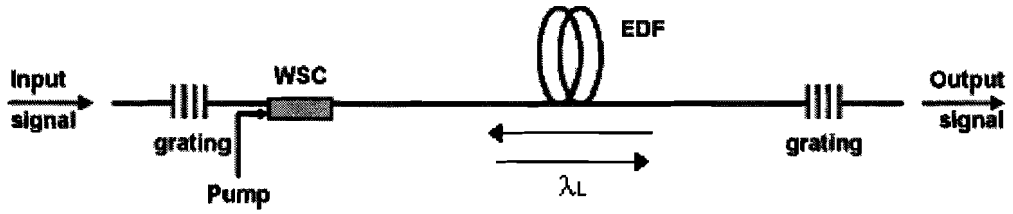

Figure 5.5: *Gain clamped amplifier with Farby Perot laser structure using fiber grating reflectors. EDF: erbium-doped fibre, WSC: wavelength selective coupler.*

5.2 Gain clamping by all optical feedback (lasing)

The all-optical gain-control technique is widely studied as a potential method to prevent signal power transients due to cross-gain saturation of EDFAs in multiwavelength optical networks [16], [17], [18]. Here, an EDFA is made to lase at a particular wavelength within the EDFA gain bandwidth, but different from signal wavelengths. The optical feedback (the laser resonator) is usually obtained by two methods:

1. The use of distributed Bragg reflector (DBR) gratings in the fiber at each end of the amplifier, causing reflective feedback at the Bragg wavelength [19], [20].

2. The use of a ring laser structure configuration [21], [22] with wavelength selective WDM filters feeding back the lasing wavelength only.

5.2.1 Using Bragg reflector

This relatively simple passive method uses lasing to control the gain of the EDFA. It uses a Fabry-Perot laser structure with two narrow bandpass fiber Bragg grating reflectors placed at the input and the output ends of the amplifier, as shown in figure 5.5. These fiber gratings will let light with all wavelengths through, except for the lasing wavelength,

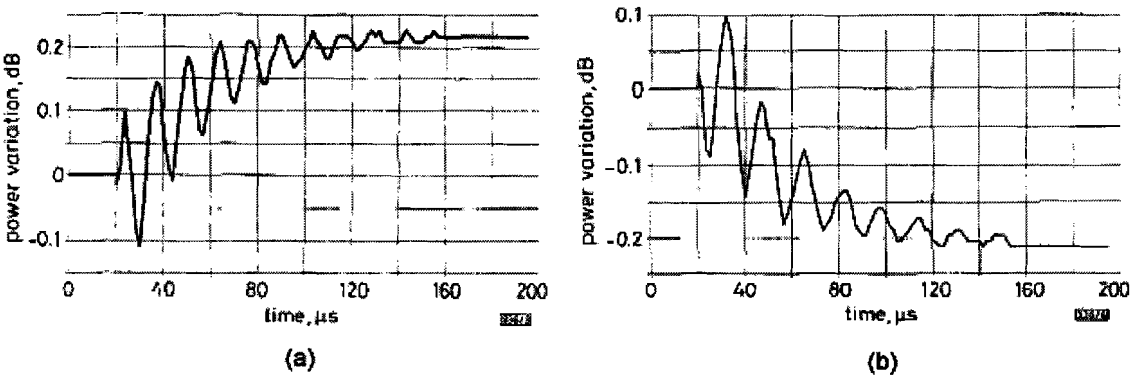

Figure 5.6: *Surviving channel power transients when seven out of eight channels are* (a)*dropped* (b)*added* [20].

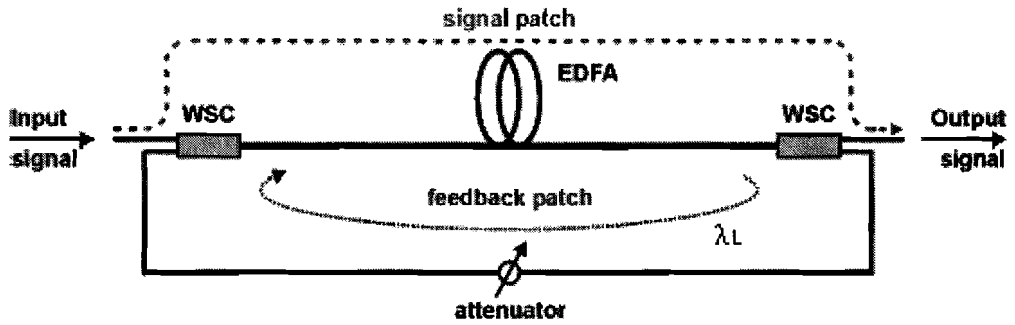

Figure 5.7: *Gain-clamped amplifier scheme in a ring laser structure. WSC: wavelength selective coupler.*

λ_L. As a result, light with this wavelength will be lasing in the EDFA, with a power that is multiple times larger than the signal powers in the EDFA. This laser will keep the inversion of the erbium ions and therefore the gain of the EDFA on an almost constant level. Figure 5.6 shows some results obtained by Landousies et al [20]. It is typical that the output power of the surviving channel suffers from relaxation oscillations because of the proportional feedback action of optical gain clamping.

5.2.2 Using ring laser structure

As shown in figure 5.7, gain control can also be achieved by operating the amplifier in a ring-laser configuration. With a wavelength selective coupler, part of the light at the output with wavelength λ_L is fed back through an optical attenuator to the input of the EDFA again. The optical attenuator is used to control the power of the feedback signal, thereby setting the gain of the EDFA to a constant value.

When the input signal power drops, the power of λ_L at the output will increase. This is fed back to the input, where its power is larger than all other signals. As a result, this

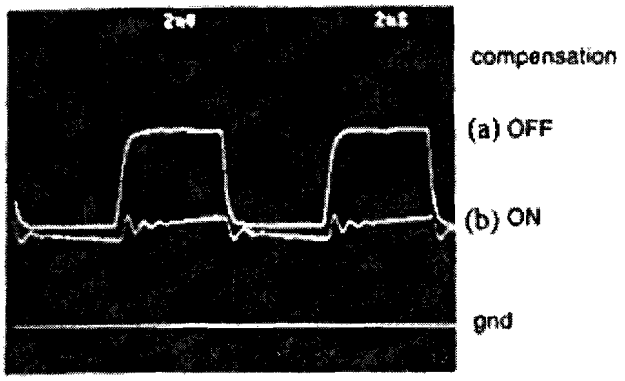

Figure 5.8: *Results obtained by Desurvire et al* [22] *using the ring laser structure of optical gain clamping.*

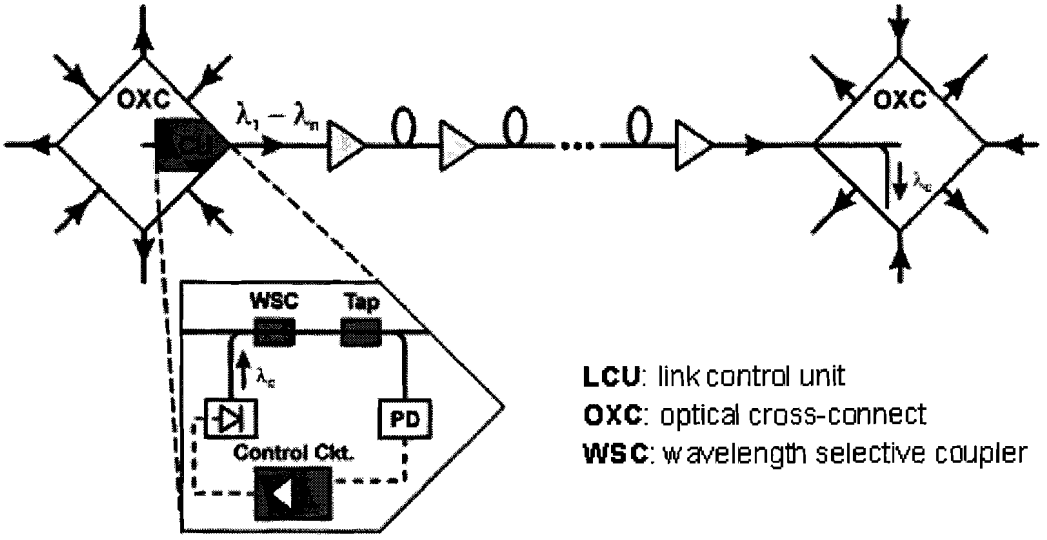

Figure 5.9: *Link control for surviving channel protection in optical networks by using a control channel* [25].

will compensate for the loss of the input signal power, keeping the gain and inversion of the EDFA constant. Just like the method using fiber Bragg gratings, the resulting output power suffers from relaxation oscillations too (see figure 5.8).

5.3 Link control by an extra compensating channel

A gain control scheme based on the use of an additional WDM channel to compensate for the variation of total optical power at the input, and thereby stabilizing all the amplifiers in a transmission link between network routing nodes, has been proposed by Zyskind and

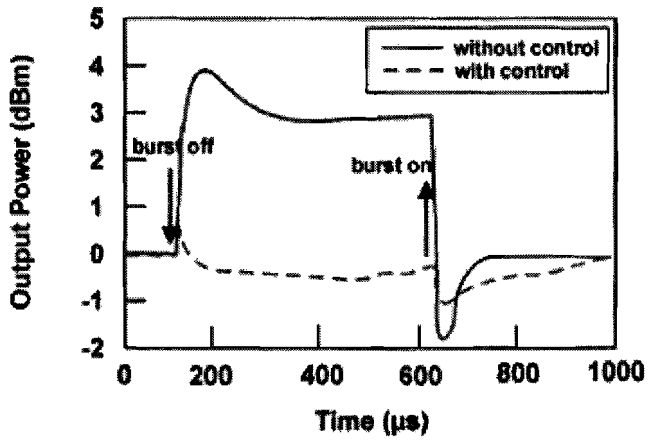

Figure 5.10: *Power excursions due to cross saturation of an EDFA cascade for a surviving channel. Five of seven WDM channels are switched on /off at 1 kHz* [25].

Srivastava et al [23], [24], [25]. The scheme, illustrated in figure 5.9, protects surviving channels on a link basis.

It can be seen that the extra link control channel λ_C is added to the input of the first optical amplifier in a transmission link (this will commonly be the output amplifier of a network node). At the end of the link, which is the next network node, the link control channel is then stripped off. The power of the link control channel is adjusted to keep the total power of the signal channels (including the link control channel) constant at the input of the first amplifier. This will maintain constant channel loading at all EDFA's cascaded in the link. Figure 5.10 shows the power excursions at the end of the transmission link for the surviving channel. In this case, six channels are transmitted and five are dropped, leaving one surviving channel. Results are shown with and without link control.

5.4 Best method to control an EDFA

With all the different EDFA gain control methods presented in previous sections, the next step is to discuss the advantages and disadvantages of these methods and to conclude which method is the best.

The main advantage of the all-optical gain control by using laser action in the EDFA is its simple implementation. However, the pump powers required for controlled operation are quite large. This is because the optical power in the gain band is always at its maximum value. Also, system performance can be degraded due to relaxation oscillations, which can be minimized, but not avoided due to the simple proportional feedback scheme. Last but not least, the speed in optical feedback (lasing) gain control is limited

by the laser relaxation oscillation which is generally in the order of tens of microseconds or slower [17].

The link control method, by using an extra channel which compensates for the power variations in an entire link, is a very cost effective way to control transients. However, this only works well for short links with a few amplifiers and a low number of channels. For long links with long amplifier chains and a high number of channels, the quality of this type of control deteriorates severely.

At this moment, the best method seems to be fast electronic gain control. The feedback signal can be filtered electronically, in order to optimize the total dynamic response and to avoid relaxation oscillations, observed with the all optical control method. It makes efficient use of the available pump power (unlike an optically stabilized EDFA where most of the pump power is converted into the lasing wavelength) while allowing fine control and adjustment of the EDFA gain, without sacrificing any of the EDFA transmission bandwidth.

It is true that fast electronic gain control is complex and costly to implement, but the results that can be achieved with this type of control currently outweigh these negative arguments. In addition, the possibilities with electronic gain control are much larger than other types of control.

Chapter 6

A multilevel gain controlled optical amplifier

Taking into mind the conclusion from the previous chapter that fast electronic gain control is currently the best method to control power transients in an EDFA, the structure and working of a multilevel gain controlled optical amplifier that is used in practice is presented and discussed in this chapter. This amplifier consists of a fast electronic feedback control combined with a feedforward control, which enhances the system performance.

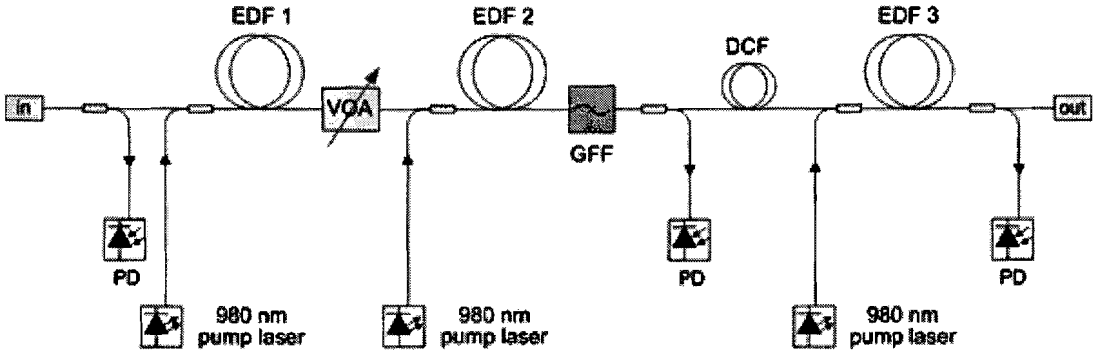

Figure 6.1: *Schematic view of a state of the art optical amplifier.*

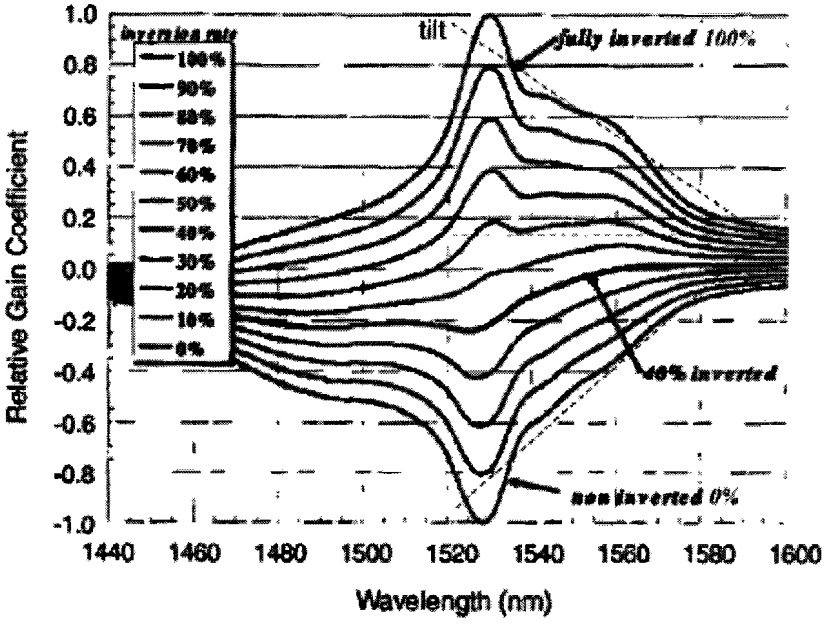

Figure 6.2: *Gain coefficients of EDFs with population inversion rate as a parameter.*

6.1 Structure of a complex optical amplifier

Figure 6.1 shows a schematic view of a state of the art optical amplifier that is used in practice. It can be seen that this amplifier consists of three EDFA stages. Each EDFA stage consists of an erbium-doped fiber (EDF), pumped codirectionally by a laser with a wavelength of 980 nm. The codirectional pumping method is used in order to achieve a low noise figure. In this three-stage optical amplifier, the first stage serves as a low noise pre-amplifier and increases the signal level for the following stages. The second stage compensates for losses due to the gain flattening filter and the dispersion compensating fiber. The third stage provides high output power.

6.1.1 Variable optical attenuator

By inserting a variable optical attenuator (VOA) between the first two stages, a simple gain tilt control is implemented in the optical amplifier. This works as follows. The gain spectrum of an EDFA changes when the population inversion of the erbium ions changes (see figure 6.2). It can be seen that in the EDFA working range of 1520 nm to 1600 nm, this gain spectrum tilts with the level of inversion. This inversion level can be changed by adjusting the pump power.

When the VOA is adjusted to give more attenuation, the pump power should be increased in order to achieve the same power at the output of the second stage. Because

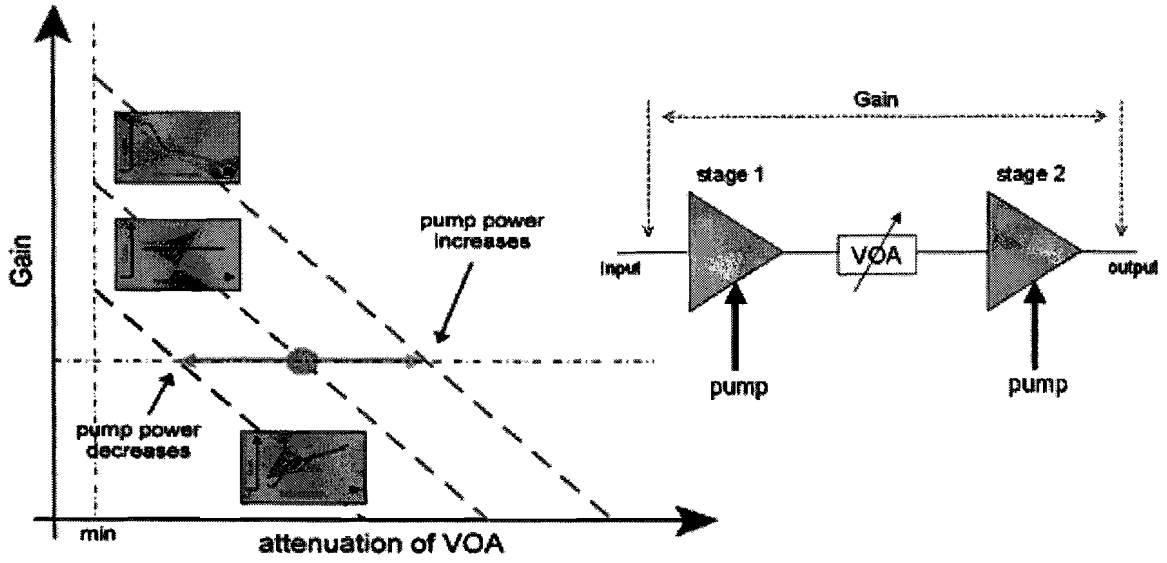

Figure 6.3: *Tilt control with a VOA*

the pump power is increased, the tilt of the gain spectrum changes. However, the power at the output of the second stage remains the same. Therefore, the total gain measured between the input of the first stage and the output of the second stage remains also the same. With this method, the gain is held constant but the spectrum experiences a tilt. A tilt control is implemented. Figure 6.3 shows this method in a diagram.

A tilt control is needed to adjust the spectral tilt of the signals coming out of the optical amplifier. This is important because a lot of elements in the optical amplifier or the transmission link can cause a tilt in the spectrum of the signals. The most important is the effect of stimulated Raman scattering (SRS), which occurs in the fiber span prior to the optical amplifier and in the DCF that is used in the amplifier. SRS causes signals with smaller wavelengths to transfer power to signals with larger wavelengths, resulting in a tilt in the spectrum of the signals. More on SRS and the negative effects of SRS on the performance of optical amplifiers can be found in the next section. Also, the attenuation in fibers doesn't have the same value for different wavelengths. This causes a tilt in the spectrum of the signals too (see figure 6.4). Finally, the non-flatness of the gain spectrum of the EDFAs and the gain flattening filters can also lead to spectral tilt in the signals.

6.1.2 Gain flattening filter

Returning back to figure 6.1, one can also find a gain flattening filter (GFF) in the optical amplifier. This GFF is used to flatten the gain spectrum of all three EDFAs in the amplifier. As shown already in figure 6.2, the gain spectrum of an EDFA is not

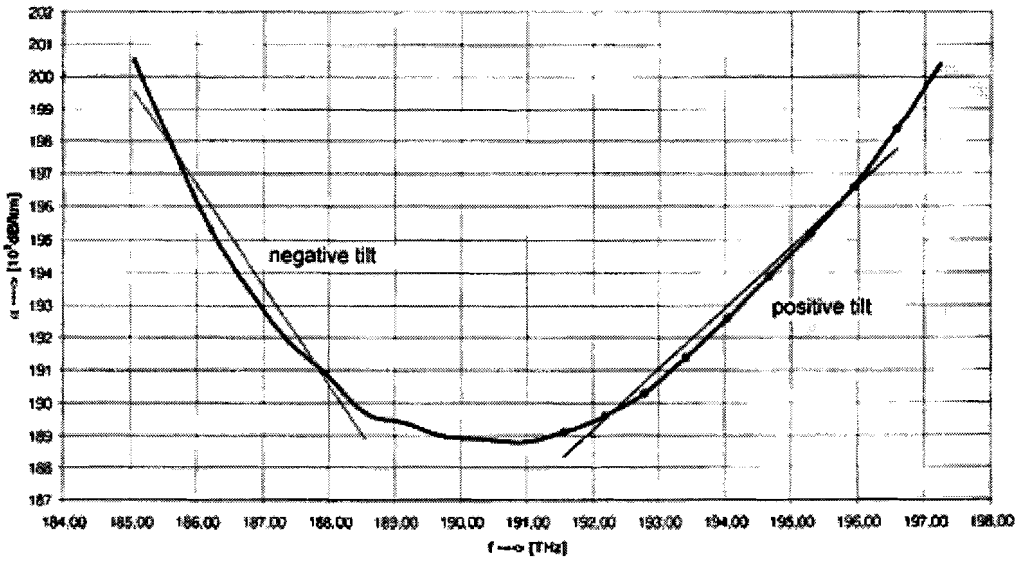

Figure 6.4: *Spectral attenuation of standard single mode fiber. It can clearly be seen that the attenuation curve is tilted.*

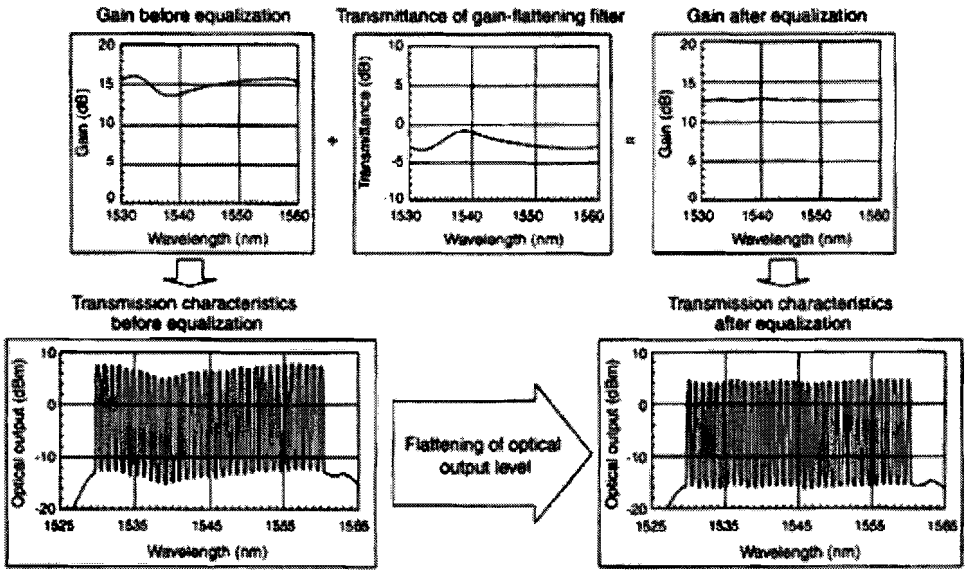

Figure 6.5: *Function of an optical gain flattening filter.*

perfectly flat. Figure 6.5 shows the function of such a gain flattening filter. A flat gain spectrum is very important because this has a lot of influence on gain control when signals are added or dropped. Ripples in the gain spectrum can cause a jump in the surviving channels even when good gain control is implemented. An extreme case of this problem is shown in figure 6.6, where only one channel at λ_s survives after the drop. In

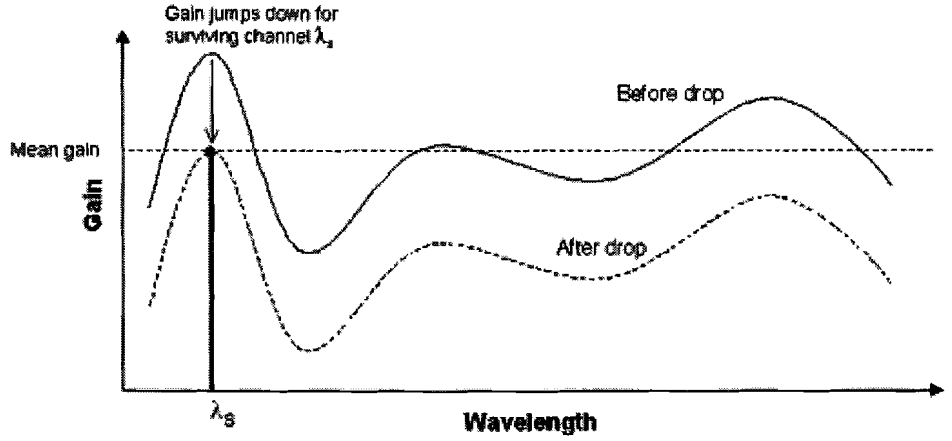

Figure 6.6: *Influence of gain ripple on gain control.*

both cases, the gain control fixes the gain to the same mean value. However, in the case after the drop, it can be seen that the actual gain of the surviving channel has decreased, resulting in a loss in the channel power.

6.1.3 Dispersion compensating fiber

The dispersion compensating fiber (DCF) is used to compensate dispersion that accumulates in the fiber spans. Dispersion causes signal pulses to broaden, resulting in an overlap with neighboring pulses. After a certain amount of overlap has occurred, adjacent pulses can no longer be individually distinguished at the receiver and bit errors will occur. This pulse broadening effect is shown schematically in figure 6.7. The DCF is placed before the second stage of the optical amplifier instead of after because of a better noise figure.

6.2 Different levels of control

In the optical amplifier, different levels of control with different complexities are implemented to ensure high system performance. There are four main different levels of control that can be differentiated:

1. Gain tilt control with VOA,
2. Electronic gain and transient control,
3. ASE correction,
4. OSNR or power preemphasis.

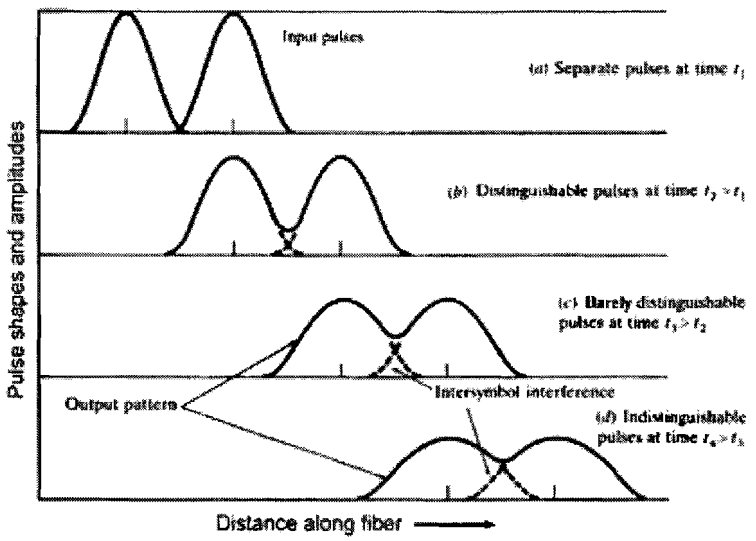

Figure 6.7: *Broadening and attenuation of two adjacent pulses as they travel along a fiber.*

In the following sections, these controls are presented and discussed.

6.2.1 Gain tilt control

As discussed in the previous section, the optical amplifier contains a gain tilt control implemented with a VOA. This is important because a lot of elements can cause a tilt in the spectrum of the signals. This tilt in the signal spectrum may affect transient behaviours, thereby interfering with the transient control. It is therefore necessary to compensate this spectral tilt.

Stimulated Raman scattering

The most important source of spectral tilt in the signal channels is stimulated Raman scattering (SRS). When light is incident on a medium, scattering occurs. This scattered light will consist mostly of light with the same frequency as the incident light. In the meantime, low intensities of light with lower frequencies may also be observed. This is due to the effect of Raman scattering and can be described quantum-mechanically as scattering of the incident photon by a molecule to a lower-frequency photon while at the same time the molecule makes a transition between its two vibrational states. Incident light acts as a pump for generating frequency-downshifted radiation called the Stokes wave.

The initial growth of the Stokes wave in a fiber is described by

$$\frac{dP_s}{dz} = \frac{g_R}{A_{eff}} P_p P_s - \alpha_s P_s, \tag{6.1}$$

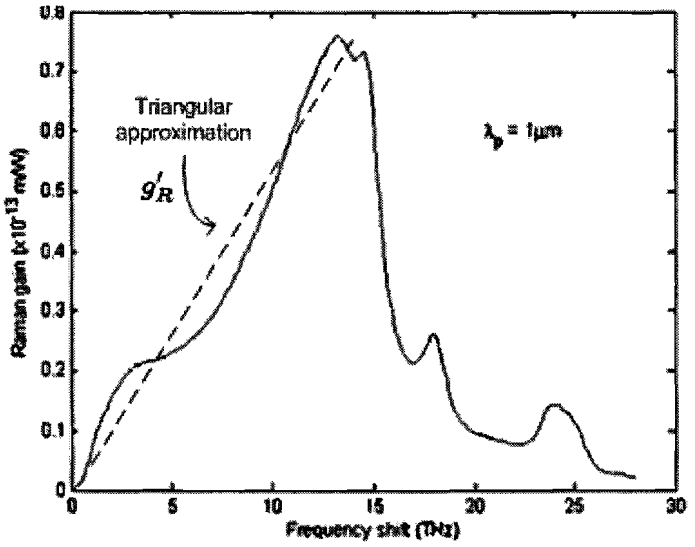

Figure 6.8: *Raman gain spectrum for SSMF at a pump wavelength $\lambda_p = 1$ μm. The Raman gain scales inversely with λ_p.*

where P_s is the power of the Stokes wave, P_p the power of the pump, A_{eff} the effective mode field diameter of the fiber, α_s the loss in the fiber for the Stokes wave, and g_R the Raman-gain coefficient. The Raman-gain coefficient describes how much power is gained from the pump depending on the frequency of the Stokes wave. This is given in figure 6.8. The evolution of the pump power in the fiber is given by

$$\frac{dP_p}{dz} = -\frac{\nu_p}{\nu_s}\frac{g_R}{A_{eff}}P_sP_p - \alpha_pP_p, \tag{6.2}$$

where ν_p is the frequency of the pump signal, ν_s the frequency of the Stokes wave, and α_p the loss in the fiber for the pump signal. Equations 6.1 and 6.2 are called the coupled equations for Raman scattering [26].

Under the assumption that $\frac{g_R}{A_{eff}}P_s \ll \alpha_p$, the depletion of the pump power $-\frac{\nu_p}{\nu_s}\frac{g_R}{A_{eff}}P_sP_p$ in equation 6.2 can be neglected. The pump power is therefore only affected by the loss of the fiber

$$\frac{dP_p}{dz} = -\alpha_pP_p. \tag{6.3}$$

Solving the coupled equations 6.1 and 6.3 yields

$$P_s(z) = P_s(0)\exp\left\{\frac{g_R}{A_{eff}}P_p(0)L_{eff} - \alpha_sz\right\}, \tag{6.4}$$

with

$$L_{eff} = \frac{1}{\alpha_p}\left[1 - \exp\left(-\alpha_pz\right)\right]. \tag{6.5}$$

Equation 6.4 describes how much power is gained from the pump for the Stokes wave and how the power changes along the fiber. If the polarizations of the pump light and the Stokes wave are not matched, equation 6.4 is written as

$$P_s(z) = P_s(0) \exp\left\{\frac{1}{2}\frac{g_R}{A_{eff}} P_p(0) L_{eff} - \alpha_s z\right\} \tag{6.6}$$

because the gain from the pump is less.

When many channels are used, every channel power acts as a Raman pump for the remaining channels of lower frequencies. Instead of equation 6.1, the growth of the power of the kth channel along the fiber in a system with N channels can be written as

$$\frac{dP_k}{dz} = P_k \cdot \sum_{j=1}^{N} \frac{g_R}{2A_{eff}} P_j - \alpha P_k. \tag{6.7}$$

In all equations mentioned before, the Raman-gain coefficient g_R is a non-linear function of the frequency difference between pump and Stokes wave. However, a triangle gain profile can be used to approximation the Raman-gain coefficient. This is shown in figure 6.8. Then, the approximated Raman-gain profile is linear with respect to the frequency difference. The approximated Raman-gain profile can then be written as

$$g_R \doteq g'_R \cdot (f_j - f_k)$$

and equation 6.7 can be written as

$$\frac{dP_k}{dz} = P_k \cdot \sum_{j=1}^{N} \frac{g'_R \cdot (f_j - f_k)}{2A_{eff}} P_j - \alpha P_k \tag{6.8a}$$

$$\frac{dP_k}{dz} = P_k \cdot \frac{g'_R}{2A_{eff}} P_{tot} - \alpha P_k. \tag{6.8b}$$

For a WDM system with N channels, equation 6.4 can then be written as

$$P_k(z) = P_k(0) \exp\left\{\frac{g'_R}{2A_{eff}} P_{tot}(0) L_{eff} - \alpha z\right\}, \tag{6.9}$$

with P_k the power of the kth channel and $P_{tot}(0)$ the total power of all N channels at the beginning of the fiber. Equation 6.9 can be splitted into two terms, a term defining SRS

$$P_k(z) = P_k(0) \exp\left\{\frac{g'_R}{2A_{eff}} P_{tot}(0) L_{eff}\right\} \tag{6.10}$$

and a term defining the loss in the fiber

$$P_k(z) = P_k(0) \exp\{-\alpha z\}. \tag{6.11}$$

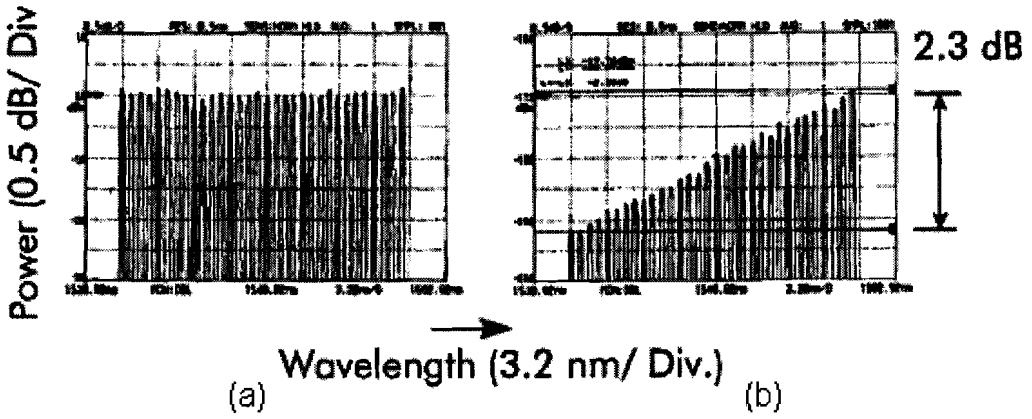

Figure 6.9: *The effect of SRS crosstalk on signals transmitted through a fiber span* [27]. (a)*Fiber input spectrum.* (b)*Fiber output spectrum after 100-km of fiber.*

The term

$$\exp\left\{\frac{g'_R}{2A_{eff}}P_{tot}(0)L_{eff}\right\}$$

from equation 6.10 can also be expressed in dB, yielding the Raman tilt to be

$$Raman\_tilt = 4.343 \cdot 10^{15} \cdot \frac{L_{eff} \cdot g'_R}{2A_{eff}} \cdot P_{tot} \ \ [dB/THz]. \tag{6.12}$$

In figure 6.9, the influence of SRS tilt on the spectrum of the signals is shown by results from Bigo et al [27]. This effect is often called SRS crosstalk and happens not only in normal transmission fibers, but also in the DCF. Therefore, gain tilt control is needed to compensate for spectral tilts in transmission fibers as well as DCF.

Fiber spectral attenuation tilt

As shown already in figure 6.4, the attenuation in fibers is frequency dependent. This also adds a tilt in the spectrum of the signals when transmitted through the fiber. Unlike SRS which causes a negative tilt in the direction of increasing frequency, this tilt can either increase positively or negatively with increasing frequency. If channels in the C-band (from 192 to 196 THz) are used, this tilt will be positive. And if channels in the L-band (from 186 to 190 THz) are used, this tilt will be negative. Although fiber spectral attenuation causes tilts in signal spectra transmitted through fibers, the effect is not as large as from SRS.

However, this tilt has also to be compensated too in order to have a flat gain spectrum for the optical amplifier so that gain control can work properly. Just like for SRS tilt, this happens also in the DCF. Compensation must therefore be done for the transmission fiber as well as DCF.

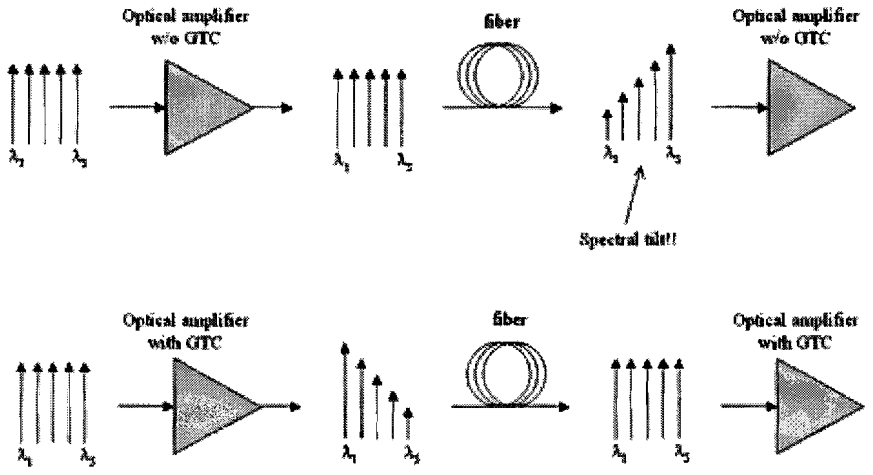

Figure 6.10: *Compensation of spectral tilt resulting from transmission fiber with and without gain tilt control (GTC).*

Gain tilt control with VOA

With SRS and fiber attenuation, the most important causes of spectral tilt in signals are discussed. In most cases, these tilts can be calculated theoretically. SRS tilts depend on the power launched into the fibers and the Raman-gain coefficients of these fibers. These values can either be measured or estimated well and the tilt can then be calculated. The same applies for fiber attenuation tilts.

A gain tilt control with a VOA can then be implemented easily. With a conversion formula, the tilt (in dB/THz) that is needed for compensation can be converted to an attenuation value (in dB) for the VOA so that the desired tilt can be achieved. Figure 6.10 shows how a gain tilt control compensates a spectral tilt to ensure a flat gain spectrum for an optical amplifier.

6.2.2 Electronic gain and transient control

In figure 6.11, a schematic view of the optical amplifier with its electronic gain control is given. While there are three EDFA stages, only two electronic gain control blocks are used. The first two EDFA stages are controlled by the first gain control group A, and the last stage is controlled by a separate control group B. The electronic control is implemented digitally in a digital signal processor (DSP). Group A sets the gain of the first two stages at a fixed value given by the user, so that the total optical output power at point P2 is equal to the input power at P1 multiplied with the set gain value. Group B does the same, but for the third stage and the total optical power at the output of the amplifier P3.

From the input of the optical amplifier, a small part of the optical input power is coupled out with a tap coupler and measured with a photodetector at P1. This

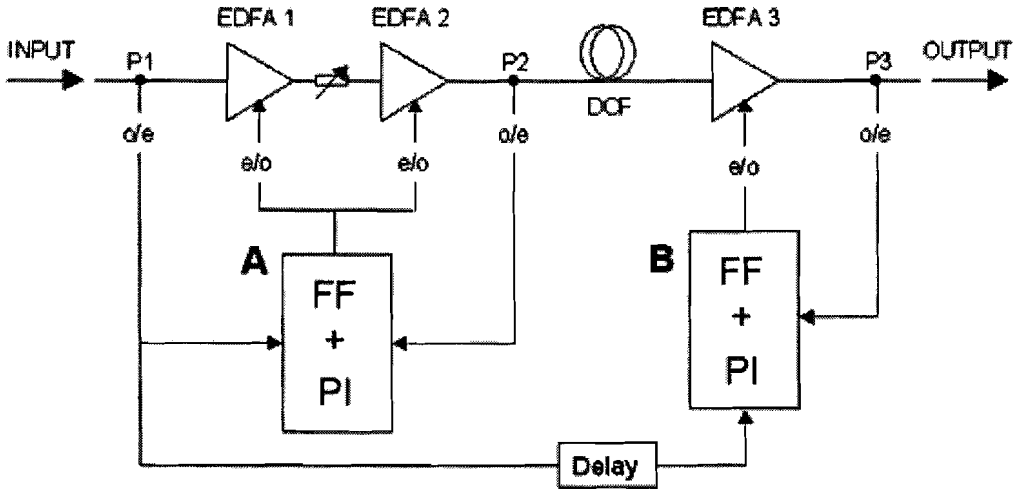

Figure 6.11: *Schematic view of optical amplifier with electronic gain control*

photodetector then converts the measured optical power to an electrical signal that is sent to the DSP. The same happens at the points P2 and P3. The electrical signals are then processed in the control groups A and B and sent as currents to the pump lasers. In the pump lasers, these currents are converted back to optical signals again. These optical signals have a wavelength of 980 nm in order to pump the EDFAs and the intensity is changed by the currents sent from the control groups. With this, an electronic gain control for the EDFAs is realized.

The basics of the two control groups are principally the same. A feedback proportional-integral control is combined with a feed-forward control to process the powers measured from the input and output of each control group. For control group A, these are the points P1 and P2 given in figure 6.11. And for control group B, these are the points P1 and P3. Figure 6.12 shows the details of a such a feedback proportional-integral control combined with feed-forward control for an EDFA.

First, a proportional-integral feedback control is used to set the pump power at such a value, that the optical power measured at the output is equal to the optical power measured at the input multiplied with a gain factor. With this, the gain of the amplifier can be set. Proportional-integral feedback is given by

$$u = K_p e + \frac{K_i}{T_I} \int e \, dt \tag{6.13}$$

where K_p is the proportional gain, e is the error between the measured output signal and the desired output signal, K_i is the gain of the integrator, T_I is the integral time, and u is the output signal of the control. The term

$$K_p e \tag{6.14}$$

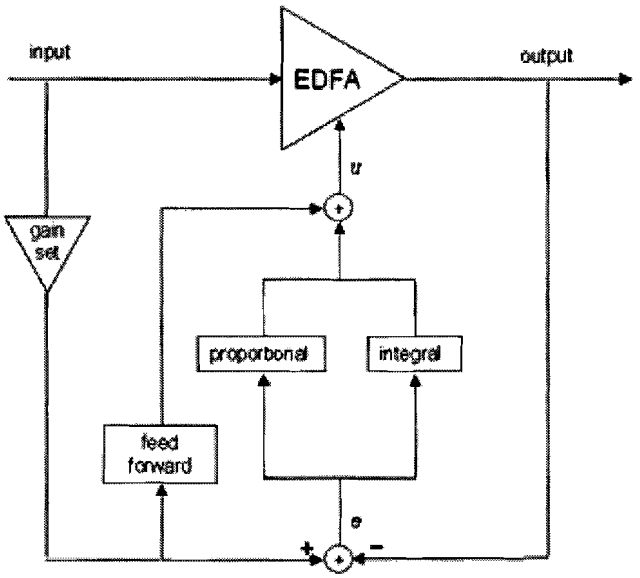

Figure 6.12: *A combined proportional integral feedback with feed-forward control.*

is called the proportional feedback and the term

$$\frac{K_i}{T_I} \int e \, dt \tag{6.15}$$

the integral feedback.

With proportional feedback, the control signal is made to be linearly proportional to the error in the measured output. This means that when the output power is higher than the set value, the error e will have a negative value, leading to a negative proportional term given in equation 6.14. The output signal u of the control will be negative and the pump of the EDFA will be turned down. This will subsequently lead to a decrease of the output power, which is the desired effect. The same follows for an output power that is too low. However, the problem of a proportional feedback control is that the error will never be zero. An error signal is always needed to be able to control the EDFA.

This is why an integral feedback control is added. This control has the primary virtue that it can provide a finite value of control signal with no error-signal e. This is because u is a function of all past values of e rather than just the instantaneous value of e, as in the proportional case. Therefore, past errors e "charge up" the integrator to some value that will remain, even if the error becomes zero and stays there. This means that with an integral control, the output power of an EDFA can be controlled to be error-free.

With such a proportional integral feedback, an effective control system can be implemented. However, the speed of the control can be further enhanced with a feed-forward control. When the input power of the EDFA drops very fast, the output power will jump

up because of a high inversion level in the EDFA. To counter this, the control signal u to the pump has to be decreased. This is done automatically by the proportional integral feedback already, but the feedback has to wait until the output power deviates before it knows how to react. This delay will have a negative influence on the speed of the control. When a feed-forward is implemented, a change in the input power of the EDFA will have an almost instantaneous effect on the pump control signal u, thereby speeding up the control.

Going back to figure 6.11, it can be seen that the first two EDFAs of the optical amplifier are controlled by one feed-forward/back control, and the last EDFA by another similar feed-forward/back control. The time constants of these two controls differ by approximately twice, so that they don't interfere with each other. The delay block in the path from input power to control group B is there because the DCF in the optical path delays the signals going to the third EDFA. For control group B to work well, the input power to the control must be delayed with the same amount of time too.

6.2.3 ASE correction

With electronic gain control by pump power adjustment, the input signal powers and the output signal powers of the optical amplifier have to be measured. This is done by using couplers at the input and output fibers of the optical amplifier. With a tap coupler, a small percentage (usually 2 to 5%) of the optical light going through the fiber can be coupled out of the system. This small amount of light is then fed to a photodiode, converting the light into electrical current. With some scaling, the current is changed to a voltage that is proportional to the optical power.

In the optical amplifier, optical power is measured at the three points that are of importance to the electronic control discussed previously. However, because of the use of a photodiode, the total optical power is measured. Therefore, the difference between ASE and signal power cannot be distinguished. This extra ASE noise decreases the performance of the electronic gain control because the gain of an amplifier stage is calculated from dividing the output power by the input power.

Ideally, when there is no ASE noise, the gain G of an amplifier stage can be calculated by the measured signal output power divided by signal input power

$$G = \frac{P^{out}_{meas}}{P^{in}_{meas}} = \frac{P^{out}_{sig}}{P^{in}_{meas}}, \tag{6.16}$$

where the signal output power $P^{out}_{sig} = P^{out}_{meas}$ because no ASE is present. However, when it is now assumed that ASE noise is present and the measured output power still has the same value as before, the gain of the amplifier stage will remain the same, given by

$$G = \frac{P^{out}_{meas}}{P^{in}_{meas}} = \frac{P^{out/}_{sig} + P_{ASE}}{P^{in}_{meas}}, \tag{6.17}$$

where $P_{sig}^{out\prime}$ is the signal output power when ASE is present. Equation 6.17 can also be written as

$$P_{sig}^{out\prime} = GP_{meas}^{in} - P_{ASE} \tag{6.18a}$$

$$P_{sig}^{out\prime} = P_{sig}^{out} - P_{ASE}. \tag{6.18b}$$

It can be seen from equation 6.18b that the signal output power $P_{sig}^{out\prime}$ is less than the signal output power P_{sig}^{out} because of the influence of ASE power P_{ASE}. In order to achieve the same signal output power P_{sig}^{out} as in the case without ASE noise, the gain must be set higher by

$$G_{corr} = \frac{P_{sig}^{out} + P_{ASE}}{P_{meas}^{in}} = \frac{P_{sig}^{out}}{P_{meas}^{in}} + \frac{P_{ASE}}{P_{meas}^{in}} = G + \frac{P_{ASE}}{P_{meas}^{in}} = G + ASE_{corr}, \tag{6.19}$$

where $P_{sig}^{out\prime} = P_{sig}^{out}$ because the same signal power has to be achieved, and ASE_{corr} is the ASE correction factor. With other words, to compensate for the ASE noise, the gain of the amplifier must be added with an ASE correction factor.

In the optical amplifier, this ASE correction is estimated from a noise figure table, which is a function of the operating conditions of the amplifier. This noise figure table is obtained from measurement results and estimates the amount of ASE noise that is generated from the optical amplifier for the different operating conditions. With the operating parameters given to the gain control, the amount of ASE noise and therefore the ASE correction factor can be estimated from the noise figure table that is stored in memory.

Under normal operating conditions, ASE forms only a small part of the total optical signal output power of an amplifier. ASE correction is not so important then. However, when the input signal powers or the gain of an optical amplifier are very low, or the number of channels is very low, ASE will be more dominant in the total optical power and ASE correction will be very important. Also, in long transmission links, where ASE noise is high, ASE correction will be more than necessary.

6.2.4 OSNR and power preemphasis

Besides a gain flattening filter (GFF) and gain tilt control (GTC), power preemphasis can also be used to flatten the spectrum of WDM channels. This is especially useful at the end of a link. The power spectrum of the WDM channels at the end of the link is measured and fed back to the booster amplifier at the beginning of the link. At the booster amplifier, this information is processed and the input spectrum of the WDM channels is adjusted accordingly so that at the output of the link, the power spectrum becomes flat. This happens after a few iterations of the algorithm.

Although power preemphasis is a good way to ensure a flat output power spectrum at the end of the link for the receiver, the noise at the end of the link can endanger

good signal detection and quality of service. A better way to qualify performance is the OSNR, taking into account the influence of noise. Therefore, instead of achieving flat output power spectrum, it is better to ensure a flat OSNR at the end of a link.

OSNR preemphasis functions in a similar way as power preemphasis. Instead of measuring the power spectrum, the OSNR is measured for the WDM channels at the end of the link and signals at the booster amplifier are adjusted accordingly so that the OSNR is flat at the end of the link. Menif et al have suggested a good method to achieve this goal [28].

Chraplyvy et al have introduced a simple but effective algorithm to achieve equalization [29], [30]. This algorithm can either be used for OSNR preemphasis or power preemphasis.

For OSNR preemphasis, the OSNRs at the end of the link can be equalized by adjusting the individual input signal powers at the beginning, while keeping the total optical power in the link constant. The power in each channel is scaled by a factor proportional to the noise present in that particular channel, yielding the new input signal power of the ith channel

$$P_{new}^{i} = P_{tot}\left(\frac{P_i/\left(SNR\right)_i}{\sum_{i=1}^{N} P_i/\left(SNR\right)_i}\right) \tag{6.20}$$

where P_{tot} is the total signal power at the input, P_i the power of the ith channel at the beginning of the link, N the total number of channels, and $\left(SNR\right)_i$ the OSNR of the ith channel at the end of the link.

For power preemphasis, the same algorithm is used, leading to

$$P_{new}^{i} = P_{tot}\left(\frac{1/G_i}{\sum_{i=1}^{N} 1/G_i}\right) \tag{6.21}$$

where G_i is the optical gain experienced by the ith signal, and the channel powers are scaled by a factor inversely proportional to the individual gain values.

Figure 6.13 shows the results for power preemphasis and OSNR preemphasis after 840 km of transmission. In figure 6.13(a), a similar OSNR of 17.43 dB for all channels is achieved and in figure 6.13(b), a flat output power spectrum can be seen.

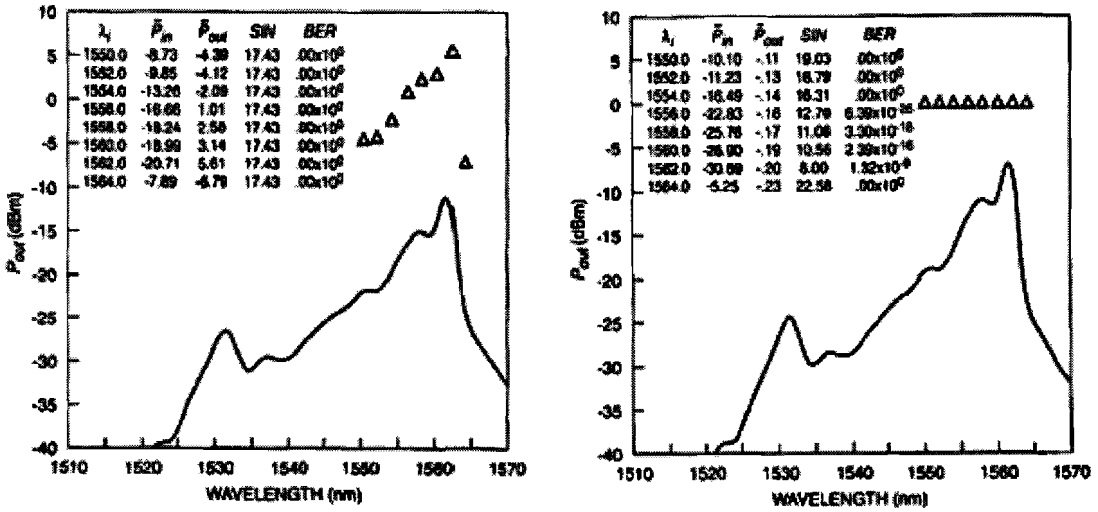

(a) (b)

Figure 6.13: *Output powers after 840-km transmission using equal input powers* [29]. *Solid curve denotes amplified spontaneous emission in 0.2-nm optical bandwidth. Triangles denote signal powers. S/N denotes optical signal-to-noise ratios.* (a)*Results of OSNR preemphasis after five iterations of algorithm.* (b)*Results of power preemphasis after second iteration of algorithm.*

6.2.5 Time constants of different control levels

Because of the different control levels implemented in the optical amplifier, the speed and therefore time constants of these controls shouldn't interfere with each other. Otherwise, these controls will work against each other instead of with each other. Table 6.1 gives the different levels of control with a range of their time constants.

Table 6.1: *Different levels of control with their time constants*

Control level	**time constant range**
Gain tilt control with VOA	30 ms
Electronic gain and transient control	1μs - 10 ms
ASE correction	30 ms
OSNR or power preemphasis	> 30 ms

Chapter 7

Simulation model of optical amplifier

Up till now, simulation models are based on either simplified EDFA models or simple control system models. These are then used to predict and analyze the effects of different design parameters and novel techniques on the behaviour of power transients in real-case complex optical EDFA systems. However, when measurements are done, the results don't correspond with those from the simulations because many different levels of complex control methods are working together in a real-case optical EDFA system, producing unexpected discrepancies.

This chapter discusses the implementation of a simulation model of the optical amplifier system presented in the previous chapter. It combines an accurate EDFA model with different levels of detailed complex gain control of the optical amplifier. This will lead to accurate simulation results that are comparable to measurements for an entire transmission link.

7.1 Structure of simulation model

The simulation model will be implemented with both Matlab and Simulink. With such an implementation, the high computation speed of Matlab and the simplicity of implementing complex dynamic models with Simulink can be combined together in the simulation model. As discussed in the previous chapter, the four main levels of control in the optical amplifier are:

1. Gain tilt control with VOA
2. Electronic gain and transient control
3. ASE correction
4. OSNR or power preemphasis.

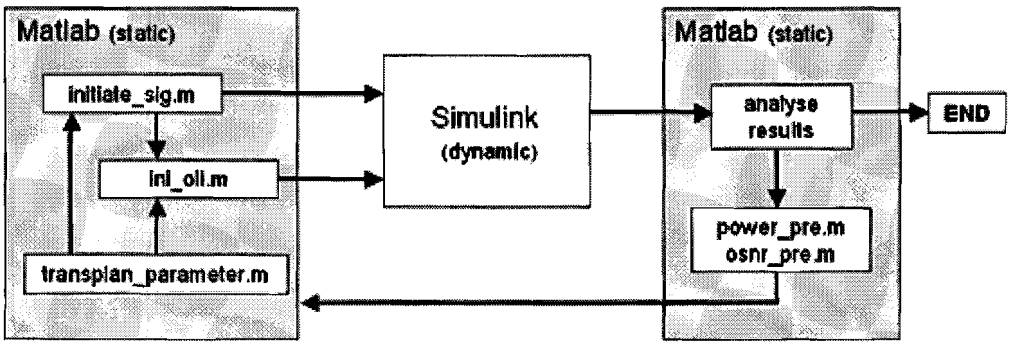

Figure 7.1: *Structure of simulation model with Matlab and Simulink.*

Because the area of interest is in power transients behaviour, the time range considered will be about a few milliseconds. In this time range, only the electronic gain control has a similar time constant (see table 6.1). Therefore, all of the control levels except the electronic control can be considered to be static for this time range. With the implementation in Matlab, these static control levels can be calculated quickly, saving a lot of computation time.

However, because the behaviour of power transients is dynamic, a part of the simulation must be done dynamically. Simulink is used for this because of the graphical interface, time-saving building blocks, and the flexibility. With the graphical interface, the structure of the simulation model is shown together with the relations of different function blocks with each other. This creates a fast and clear overview of the entire simulation model so that different functions can be understood very quickly. Also, because of the presence of basic functional blocks, new complex function blocks can be created in a short amount of time. This way, a simulation model can be built in a little amount of time and different function blocks can be modified, added, or deleted easily. This creates flexibility which is of advantage to testing different designs.

A disadvantage of Simulink is the computation time. Before the implementation of the simulation model, the choice had to be taken whether or not to include the use of Simulink into the simulation model. The dynamic EDFA routine was used to compare the time performance of Matlab with Simulink. Results however showed that Simulink was not much slower than Matlab, adding just about 5% of overhead to the computation time for one EDFA routine. It is expected that when more EDFA routines are used, for example in a transmission link simulation, the overhead will increase. But the advantages gained with using Simulink overweigh the disadvantage of longer computation time. With this conclusion, the optical elements of the amplifier together with the electronic gain control are chosen to be implemented in Simulink.

Figure 7.1 shows the structure of the simulation model with Matlab and Simulink. First, Matlab programs are used to initialize and define starting parameters for the simu-

lation in Simulink. This happens in the initialization Matlab file, called the `initiate_sig.m`. This file is used to initialize the starting values for the simulation. The values that `initiate_sig.m` initializes are:

- the number of input channels as well as their power,
- the frequency spectrum and power of the ASE entering the amplifier,
- the coefficients of the gain flattening filter.

The main gain control software for the amplifier is implemented as a Matlab function called `ini_oli.m`. This function calculates the gains of the amplifiers so that the desired output power given in `transplan_parameter.m` is achieved. Also, the gain tilt control and ASE correction are implemented in this function.

In `transplan_parameter.m`, parameters that are used by `ini_oli.m` and `initiate_sig.m` are defined. These parameters involve:

- total optical input power,
- output power per channel,
- DCF properties,
- length of fiber spans.

After this initialization by Matlab, it can be seen in figure 7.1 that the values are passed on to Simulink and the dynamic simulation involving the EDFA routines, optical elements, and electronic gain control is run. When simulation ends, the results are saved in Matlab files and with Matlab programs, these files are analyzed. When no power or OSNR preemphasis is used, the simulation is done and the programs are ended. Otherwise, when power preemphasis is chosen, the Matlab function `power_pre.m` will be called to process the results and a new input signal power spectrum will be sent to `initiate_sig.m`. After this, the simulation will start again. This process repeats itself until the given number of iterations for power preemphasis is met. In the case of OSNR preemphasis, the same applies. But instead of `power_pre.m`, the function `osnr_pre.m` is called.

In figure 7.2, a more detailed schematic diagram of the different Matlab programs and their specific functions are given. This gives an overview of the relations between the different programs and what values and parameters are passed to each other. It also shows that `ini_oli.m` is a part of `initiate_sig.m`.

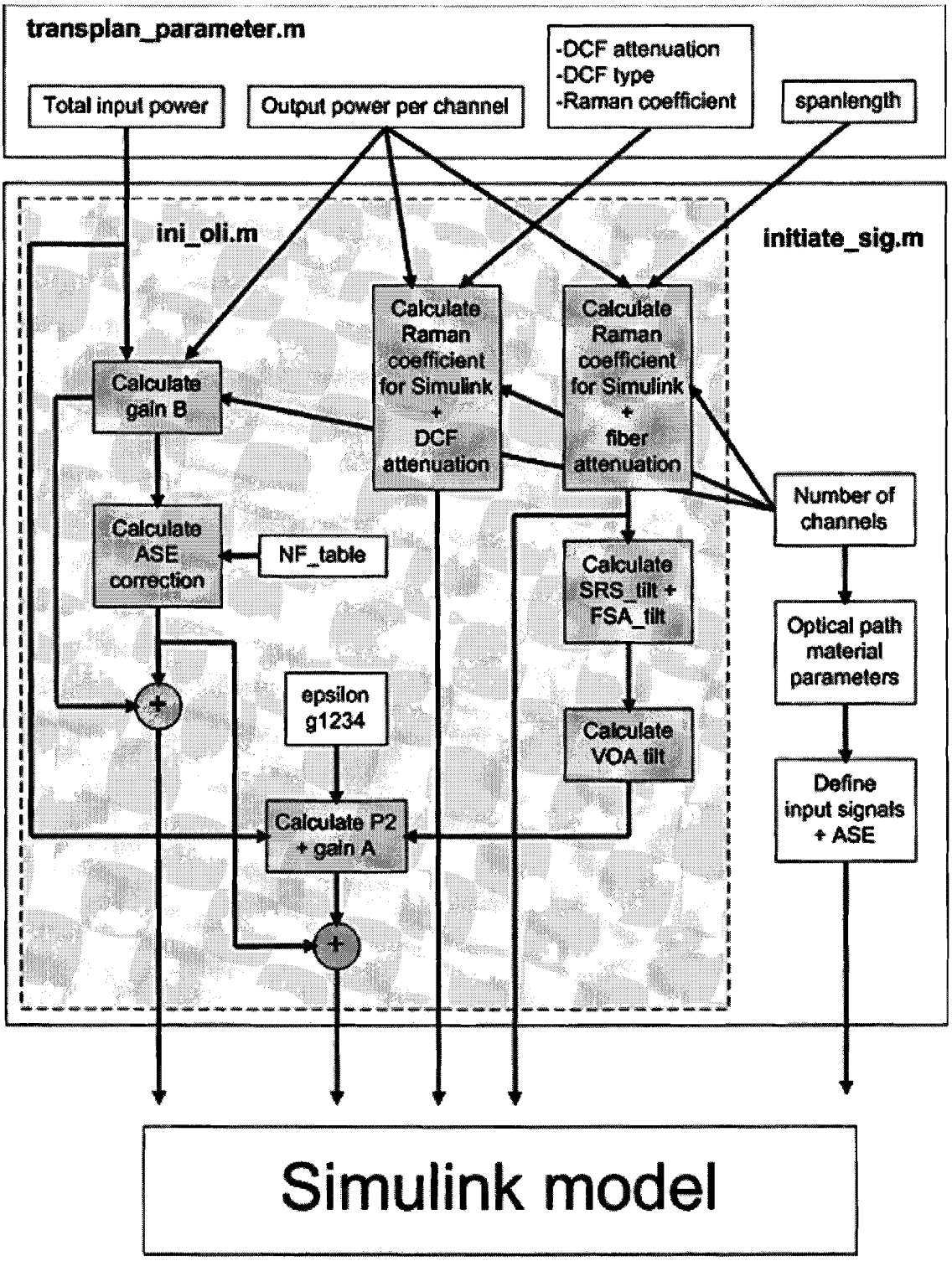

Figure 7.2: *Schematic view of the simulation model containing the different Matlab programs and their functions. White function blocks are values that are defined already and gray function blocks involves calculation and processing.*

7.2 Implementation of model in Matlab

In this section, the implementation of the different gain control levels in Matlab are discussed. This involves the gain tilt control with VOA, the ASE correction, and the power and OSNR preemphasis.

7.2.1 Gain tilt control with VOA

The gain tilt control with VOA is implemented in Matlab as a program block within a function called the `ini_oli.m`. As discussed before, SRS and fiber attenuation are the main causes of spectral tilt in the transmission link. With a gain tilt control in the optical amplifier, these tilts can be compensated for.

In the software, just like in real-case, the spectral tilt caused by SRS and fiber attenuation is estimated and pre-compensated in the optical amplifier. For every optical amplifier system, the spectral tilt caused by the fiber span that follows the amplifier system is pre-compensated. Although the spectral tilt caused by the DCF in each optical amplifier is also important, this is not compensated by the amplifier software. This is because the simulation results will be compared to measurements of a version of an amplifier system without DCF-induced spectral tilt compensation.

The spectral tilt caused by the fiber span following the amplifier system is estimated by the same formula given by equation 6.12, which is

$$SRS\_tilt = 4.343 \cdot 10^{15} \cdot \frac{L_{eff} \cdot g'_R}{2A_{eff}} \cdot P_{tot} \quad [dB/THz]. \tag{7.1}$$

The Raman-gain coefficient g'_R is approximated by a triangular gain profile as given previously in figure 6.8. From a given effective length of the fiber span L_{eff}, effective mode field diameter of the fiber A_{eff}, and the total signal output power from the optical amplifier P_{tot}, the SRS tilt can be calculated using this equation.

The fiber spectral attenuation tilt can be estimated by using the attenuation spectrum of a standard single mode fiber (SSMF) as given in figure 6.4. The number of channels and their frequencies are evaluated and their output power spectrum is multiplied by the attenuation spectrum of the SSMF. From this resulting spectrum, a linear fit with the following equation

$$P_{tot}(f) = FSA\_tilt \cdot f + offset \tag{7.2}$$

is made, where $P_{tot}(f)$ is the output power spectrum of the amplifier as a function of the frequency channels, f is the frequency of the channels, and $offset$ is the remaining term of the linear fit. FSA_tilt is then the fiber spectral attenuation tilt given in $[dB/THz]$.

With the *SRS_tilt* and *FSA_tilt*, the attenuation of the VOA that is needed to provide such an inverse total tilt is calculated using a linear conversion formula. The Matlab program for this gain tilt control takes as input the length of the fiber span, the total optical output power of the amplifier, and the number of channels. The output is the VOA attenuation.

7.2.2 ASE correction

The ASE correction of the optical amplifier is also implemented in Matlab as a program block within the function `ini_oli.m`. This correction is important because the measured output power that is sent to the electronic control is not the ideal signal output power, but added with ASE noise. Therefore, the gain that is set by the electronic control for the pump laser should be added with an extra correction factor, the ASE correction. This was discussed and given in the previous chapter by equation 6.19.

Because the ASE cannot be measured, it has to be estimated so that the correct amount of ASE correction can be applied. This is done by using a noise figure table, where the noise of the amplifier is measured and stored in a table for different operating conditions. Both the gains set by control group A and B are corrected for ASE using the same noise figure table.

The Matlab program for ASE correction takes as input the average optical input power and the gain of the respective groups. These values are fed into the noise figure table and the corresponding noise figure is found by the table. With a few formulas, the ASE correction factor for the gain is calculated.

7.2.3 OSNR and power preemphasis

Unlike the gain tilt control and the ASE correction, OSNR and power preemphasis are applied to an entire transmission link instead of a single optical amplifier. For OSNR preemphasis, the goal is to obtain a flat OSNR at the end of the link and for power preemphasis, to obtain a flat power spectrum. Because the amount of noise influences signal detection and quality of service, it is better to ensure a flat OSNR at the end of a link than a flat power spectrum. For good system performance, it is therefore important to include OSNR preemphasis. This is also the case for the optical amplifier.

The OSNR preemphasis, based on the algorithm by Chraplyvy et al [29], [30] and equation 6.20, is implemented as a standalone Matlab function called `osnr_pre.m` with the inputs:

- optical power spectrum at the input of the booster amplifier (beginning of link)
- optical power spectrum at the output of the pre-amplifier (end of link).

The output of this function is the new input power spectrum at the beginning of the link. In most cases, one iteration of this function is enough to obtain a flat OSNR at the end of the link.

However, in practice, it is not always easy to measure the OSNR. The alternative is to measure the output power and use power preemphasis. This is also implemented in the Matlab function called `power_pre.m`. The method is based also on the algorithm by Chraplyvy et al given by equation 6.21. One or two iterations will in most cases suffice.

7.3 Implementation of model in Simulink

Besides the Matlab implementation of the control levels, the optical elements of the optical amplifier as well as the electronic gain control have to be implemented too in order to have a functional simulation model. As discussed previously, these are done in Simulink. This section discusses in more detail how the implementations are done.

7.3.1 Optical path

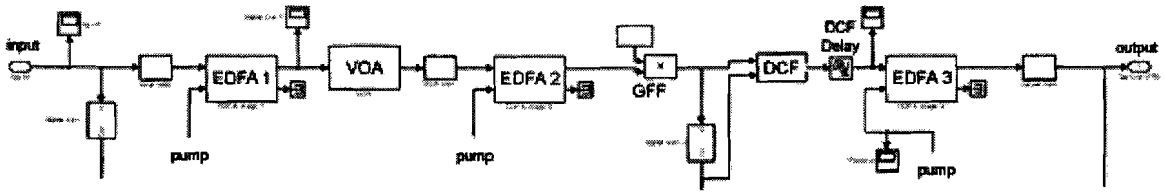

Figure 7.3: *Simulink model of the optical path in the amplifier.*

Figure 7.3 gives the optical path of the optical amplifier that is implemented with Simulink. Its structure is similar to what was given in figure 6.1. Unlike the Matlab implementations, these Simulink function blocks work dynamically. That is, the in- and outputs of each block are re-evaluated after every time step.

The EDFA blocks work with the dynamic routine that was described in chapter 3. The pump power is given as input to the routine and it calculates the output power for every channel dynamically, based on the input. The input signals of the amplifier are defined by `initiate_sig.m`. Additionally, ripples in the gain spectra of the EDFAs are also introduced into the simulation model for better correspondance with measurement results. The values of these gain ripples were obtained from measurements.

The VOA gets its value from the gain tilt control implemented in Matlab. This remains a time-independent value that is fixed for the rest of the simulation. With the

coefficients initialized by `initiate_sig.m`, the frequency spectrum of the gain flattening filter (GFF) is set. This spectrum remains also the same for the entire simulation.

The DCF is implemented as a frequency dependent attenuation block. This attenuation spectrum is derived from measurement results. Also, the Raman coefficient R_coeff of the DCF is given in `transplan_parameter.m`. This must not be confused with the Raman-gain coefficient g_R. From equation 7.1,

$$SRS\_tilt \ \ [dB/THz] = 4.343 \cdot 10^{15} \cdot \frac{L_{eff} \cdot g'_R}{2A_{eff}} \cdot P_{tot},$$

the Raman coefficient R_coeff given in `transplan_parameter.m` is equal to the term

$$4.343 \cdot 10^{15} \cdot \frac{L_{eff} \cdot g'_R}{2A_{eff}}, \tag{7.3}$$

with the unit $[dB/(W \cdot THz)]$. This Raman coefficient is obtained from measurement results of the Raman-gain coefficient g_R for the DCF and approximated by the triangular gain profile. With this Raman coefficient, the spectral tilt of the signals as a result of the DCF can be calculated easily.

Because the SRS tilt is instantaneous, this routine has to be implemented in the DCF block as a dynamic function. From equation 7.1, it can be seen that the only time-dependent value is the total optical power P_{tot} launched into the DCF. In order to save computation time, all equations concerning the SRS tilt are precalculated already in the Matlab function `ini_oli.m`. This precalculated value is then passed on to Simulink as a constant which is then multiplied by the time-dependent total P_{tot} in the Simulink block at every time step.

7.3.2 Electronic gain and transient control

Figure 7.4 shows the implementation of the optical amplifier with the electronic gain control in Simulink. The optical path that can be seen was already given in figure 7.3. The electronic gain control is implemented as a proportional integral control combined with a feed forward as was shown in figure 6.12.

There are a few elements in the implementation that have to be pointed out in detail. These are some correction terms that have been introduced to correct the values of the simulation model compared to the real-case amplifier. This is because in real-case systems, there are always errors, nonlinearities, and uncertainties that influence the performance according to the theoretical model.

One of these is the offset in the photo-detectors. Because of threshold voltages, nonlinearity, and background light (noise), an offset value is almost always present at the output of the photo-diodes. This means that even when there is no optical output

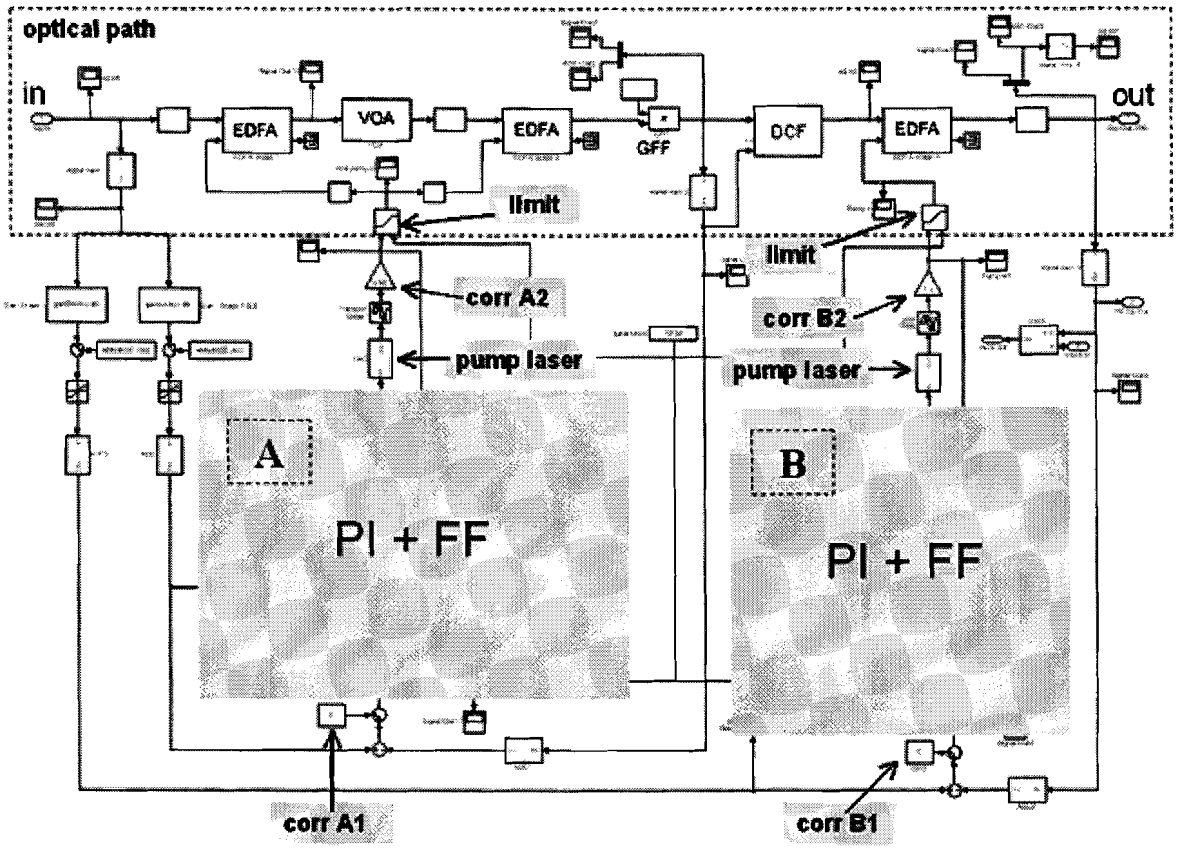

Figure 7.4: *Simulink model of optical amplifier with optical path and electronic gain control.*

power, the output current given by the photo-detector is not equal to zero. That is, there is always an offset value. This offset value also differs for different photo-detectors.

For control group A, the measurement of optical powers by the photo-detectors at the input of the optical amplifier and after the GFF. These values are converted to electrical signals which are compared to each other before being processed by the PI + FF control. Because of offset values in the photo-detectors, the resulting signal going to the PI + FF control suffers from errors. By adding a correction factor **A1** to the resulting signal, this error can be introduced into the simulation model so that the simulation results match those from the measurements. By comparing simulation and measurement results, a nominal value for this correction factor can be determined. The same analysis applies for correction factor **B1** (see figure 7.4).

In general, pump lasers for EDFAs may suffer from non-linearities such as threshold current, kink, and power saturation. Also, laser performance deteriorates after time because of internal degradation. In the optical amplifier, kink-free pump lasers are

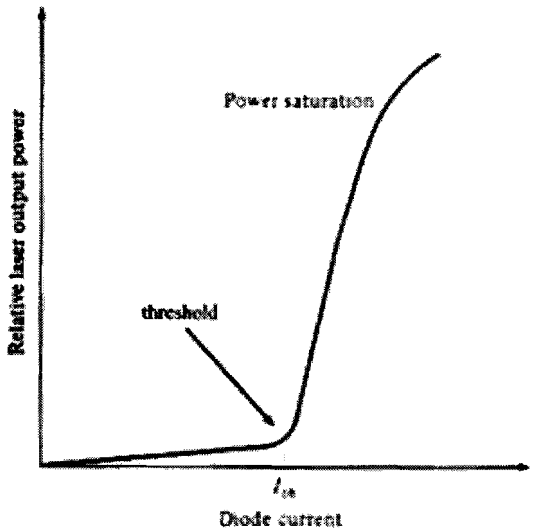

Figure 7.5: *Example of non-linear distortions in the optical output power of a laser diode as a function of its drive current .*

used. Despite this, the threshold current and performance deterioration will contribute to differences between simulation and measurement results. These effects are shown in figure 7.5. In order to correct these, measurement results of the pump lasers are gathered and an approximated curve of optical output power against the diode current is derived. This curve is then implemented in the Simulink pump laser block.

In addition, delay blocks are introduced between the pump laser blocks and the correction factors **A2** and **B2**. This is because in real-case, it takes time for the measured powers to be first passed to the electronic gain control, processed, and then sent as a current to the pump laser to change the optical pump power into the EDFA. All these delays are added together and implemented as a delay block between the pump laser block and the correction block per control group.

Further, the factors **A2** and **B2** given in figure 7.4 are introduced as gain factors to correct all other errors occurring in the optical amplifier. For example, the measured optical powers have to be converted into electrical voltages and sent to the electronic gain control. Because this gain control is implemented in a digital signal processor (DSP), these values have to be converted into bits. Because of all these conversions, it is very difficult to calculate what the exact conversion factor is so that approximations are used. The errors that occur because of this and also quantization errors can be corrected by these gain correction factors **A2** and **B2**. The errors that occur from the conversion of bits out of the DSP to pump current can also be corrected by the same factors. Last but not least, the output power curve of the pump laser is not the same for different pump lasers (sample dependence), these discrepancies can also be corrected by the gain correction factors as well as the coupling losses of optical power travelling from pump

laser to EDFA.

Finally, the powers of the pump lasers are limited by using saturation blocks. That is, the pump lasers cannot provide infinite high output power. The maximum values are obtained from specifications, adjusted for the correction factors **A2** and **B2**. This means for example that when **A2** has a value of x, the upper limit in the saturation block is equal to the maximum value from the specifications multiplied by a factor x. Also, the lower limit is not completely equal to zero because of nonlinearities in the laser. By comparing simulation with measurement results, this minimum value is determined and implemented in the model.

To summarize, two correction factors are introduced per control group to compensate for errors, nonlinearities, uncertainties, and sample dependence occurring in the optical amplifier. These are the factors **A1** and **A2**, and **B1** and **B2** shown in figure 7.4. With a more analytical approach, it can be seen that for control group A, a correction factor **A1** is added to the control signal and a correction factor **A2** is multiplied with this signal. In essence, the pump power P_{pump} is a function of the control signal $S_{control}$ coming from the electronic gain control and can be given by

$$P_{pump}(S_{control}) = f(S_{ideal} + S_{error}). \tag{7.4}$$

In this equation, S_{ideal} is the ideal control signal and S_{error} is the error because of nonlinearities, uncertainties, etc. This S_{error} is a nonlinear function and cannot be calculated exactly. With the implementation of **A1** and **A2**, this error-signal is approximated by the following equation

$$S_{error} \approx A1 + A2 \cdot S_{ideal}, \tag{7.5}$$

which is a first order approximation function for the nonlinear error-signal. From comparison with measurement results, this seems to be a satisfying approximation. Similar analysis applies for the correction factors **B1** and **B2**. In the Simulink model, values of **A1** and **B1** are about 2% to 5% of the total control signal, and **A2** and **B2** are values between 0.95 to 1.2. This shows that the simulation model is a very accurate model with small deviations from measurement results.

Because of this accuracy, it is therefore good enough to leave out these correction factors in general. Also, simulations of transmission links containing several or more amplifiers can be done without these correction factors. The sample dependence of the different amplifiers will cancel each other out so that correction factors are highly unnecessary. Moreover, these correction factors are introduced for simulation of specific optical amplifiers. With these correction factors, the simulation model can be customized to simulate a single specific optical amplifier with its own sample dependence so that it can be compared to measurement results almost exactly.

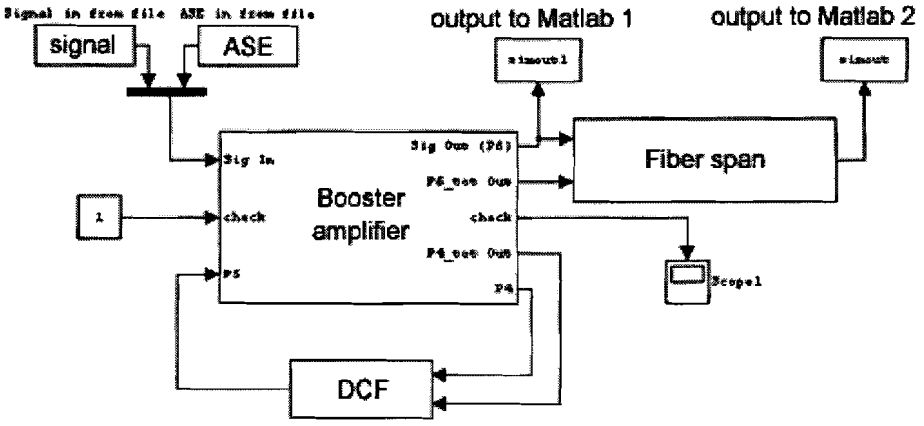

Figure 7.6: *Total simulation model of optical amplifier with fiber span and DCF given in Simulink.*

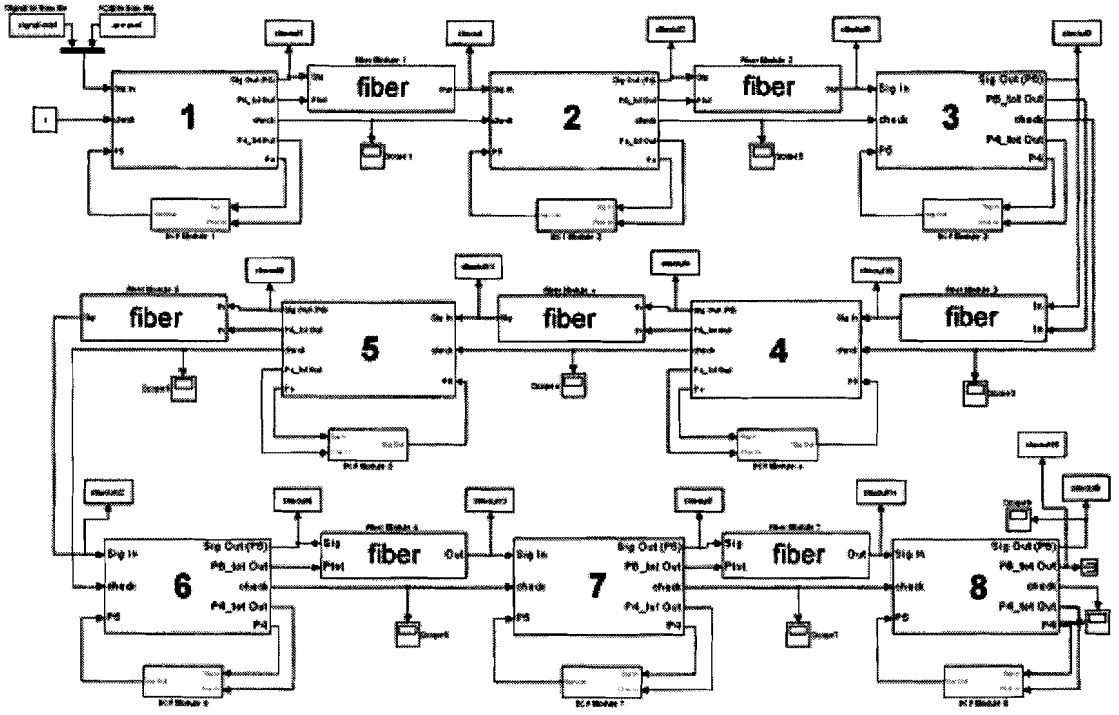

Figure 7.7: *Simulation model of a transmission link with 7 fiber spans and 8 amplifiers.*

7.4 Total simulation model with Matlab and Simulink

In figure 7.6, the total simulation model for one optical amplifier with a fiber span is given. This model structure is implemented in Simulink and the Matlab program is run in the background. In the total simulation model, the input signals and ASE

are initialized and defined by the Matlab program `initiate_sig.m` and the values are passed to the Simulink model. After the dynamic simulation, the output values are passed back to Matlab to be further processed. The implementation of the fiber span is similar to that of the DCF. A fiber spectral attenuation curve is loaded into the fiber span Simulink block and multiplied with the input signal spectrum. From the length and Raman-gain coefficient defined in Matlab, the SRS tilt is calculated and implemented as a dynamic function in the Simulink block. In figure 7.7, a simulation model of an entire transmission link is given. This will be used for comparison with measurement results.

Chapter 8

Simulation and measurement results

Along with the implementation of the simulation model, measurements are made to compare and determine the accuracy with the real amplifier. In this chapter, the results are compared and discussed for simulations and measurements on both a single optical amplifier, as well as an entire transmission link consisting of 7 fiber spans with a total length of 500 km and 8 optical amplifiers.

8.1 Results for a single optical amplifier

8.1.1 Measurement setup

In order to have a good and accurate simulation model, comparisons have to be done first on one single amplifier to determine its accuracy before moving to an entire transmission link. Therefore, measurements for one single optical amplifier are done and compared to the simulation results.

Figure 8.1 shows the corresponding measurement setup. In this setup, 20 lasers with different frequencies are used to obtain 20 WDM channels entering the optical amplifier. The frequencies and wavelengths of these channels are given in table 8.1. 19 of them are multiplexed together and fed through a mechanical switch before being coupled together with the remaining single channel. The switch, with a speed of 160 μs, is used to switch off the 19 channels, thereby simulating a drop. The remaining single channel comes from a tunable laser source so that the frequency of the surviving channel can be adjusted. The VOA and polarization scrambler are used to adjust the properties of the channels entering the optical amplifier.

Regarding the optical amplifier, two different types exist. The difference lies in the EDFAs that are used, which come from two different suppliers. In the measurements, both types are measured separately and their results compared to simulations. In the

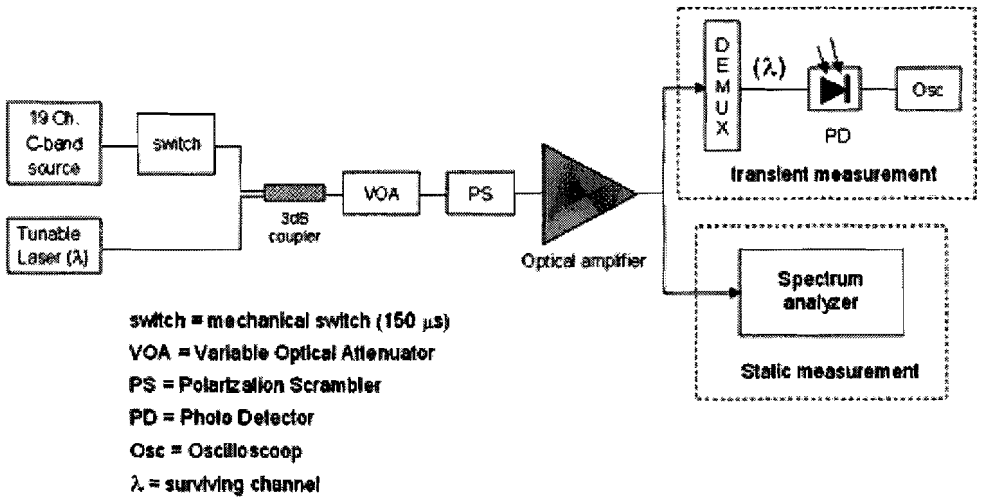

Figure 8.1: *Measurement setup for static and transient measurement of the single optical amplifier.*

simulation model, these two different types of optical amplifiers are both implemented with their own specific properties. The user can choose between these two by using an option in the simulation model. In order to be able to distinguish between the two types of optical amplifiers, the terms **Type A** and **Type B** optical amplifiers are used in the following sections.

At the output of the amplifier, it can be seen from figure 8.1 that two different measurements are done: a static measurement and a transient one. In the static measurement, an optical spectrum analyzer is used to measure the output power spectrum of the optical amplifier before the 19 channels are dropped. This measurement is used to compare results regarding the (quasi-)static performance of the optical amplifier such as the gain spectrum and the gain tilt control with VOA.

Table 8.1: *Channels used for single optical amplifier measurements*

nr.	frequency [THz]	wavelength [nm]	nr.	frequency [THz]	wavelength [nm]
1	196.1	1528.77	11	193.5	1549.32
2	195.9	1530.33	12	193.3	1550.92
3	195.7	1531.90	13	193.1	1552.52
4	195.5	1533.47	14	192.9	1554.13
5	195.3	1535.04	15	192.7	1555.75
6	195.1	1536.61	16	192.5	1557.36
7	194.9	1538.19	17	192.3	1558.98
8	194.7	1539.77	18	192.1	1560.61
9	194.5	1541.35	19	191.9	1562.23
10	194.3	1542.94	20	191.7	1563.86

In the transient measurement, the surviving channel is demultiplexed from the output of the amplifier and its optical power is measured with a photo detector followed by an oscilloscope. This oscilloscope measures the power change of the surviving channel during the drop. With this setup, the transient behaviour of the surviving channel and the optical amplifier can be measured and compared to the simulation results. In the following sections, both the static and transient/dynamic results will be presented and discussed.

8.1.2 Static results

Before showing and discussing the results, it must be remarked that the gain of the optical amplifier can be set in two different ways:

1. The gain values of control group A and B (see figure 6.11) are set **manually** by the user, thereby achieving a specific output power per channel indirectly.
2. The output power per channel is set directly by the user and the electronic gain control will **automatically** calculate and set the gain values for control group A and B.

These two different methods of setting the gain can lead to different gain values for control group A and B. As a result, the transient behaviour can differ even when the gain and the output power of the amplifier are equal for both cases. When the gain control is chosen to automatically set the gain values, a clever algorithm is used to calculate the best values for control group A and B.

The first set of results are obtained by setting the gain values of the optical amplifier manually. The number of channels used is 20 and the spacing between these channels is 200 GHz. The channels used are in the C-band with wavelengths as given in table 8.1. A flat input spectrum with channel power of -18 dBm is used, yielding a total input power of -5 dBm. The gains of control group A and B are set manually, thereby achieving a total output power of 15 dBm for the optical amplifier. These operating conditions are summarized and given again in table 8.2.

Figure 8.2 shows the static simulation results compared to those from measurement. The simulation model used is similar as the one given in figure 7.6. The measurements

Table 8.2: *Operating conditions for manual gain setting results in figure 8.2*

gain setting method	manual
number of channels / channel spacing	20 / 200 GHz
single channel input power (flat input spectrum)	-18 dBm
total input power / total output power	-5 / 15 dBm
gain A / B	17.5 / 20 dB

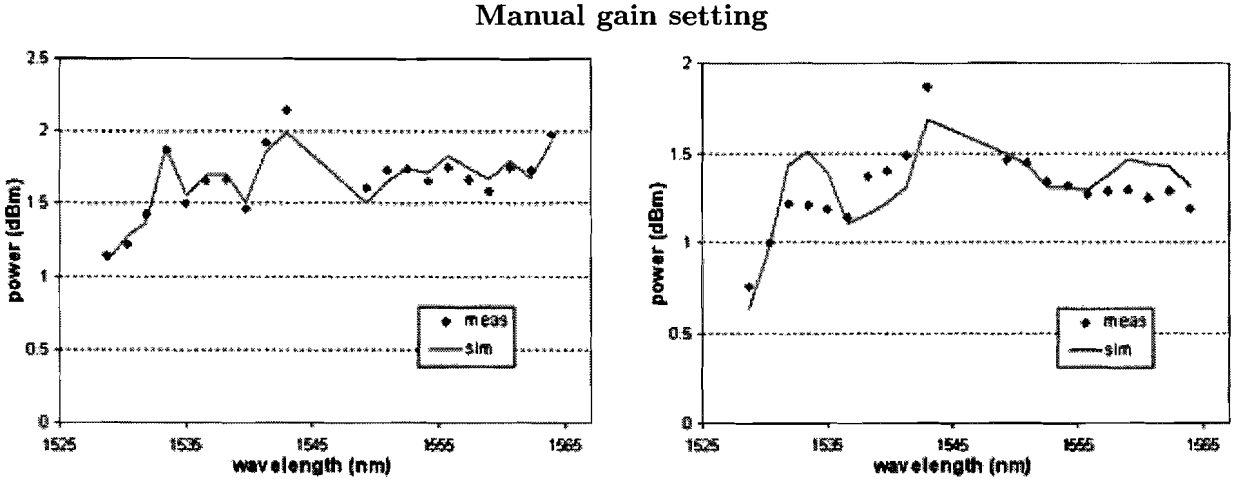

Figure 8.2: *Simulation and measurement results of output power spectrum for one single amplifier with manual gain setting.* (a) *Type A amplifier.* (b) *Type B amplifier.*

were done with the setup given in figure 8.1. In figure 8.2(a), the results are given for a Type A amplifier and in figure 8.2(b), the results for a Type B amplifier. As mentioned previously, the difference between Type A and B lies in the suppliers of the EDFAs, which lead to different optical properties and behaviour.

From the figures, it can be seen that the simulation results resemble the measurement results very well with error margins of less than 0.25 dB. The shapes of the power spectra correspond amazingly well.

The same applies for the results obtained by letting the gain control calculate the gain values automatically. The same operating conditions as for the manual gain setting are used except that the output power per channel is set at -2 dBm, yielding a total output power of 11 dB. The gain values for control group A and B are then calculated and set automatically. The operating conditions are given in table 8.3 and the results are given in figure 8.3. Again, the results correspond very well with errors not more than 0.25 dB.

Table 8.3: *Operating conditions for automatic gain setting results in figure 8.3*

gain setting method	automatic
number of channels / channel spacing	20 / 200 GHz
single channel input power (flat input spectrum)	-18 dBm
total input power / total output power	-5 / 11 dBm
gain A / B	14.6 / 16 dB

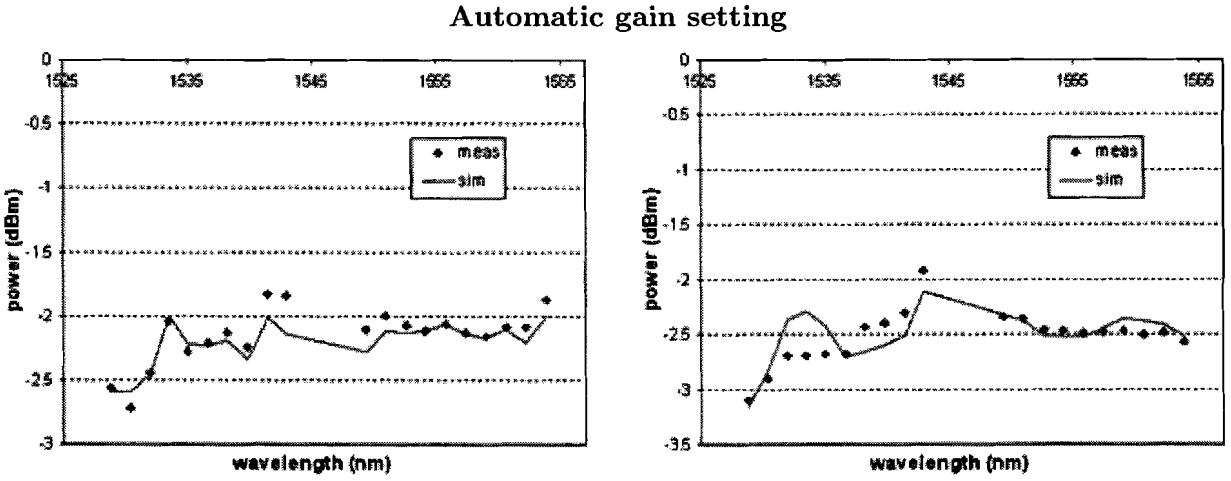

Figure 8.3: *Simulation and measurement results of output power spectrum for one single amplifier with automatic gain setting.* (a) *Type A amplifier.* (b) *Type B amplifier.*

8.1.3 Dynamic results

As mentioned before, the transient/dynamic measurement results are obtained together with the static results in the same setup given already in figure 8.1. Therefore, the same operating conditions apply for both the static and the dynamic measurements. Actually, the static measurements show the power spectrum at the output of the optical amplifier before the drop, portrayed by the 20 channels (see table 8.1) used.

For the dynamic measurements, 19 of the 20 channels are dropped and the surviving channel power is measured during this drop. In all measurements, the surviving channel is chosen to be in the middle of the C-band, with a frequency of 194.3 THz. This is because frequency channels in the middle of the C-band will suffer the least from any spectral (gain) tilt so that the results can be compared to each other with more accuracy and certainty.

In the case of manual gain setting, where the gain values of control group A and B are set manually, table 8.4 gives the operating conditions again. These are the same as previously given in table 8.2 for the static measurements except that now, 19 of the 20 channels are dropped with the surviving channel at 194.3 THz.

As shown already in figure 6.11, the optical amplifier consists of two electronic gain control groups: A and B. By measuring the surviving channel power at point P2 instead of P3 given in figure 6.11, the performance of control group A in the optical amplifier can be determined. This is done for the results given in figure 8.4. Figure 8.4(a) shows the simulation (smooth darker line) and measurement (noisy lighter line) results for a Type A amplifier and figure 8.4(b) the results for a Type B amplifier. The results show

Table 8.4: *Operating conditions for results in figures 8.4 and 8.5*

gain setting method	manual
number of channels / channel spacing	20 / 200 GHz
single channel input power (flat input spectrum)	-18 dBm
total input power / total output power	-5 / 15 dBm
gain A / B	17.5 / 20 dB
number of dropped channels	20 to 1
drop time	$\sim$ 160 μs

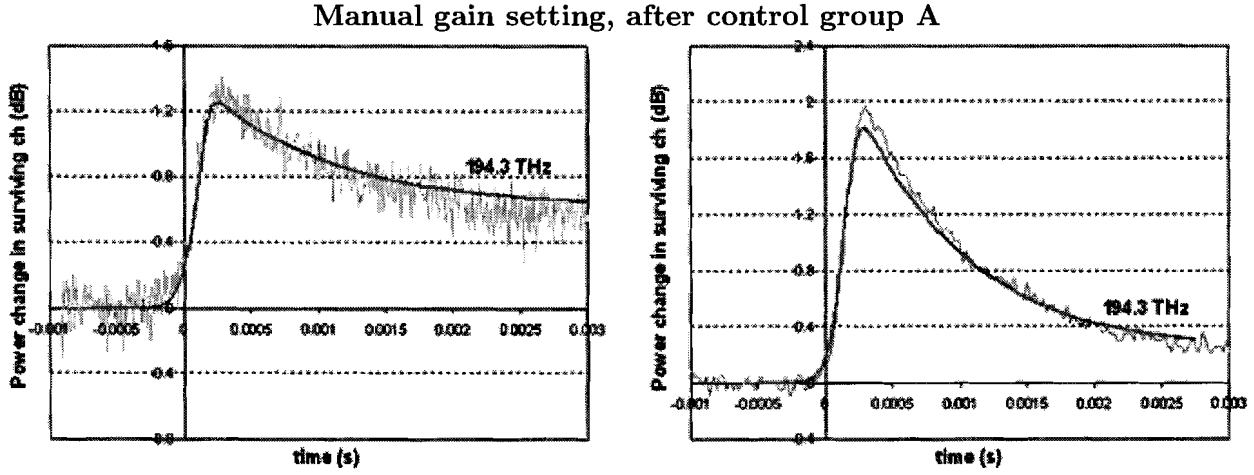

Figure 8.4: *Dynamic simulation and measurement results of relative surviving channel power change for one single amplifier with manual gain setting when 19 of 20 channels are dropped.* (a)*Results after control group A for surviving channel frequency 194.3 THz and Type A amplifier.* (b)*Same as (a), but for a Type B amplifier.*

the relative change of power in the surviving channel at 194.3 THz after being controlled by control group A during the 20 to 1 channel drop.

It can be seen that the electronic gain control is modeled well in the simulation, giving very good corresponding results. Also, the ASE correction of the amplifier is modeled well so that the steady state values are almost similar. This conclusion can be drawn because after the drop, only one WDM channel survives. Relatively, the ASE power will make up a large part of the total output power, just like the ASE correction. This influences the power of the surviving channel significantly after the drop, giving rise to errors when the ASE correction factors are calculated inaccurately.

By measuring the surviving channel power at the output of the amplifier (point P3 in figure 6.11), the combined performance of electronic control group A and B can be determined. This is equal to the total dynamic performance of the entire optical

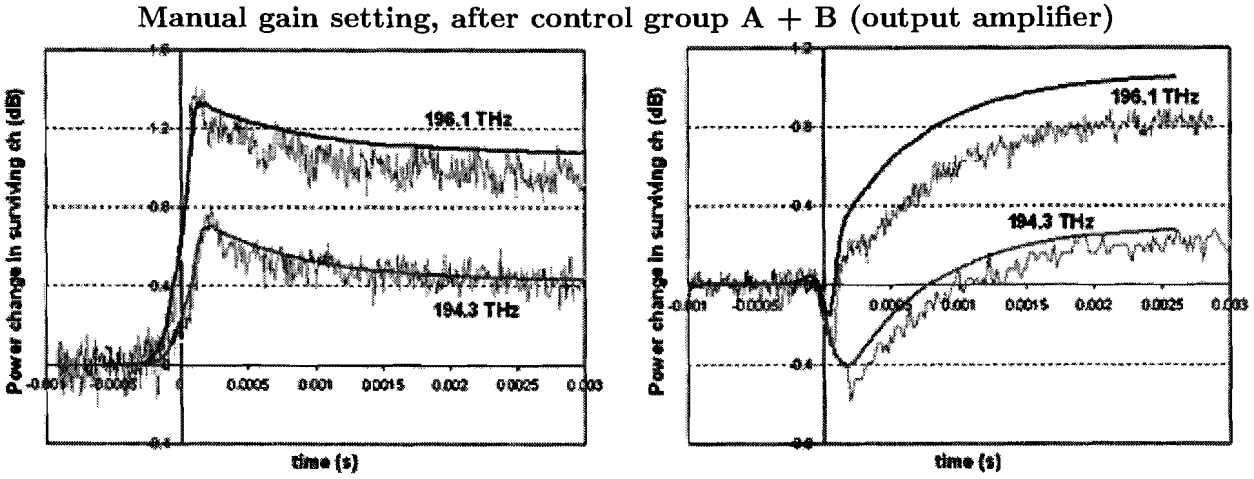

Figure 8.5: *Dynamic simulation and measurement results of surviving channel power change for one single amplifier with manual gain setting when 19 of 20 channels are dropped.* (a)*Results at output of optical amplifier for surviving channel frequency 194.3 THz and 196.1 THz alternately and Type A amplifier.* (b)*Same as (a), but for a Type B amplifier.*

amplifier. Figure 8.5 shows the results for the same 20 to 1 channel drop, at the output of the amplifier. In this case, two different dynamic measurements are done. First, the surviving channel is chosen to be at the frequency 194.3 THz. Also, a similar 20 to 1 measurement is done but with surviving frequency at 196.1 THz, in order to test the simulation model for other surviving channel frequencies. The frequency of 196.1 THz is chosen because this channel suffers the most from spectral gain tilts and plays an important part in non-linear effects as a result of its high frequency.

Figure 8.5(a) shows the results for a Type A amplifier and figure 8.5(b) the results for a Type B amplifier. Again, the smooth darker lines are the simulation results and the noisy lighter lines are measurement results. First, it can be seen that the results of 194.3 THz correspond very well, with errors of 0.1 dB or less occurring in the Type B amplifier. For 196.1 THz, the figures show that larger errors of up to 0.3 dB occur. The simulation model seems to give higher values than those measured.

This is presumably because of a phenomenon called spectral hole burning [36]-[39]. Spectral hole burning (SHB) occurs when a strong laser beam is being amplified by an optical amplifier. This strong laser beam causes the gain of the amplifier to saturate, leading to inhomogeneous broadening of the gain of the EDFs. The gain at this specific frequency will therefore decrease, leading to a hole in the gain spectrum of the optical amplifier (see figure A.1). More on spectral hole burning can be found in Appendix A, where this phenomenon will be presented and discussed in detail.

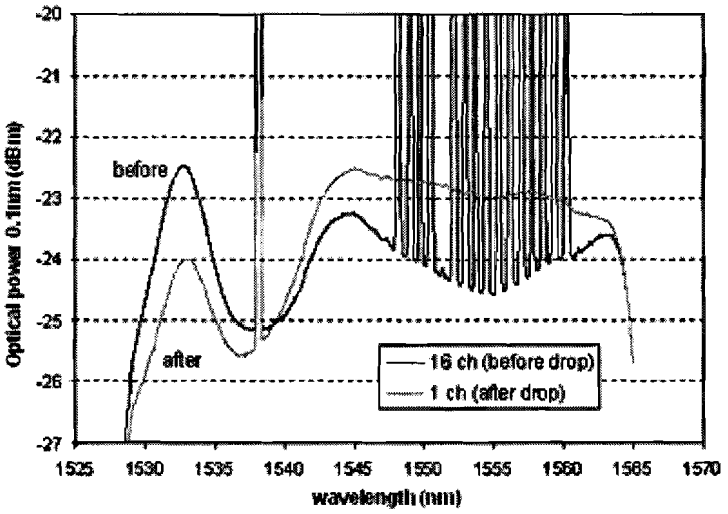

Figure 8.6: *Measurement of ASE power in an optical amplifier before and after a 16 to 1 channel drop. The effects of SHB can clearly be seen.*

Most important about SHB is that it has a greater effect for signals with smaller wavelengths (high frequencies) than for those with larger wavelengths. Therefore, it will have more effect on the WDM channel at 196.1 THz than the channel at 194.3 THz. Also, the gain will decrease when the channel power increases. The effect of SHB is shown in figure 8.6 where the ASE power is measured before and after a 16 to 1 channel drop for a single optical amplifier. It can clearly be seen that after the drop, the ASE power around the surviving channel decreases. This is because the surviving channel jumps up in power, thereby saturating the gain and creating a spectral hole. As a result of this, the surrounding ASE power decreases and the channel power will not jump as high as it should in the first place.

The same occurs for the results given in figure 8.5. Because SHB is not implemented in the simulation model, the surviving channel powers at 196.1 THz do not suffer from a lower gain as a result of SHB, thereby leading to higher powers when compared to measurement results. The greatest errors come from the frequency channel of 196.1 THz because SHB has a larger effect on higher frequency channels than lower frequency ones (see figure A.4).

In the case of automatic gain setting, the dynamic results at the output of the optical amplifier are given in figure 8.7. The operating conditions are similar as given in table 8.3, except for the drop of 19 channels. Table 8.5 sums these conditions up again.

Again, two measurements are done for each type of amplifier. One with surviving channel at 194.3 THz, and another with surviving channel at 196.1 THz. It can be seen that the simulation results (smooth darker line) correspond very well with the measurements (noisy lighter line). Although SHB is not implemented in the simulation

Table 8.5: *Parameters for simulations in figure 8.7*

gain setting method	automatic
number of channels / channel spacing	20 / 200 GHz
single channel input power (flat input spectrum)	-18 dBm
total input power / total output power	-5 / 11 dBm
gain A / B	14.6 / 16 dB
number of dropped channels	20 to 1
drop time	$\sim 160\ \mu s$

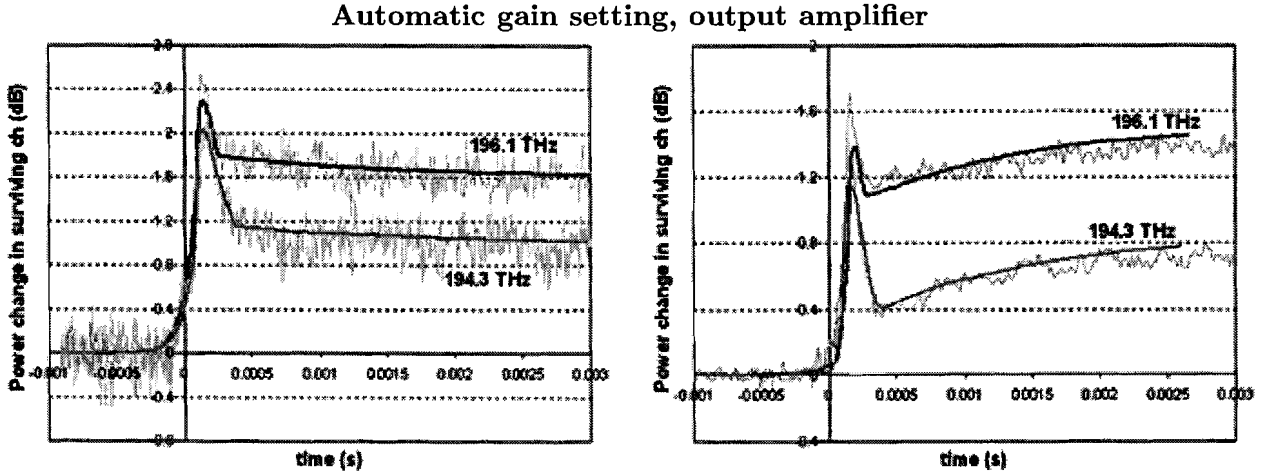

Figure 8.7: *Dynamic simulation and measurement results of surviving channel power change for one single amplifier with automatic gain setting when 19 of 20 channels are dropped.* (a)*Results at output of optical amplifier for surviving channel frequency 194.3 THz and 196.1 THz alternately and Type A amplifier.* (b)*Same as (a), but for a Type B amplifier.*

model, the results for 196.1 THz correspond quite well too. This is because of the lower channel power and lower amplifier gain calculated and set by the electronic gain control in automatic gain setting mode. Because of this, the effects of SHB are not so strong, leading to a better correspondence between simulation and measurement results.

8.2 Results for an optical transmission link

8.2.1 Measurement setup

In the previous section, simulation and measurement results were compared for a single optical amplifier. Although SHB effects are not implemented in the simulation model, the results show good correspondence with typical error margins of around 0.1 dB for

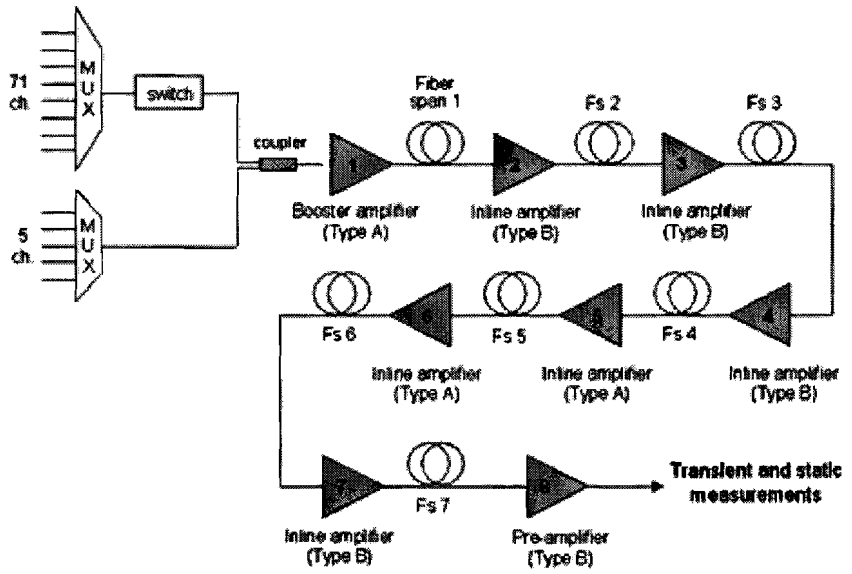

Figure 8.8: *Measurement setup for static and transient measurements of a transmission link with 7 spans.*

a single amplifier. When SHB effects are strongly present, errors of about 0.3 dB may occur for channels with higher frequencies.

In this section, results for a transmission link with 7 spans and 8 amplifiers are simulated and compared to measurement data. With 8 amplifiers, it is logical to assume higher error values between simulation and measurement results than for a single amplifier. This section will show these comparisons and the magnitude of the errors that occur.

Figure 8.8 shows the measurement setup of the entire transmission link schematically. It can be seen that instead of 20 channels, 76 are used. Now, a drop from 76 to 5 channels is used to obtain the dynamic results. With the use of more channels, more accurate spectral results can be obtained. Also, ASE power and ASE correction will play a smaller role after the drop when 5 channels are present instead of 1. This will reduce the errors cause by noise, leading to a better correspondence between simulation and measurement results.

The 76 channels used are all chosen to be in the C-band, having frequencies corresponding to the ITU grid. Four channels are thereby left out: 192.7, 193.25, 194.15, and 195.9 THz. The channel spacing is 50 GHz. In order to obtain the dynamic/transient results, a 76 to 5 channels drop is done. However, instead of one drop from 76 to 5 channels, two different cases of channel drops are considered: blue surviving channels and red surviving channels. In the case of blue surviving channels, channels with frequencies at the blue end of the C-band are chosen to survive the drop. In the case of red surviving

Table 8.6: *Surviving channels for two different cases of 76 to 5 channels drop*

blue surviving channels		**red surviving channels**	
frequency [THz]	wavelength [nm]	frequency [THz]	wavelength [nm]
196.1	1528.77	192.1	1560.61
196.0	1529.55	192.0	1561.42
195.7	1531.89	191.9	1562.23
195.6	1532.68	191.8	1563.05
195.5	1533.47	191.7	1563.86

channels, frequency channels at the red end survive. Table 8.6 gives the frequencies and wavelengths of the surviving channels of these two different cases.

Figure 8.8 also shows the individual optical amplifiers that are used as well as the type of amplifier. This is important because Type A and Type B amplifiers have different optical properties and give different transient results as shown previously in the single optical amplifier results. Finally, the same transient and static measurements as given in figure 8.1 are done at the output of the preamplifier (end of the transmission link).

8.2.2 Static results

For simulation of the transmission link results, the model given in figure 7.7 is used. It can be seen that this model resembles the measurement setup given in figure 8.8.

In the transmission link, the first amplifier (booster) is used to amplify the powers of the channels coming from the multiplexers to an appropriate level before launching into the link. The rest of the amplifiers (numbers 2 to 8) are used to compensate for the losses of the fiber spans prior to each amplifier. For the first set of transmission link results, each fiber span has a loss of 15 dB. Excluding the booster amplifier, all amplifiers therefore have a gain of 15 dB. Also, all amplifiers are set to automatic gain setting mode, where the values of the gains of the amplifiers are calculated and set automatically by the electronic gain control software. The single channel output power of every amplifier is thereby manually set to -1 dBm. Table 8.7 gives a summary of the operating conditions for the first set of results.

Just like for the single optical amplifier results, the static transmission link results give the power spectra of the channels at the output of the link before the channel drops occur. Figure 8.9 gives the static spectral results prior to the two different cases of channel drops as mentioned before in the previous section: blue surviving channels and red surviving channels. Naturally, the static power spectra of the channels prior to the two different cases of channel drops should be the same and not depend on which channels are dropped. However, for the measurements, the channels to be dropped are connected to a mechanical switch, leading to different channel power levels for the two

Table 8.7: *Parameters for simulations in figure 8.9*

gain setting method	automatic
number of channels / channel spacing	76 / 50 GHz
single channel power (booster amplifier) input / output	-20.5 / -1 dBm
total power (booster amplifier) input / output	-1.7 / 17.8 dBm
single channel power (rest of amplifiers) input / output	-16 / -1 dBm
total power (rest of amplifiers) input / output	2.6 / 17.7 dBm
span loss / amplifier gain	15 / 15 dB

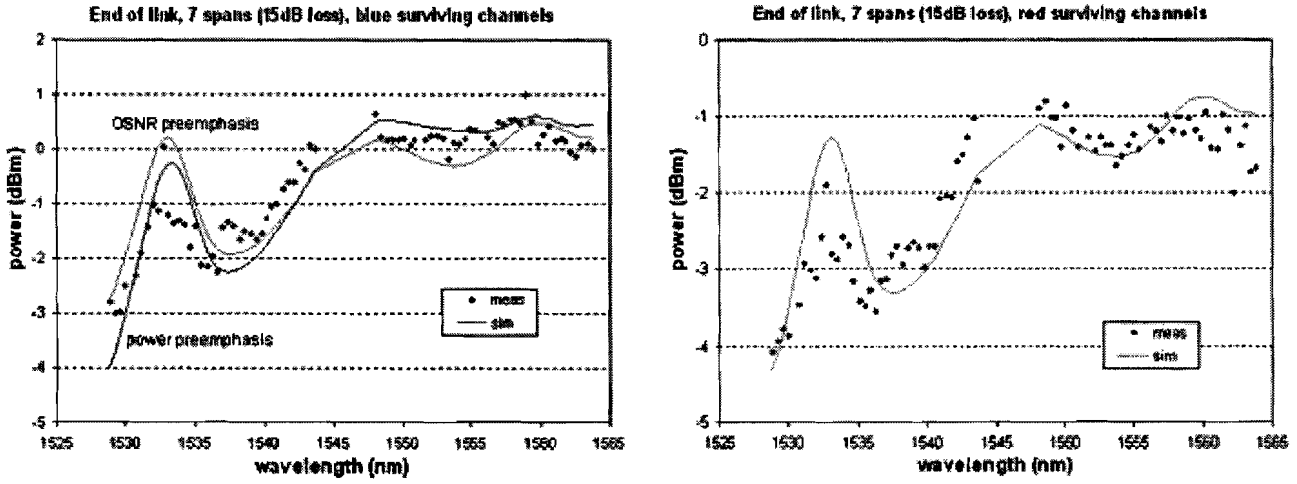

(a) (b)

Figure 8.9: *Simulation and measurement results of pre-amplifier output power spectrum at the end of a transmission link with 7 fiber spans of 15 dB loss each.* (a)*Static results prior to a drop where the blue channels survive.* (b)*Static results prior to a drop where the red channels survive.*

different cases. Therefore, two different simulations are done for the two different cases. The blue surviving channels results are given in figure 8.9(a) and the red surviving channels results in figure 8.9(b).

Additionally, figure 8.9(a) gives two different simulation results, obtained separately with OSNR preemphasis and power preemphasis. Because the results are on transmission link level, preemphasis is used to control the spectral tilt of the signal channels in the link. For all measurement results, only OSNR preemphasis is used. However, for comparison purposes, figure 8.9(a) not only shows the simulation results for OSNR preemphasis, but also for power preemphasis. It can be seen that there are minor differences between these two different methods of preemphasis. Both methods achieve almost similar results for the power spectrum at the end of the transmission link. In all following results, only OSNR preemphasis is used.

From both figures 8.9(a) and (b), it can be seen that the static results of simulation and measurement correspond well. The biggest errors are not more than 1 dB, which is actually very good for an entire transmission link consisting of 8 optical amplifiers and 7 fiber spans. In the previous section, maximum errors of about 0.25 dB were observed in the static results for a single optical amplifier. For a transmission link with 8 optical amplifiers, the theoretical maximum error should be 8×0.25 dB $= 2$ dB.

However, it must be taken into account that the fiber spans and optical amplifiers exhibit sample dependence in the gain/attenuation spectra, so that variations from nominal values may occur. These variations can be higher or lower than the nominal values assumed in the simulation model, so that errors may cancel each other out when more amplifiers are used. This statistical error cancellation works positively on the errors occurring in the static link results so that the maximum errors (1 dB) observed are less than the theoretical maximum error of 2 dB.

For longer transmission links with more optical amplifiers, it is then logical to assume that the errors will not add up proportionally but will take on comparable values because of sample dependence. It can therefore be concluded that the simulation model gives good results that correspond well with the measurements. With this, the choice of using nominal values in the simulation model proves to be simple but effective for simulating transmission link results accurately.

For the second set of results, the same setup as in figure 8.8 is used, except that the fiber spans have a loss of 25 dB each. This means that all amplifiers except the booster have a gain of 25 dB too. Table 8.8 gives a summary of the operating conditions.

For the case of blue surviving channels, figure 8.10(a) gives the static power spectrum of the pre-amplifier at the end of the transmission link before the drop. Figure 8.10(b) gives the same but for the case of red surviving channels. Once again, it can be seen that the simulation results correspond very well to those from the measurements. Errors of less than 1 dB are observed at the end of the transmission link.

Because the static measurements of the power spectra are only done at the end of the link, it cannot be seen how the power spectra of the WDM channels change along

Table 8.8: *Parameters for simulations in figure 8.10*

gain setting method	automatic
number of channels / channel spacing	76 / 50 GHz
single channel power (booster amplifier) input / output	-20.5 / -1 dBm
total power (booster amplifier) input / output	-1.7 / 17.8 dBm
single channel power (rest of amplifiers) input / output	-26 / -1 dBm
total power (rest of amplifiers) input / output	-7.3 / 17.7 dBm
span loss / amplifier gain	25 / 25 dB

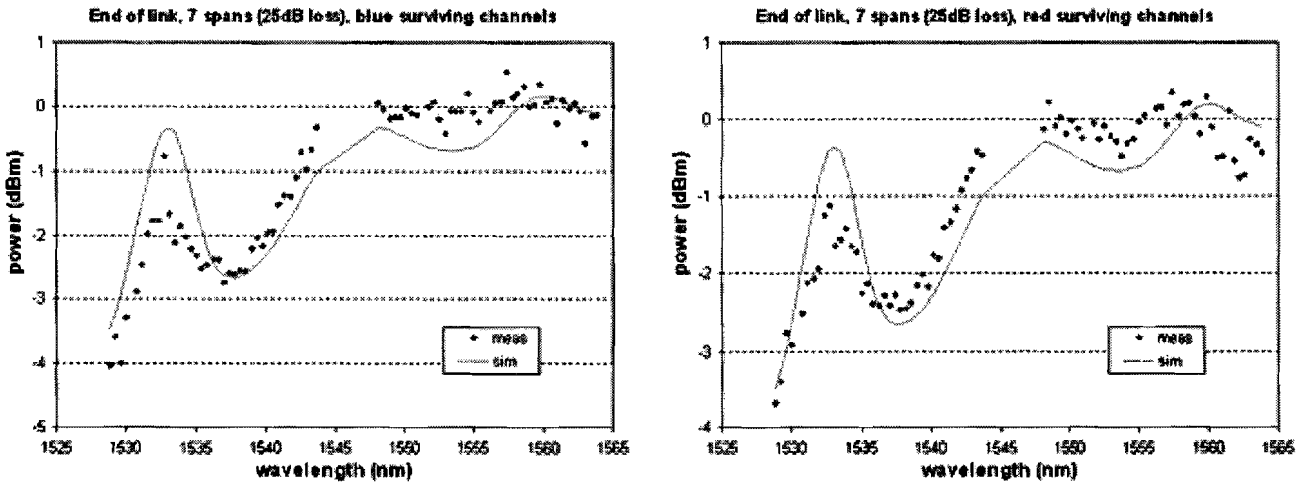

(a) (b)

Figure 8.10: *Simulation and measurement results of pre-amplifier output power spectrum at the end of a transmission link with 7 fiber spans of 25 dB loss each.* (a)*Static results prior to a drop where the blue channels survive.* (b)*Static results prior to a drop where the red channels survive.*

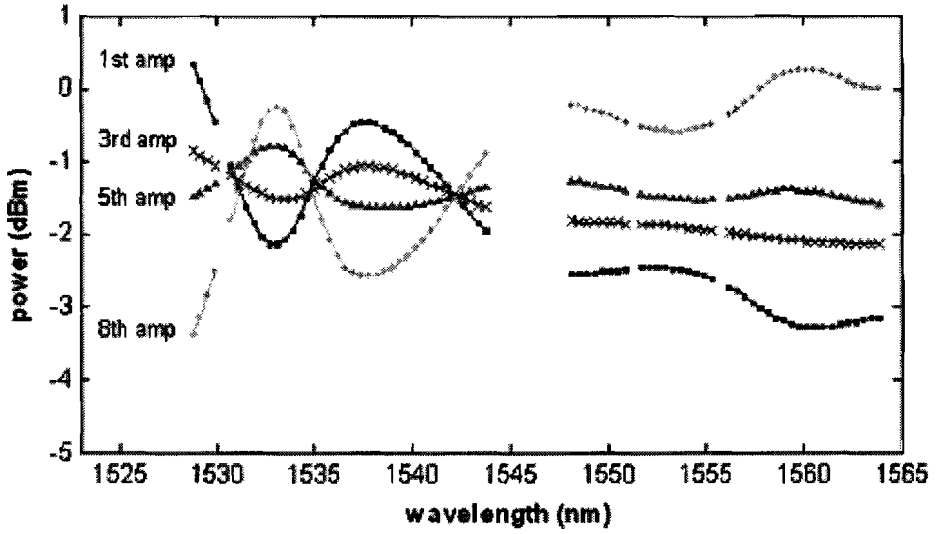

Figure 8.11: *Simulated power spectra of WDM channels along the transmission link after the 1st, 3rd, 5th, and 8th (last) amplifier.*

the transmission link. However, by using the simulation model, the variation of the power spectra along the link can be simulated and plotted. Figure 8.11 shows such a power spectrum of the WDM channels along the transmission link after the first, third, fifth, and last amplifier. These results are simulated by using the simulation model for

the same operating conditions as in figure 8.10(a). The spectrum after the eighth (last) amplifier is the same as the simulation curve given in figure 8.10(a).

From figure 8.11, it can be seen that the power spectrum of the WDM channels exhibits a spectral tilt along the transmission link. This is mainly a result of stimulated Raman scattering (SRS) which was already discussed in the previous chapters. Although the VOA gain tilt control has compensated the SRS-tilt for all fiber spans in the link, a spectral tilt can still be observed along the link. The tilt changes from a negative value at the first amplifier to a positive value at the end of the last amplifier. This is because the DCFs in the link also cause a spectral tilt due to SRS. In the particular case shown, the VOA gain tilt control is set not to compensate for the SRS-tilt caused by the DCFs, which leads to the observed spectral tilt along the transmission link. However, the setting can be changed to correct the SRS-tilt caused by the DCFs so that no spectral tilt occurs along the link. Finally, it can be seen how the use of an oppositely tilted spectrum at the beginning of the link can compensate for the negative effects of SRS so that the spectrum at the end of the link is not too seriously tilted.

By changing the parameters in the gain tilt control of the amplifiers and the OSNR preemphasis, the input power spectra at the beginning of the link can be manipulated to achieve different output power spectra at the end of the link.

8.2.3 Dynamic results

For the first set of dynamic/transient results on link level, the operating conditions given in table 8.9 are used. These operating conditions are in fact similar to those given previously in table 8.7 for the static results except that now, a drop from 76 to 5 channels takes place. As shown in figure 8.8, this drop is realized by switching off 71 WDM channels with a mechanical switch with a speed of about 160 μs. The transmission link consists of 7 fiber spans with a loss of 15 dB each, meaning that each optical amplifier following a fiber span also has a gain of 15 dB.

Table 8.9: *Parameters for simulations in figures 8.12, 8.13 and 8.14*

gain setting method	automatic
number of channels / channel spacing	76 / 50 GHz
single channel power (booster amplifier) input / output	-20.5 / -1 dBm
total power (booster amplifier) input / output	-1.7 / 17.8 dBm
single channel power (rest of amplifiers) input / output	-16 / -1 dBm
total power (rest of amplifiers) input / output	2.6 / 17.7 dBm
span loss / amplifier gain	15 / 15 dB
number of dropped channels	76 to 5
drop time	$\sim$ 160 μs

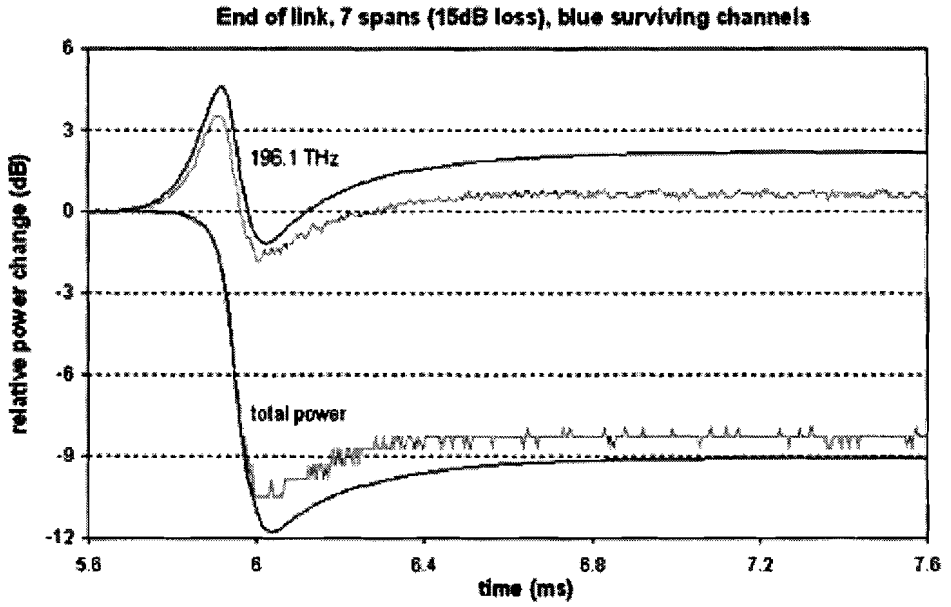

Figure 8.12: *Relative power change for surviving channel at 196.1 THz as well as the total power. Results are at the end of a transmission link with 7 spans of 15 dB loss each in case of a 76 to 5 channels drop with blue surviving channels. Dark lines represent simulation results and gray lines represent measurement results.*

Figure 8.12 shows the dynamic results at the end of the transmission link for the case of blue surviving channels during the drop from 76 to 5 channels. The 5 blue surviving channel frequencies and their corresponding wavelengths in this case were already given in table 8.6 of the previous section. In figure 8.12, the relative power change as a function of time is shown for one of the 5 surviving channels (196.1 THz) as well as the total power, both at the end of the link.

It can be seen from figure 8.12 that the simulation results (dark lines) correspond quite well to those from the measurements (gray lines) both qualitatively and quantitatively. Qualitatively, the shapes of the transient curves correspond very well for both the channel power as well as the total power. However, for quantitative values, slight errors of typically 1 dB occur. When the channel power at 196.1 THz reaches its steady-state value after about 6.6 ms, it can be seen that the error increases to 2 dB. This error may ocuur due the spectral hole burning (SHB) effect, which was already observed in figure 8.5. SHB effects are not implemented in the simulation model so that larger discrepancies may occur when SHB effects are strong. However, it must not be excluded that other effects like inaccuracies in the ASE noise or Raman coefficients used in the simulation may contribute to the error as well.

For the dynamic results along the transmission link, the relative power change of the surviving channel at 195.6 THz is shown along the link in figure 8.13. These results are

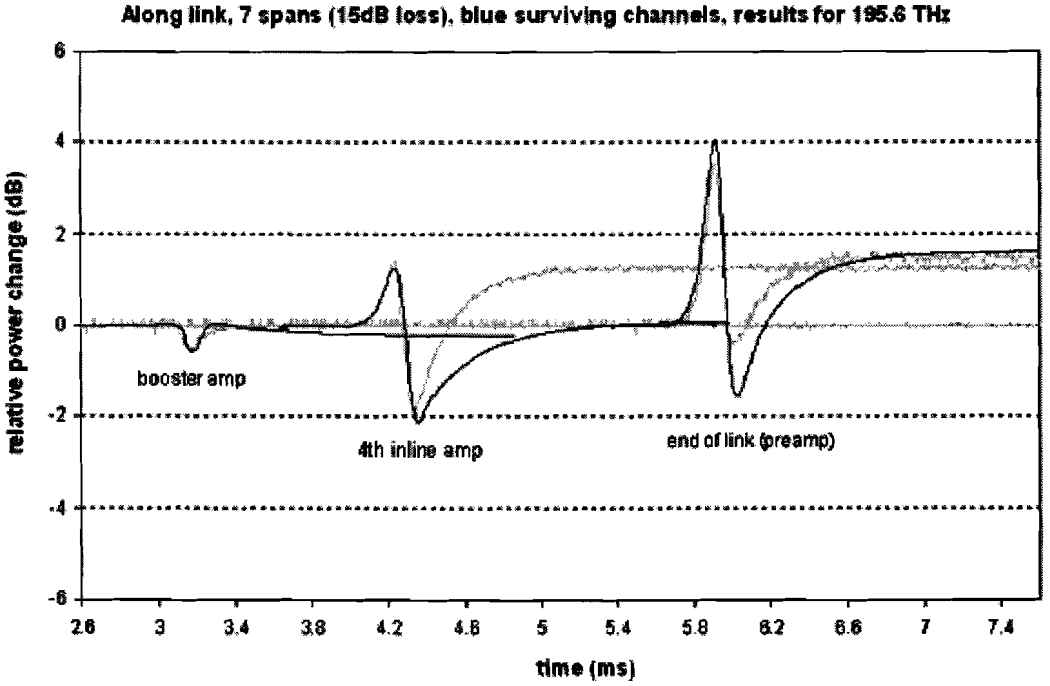

Figure 8.13: *Relative power change for surviving channel at 195.6 THz along the transmission link. Results are for a 76 to 5 channels drop with blue surviving channels and a link consisting of 7 spans with 15 dB loss each. Dark lines represent simulation and gray lines represent measurement results.*

obtained for the same 76 to 5 channels drop where the blue channels survive. It can be seen that the simulation (dark lines) and measurement (gray lines) results correspond very well, except for the 4th amplifier. For the 4th amplifier, errors start to occur when the channel power starts to reach its steady state value. Because the results at the end of the link don't show much discrepancies, SHB cannot be the cause of the errors. A possible reason for the errors occurring in the steady state value of the 4th amplifier may be the tilt of the power spectrum.

Because of different fiber spans and DCFs used in the link, the SRS tilt coefficients may differ from the values assumed in the simulation. Also, the SRS tilt correction factors set by the optical amplifiers may differ so that the simulated power spectra may differ from the real power spectra along the link. Because no measurement results are available for the power spectra along the link, it is unsure whether the power spectra correspond with the simulated results along the link. The only certainty is that the spectra correspond well at the end of the link, as already given in figure 8.9(a). It is possible that the real spectrum at the 4th amplifier is tilted more than the simulated results and the spectrum at the 5th amplifier less. Effectively, the spectral tilt at the end of the link will remain the same but the spectra along the link may differ. This difference in spectral tilt can be the cause of the errors occurring between the simulation

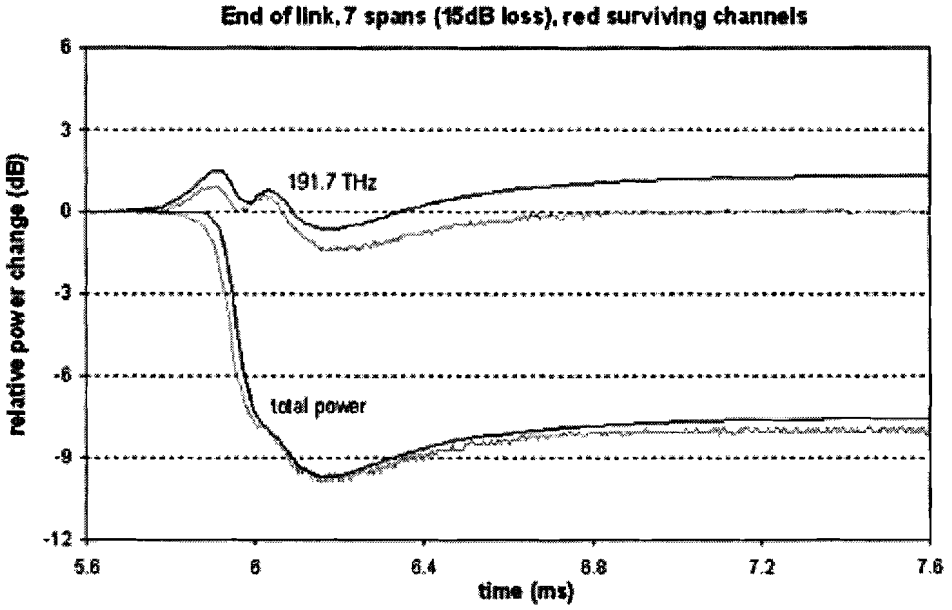

Figure 8.14: *Relative power change for surviving channel at 191.7 THz as well as the total power. Results are at the end of a transmission link with 7 spans of 15 dB loss each in case of a 76 to 5 channels drop with red surviving channels. Dark lines represent simulation results and gray lines represent measurement results.*

and measurement results in the 4th amplifier.

With the same transmission link setup and the same operating conditions as given in table 8.9, figure 8.14 shows the dynamic results at the end of the link in the case of 5 red surviving channels. The frequencies of these 5 red channels surviving the 76 to 5 channels drop can be found in table 8.6. In figure 8.14, the relative power change of the surviving channel at 191.7 THz as well as the total power are given as a function of time. The dark lines represent simulation and gray lines the measurement results.

The correspondence between simulation and measurement results is very good with maximum errors of about 1 dB for the single channel results. As discussed before, if SHB is presumed to be the main cause of errors between measurement and simulation results, its effects are smaller for channels at the red end of the C-band (see also appendix A), which may explain why the errors occurring in figure 8.14 (red surviving channels) are smaller than those in figure 8.12 (blue surviving channels).

For the second set of dynamic results, the operating conditions are given in table 8.10. These conditions are the same as given in table 8.8 for the static results with the exception that now, a drop of 76 to 5 channels occurs. Also, the transmission link setup used now consists of fiber spans with 25 dB loss instead of 15 dB loss. The amplifier gain is therefore also 25 dB for every amplifier following a fiber span.

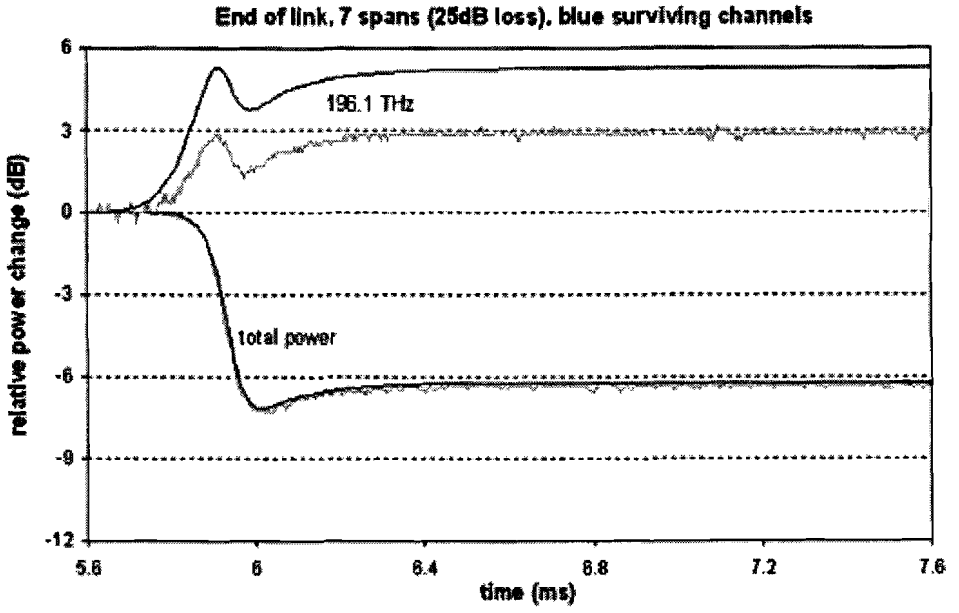

Figure 8.15: *Relative power change for surviving channel at 196.1 THz as well as the total power. Results are at the end of a transmission link with 7 spans of 25 dB loss each in case of a 76 to 5 channels drop with blue surviving channels. Dark lines represent simulation results and gray lines represent measurement results.*

Figure 8.15 shows the dynamic results at the end of the transmission link for the case of blue surviving channels. In the figure, the relative power change of the surviving channel at 196.1 THz as well as the total power are given. Because the amplifier gain is now 25 dB instead of 15 dB for each amplifier in the link, SHB effects are larger. This may explain the larger errors occurring in the single channel results when compared to the results in figure 8.12. The simulation results correspond very well with the measurements qualitatively. But when compared quantitatively, errors of 2.5 dB occur for the single

Table 8.10: *Parameters for simulations in figures 8.15 and 8.16*

gain setting method	automatic
number of channels / channel spacing	76 / 50 GHz
single channel power (booster amplifier) input / output	-20.5 / -1 dBm
total power (booster amplifier) input / output	-1.7 / 17.8 dBm
single channel power (rest of amplifiers) input / output	-26 / -1 dBm
total power (rest of amplifiers) input / output	-7.3 / 17.7 dBm
span loss / amplifier gain	25 / 25 dB
number of dropped channels	76 to 5
drop time	$\sim$ 160 μs

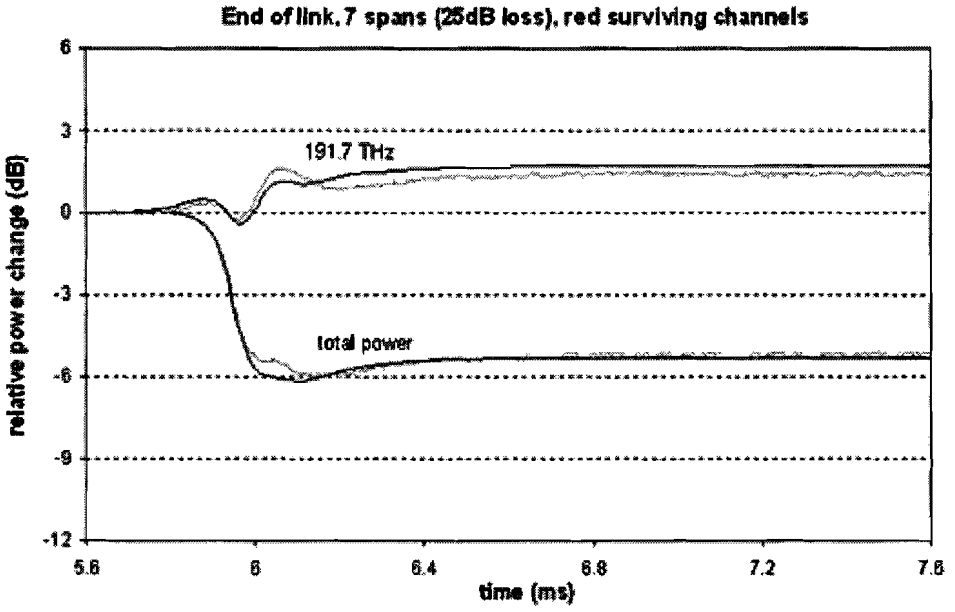

Figure 8.16: *Relative power change for surviving channel at 191.7 THz as well as the total power. Results are at the end of a transmission link with 7 spans of 25 dB loss each in case of a 76 to 5 channels drop with red surviving channels. Dark lines represent simulation results and gray lines represent measurement results.*

channel results. Once again, this can be because SHB effects are not implemented in the simulation model.

In figure 8.16, the dynamic results at the end of the transmission link for the case of red surviving channels are given. It can be seen that the results correspond very well with errors of less than 1 dB. SHB effects are not so strong so that the correspondence between simulation and measurement results is very good.

8.3 Discussion

In the first section of this chapter, simulation and measurement results were compared for a single optical amplifier. The static results corresponded very well with occasional errors of at most 0.25 dB. The dynamic results also showed very good correspondence with small errors of 0.1 dB when spectral hole burning (SHB) effects are weak. However, when SHB effects are strong, errors may increase to about 0.3 dB for channels with higher frequencies.

This is because the effect of SHB is not implemented in the simulation model. Firstly, SHB is not implemented because of the complexity of the phenomenon. Secondly, it is

not implemented in order to find out how well measurement results still can be simulated without taking SHB effects into consideration in the simulation model.

In the second section of this chapter, simulation and measurement results were compared for an entire transmission link consisting of 7 fiber spans and 8 optical amplifiers. By taking into mind the errors for a single amplifier, the worst case error margin for the link results when taking SHB effects into consideration can be estimated to be about: 8×0.3 dB $= 2.4$ dB. Such large errors can be expected to occur when high-frequency channels in the C-band are chosen to survive the channel drop.

In the dynamic results for the link, this error could be observed in figure 8.15. For all other dynamic results, errors of less than 1 dB occur between simulation and measurement data. Also, it could be noticed that the results for red surviving channels correspond better than the results for blue surviving channels. For the static results of the transmission link, sample dependence of the optical components influenced the errors positively, leading to errors of not more than 1 dB.

Finally, it can be concluded that the simulation model can simulate measurement results of a transmission link very well. The correspondence between simulation and measurement data is both qualitatively and quantitatively good when SHB effects are weak. However, when SHB effects are strong, larger errors tend to occur. The results are still comparably good with maximum error margins of 2.5 dB but better results can be obtained if SHB is implemented in the simulation model. For best results, it is therefore advisable to implement SHB effects in the simulation model.

Chapter 9

Analysis of transients based on simulations

As discussed before at the beginning of this thesis, adding and dropping of WDM channels will cause power transients in optical amplifiers. The fundamental cause of these transients is the population of erbium ions in excited state, when erbium-doped fibers are pumped with a laser. When WDM signals going into an EDFA are added or dropped, the total input signal power changes whereas the population of excited erbium ions remains the same. This influences the gain of the remaining WDM channels, which leads to transient behaviour of the signal channel powers at the output of the EDFA.

However, besides this fundamental cause, there are other factors that effect the magnitude and speed of these power transients. In chapter 4.4, a few of these factors such as the number of channels dropped, the number of EDFAs used, and the speed of the drop were already introduced. Simulation results by Schilling [33] given in figures 4.9 to 4.12 showed their effects on the behaviour of power transients. Other factors that can effect the behaviour of power transients are:

- Surviving channel configurations
- SRS effects and tilt
- Ripple in gain spectrum of amplifier
- ASE correction

In this chapter, these factors will be discussed in more details and the simulation model will be used to demonstrate and analyze their influences on power transients.

9.1 Surviving channel configurations

Figures 9.1 to 9.4 show simulations of the channel power as a function of the time at the end of a transmission link for a 76 to 5 channels drop. In the figures, all 76 channel powers are shown as a function of time, including those that are dropped. The drop of the channels starts at a time of 0.75 ms, which can be observed in the figures. The operating conditions are kept the same for all simulations except for the frequencies of the surviving channels.

It can be seen that for different configurations of the 5 surviving frequency channels, different transient behaviour may occur. The results in figure 9.2 show that the shapes of the power transients can even differ a lot depending on the configuration of the surviving channels.

Therefore, when WDM channels are used in add/drop networks, it is advisable to research different channel configurations and choose the frequency channels appropriately so that power transients can be minimized.

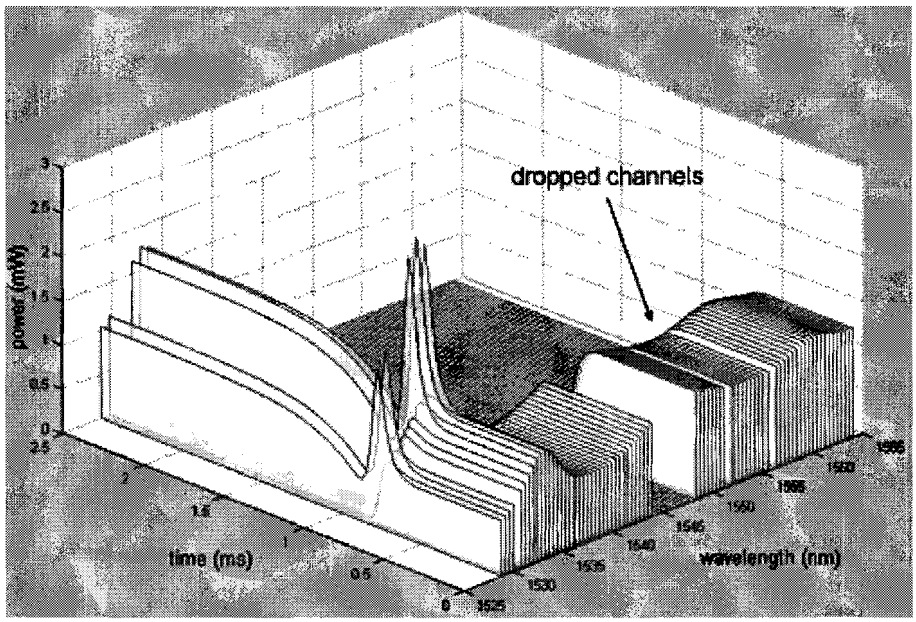

Figure 9.1: *Simulation results of the channel powers at the end of a transmission link for a 76 to 5 channels drop. Results are plotted for every present WDM channel as a function of the time. Surviving channels are blue at 196.1, 196.0, 195.7, 195.6, and 195.5 THz.*

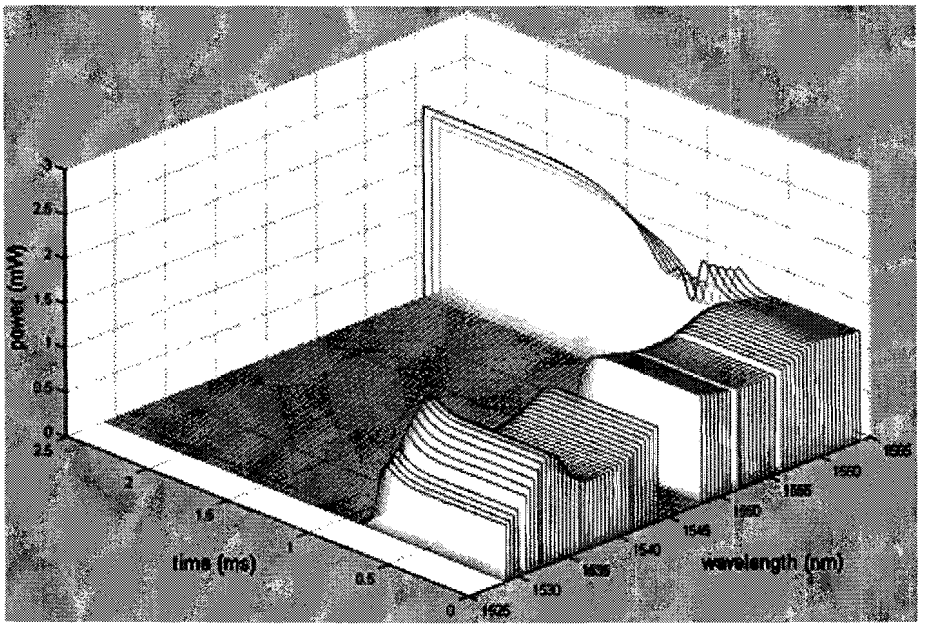

Figure 9.2: *Same as in figure 9.1, but for red surviving channels at 192.1, 192.0, 191.9, 191.8, and 191.7 THz.*

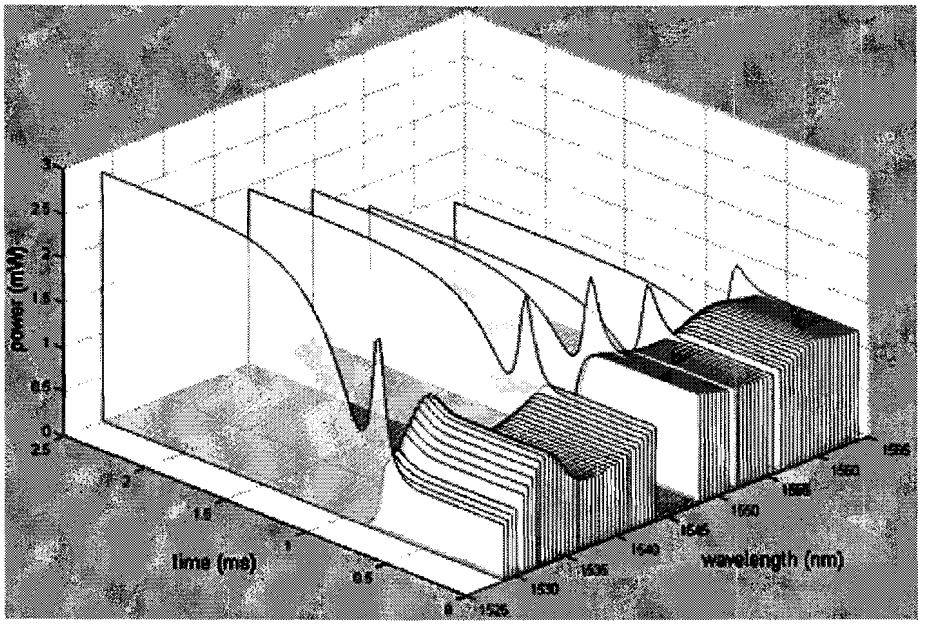

Figure 9.3: *Same as in figure 9.1, but for mixed surviving channels at 196.1, 194.25, 193.45, 192.75, and 191.7 THz.*

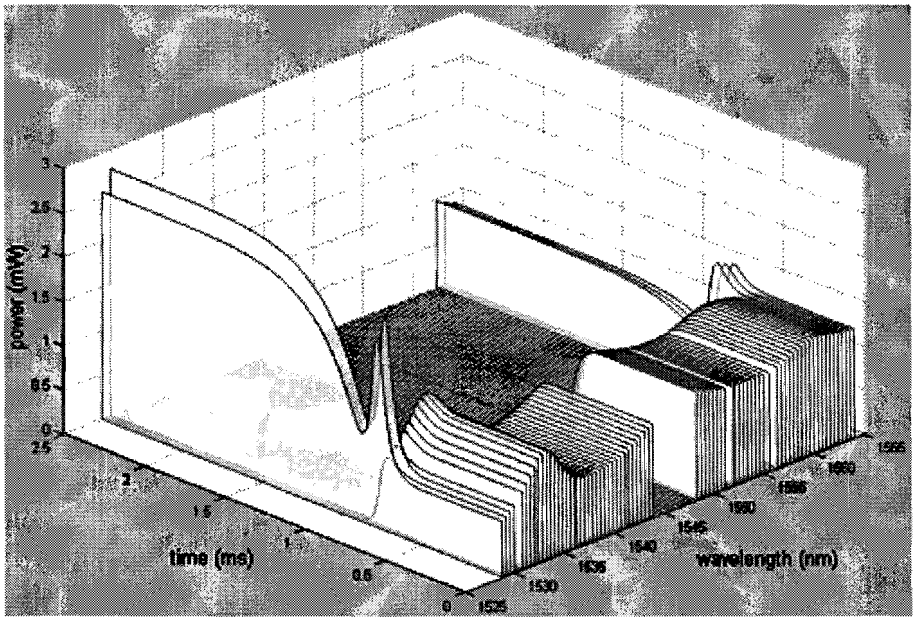

Figure 9.4: *Same as in figure 9.1, but for separated surviving channels at 196.1, 196.0, 191.9, 191.8, and 191.7 THz.*

9.2 SRS effects and tilt

Besides channel configuration, the effects of stimulated Raman scattering (SRS) can also cause power transients to become worse. In a transmission link, SRS crosstalk happens mainly in the fiber spans, causing tilts in the power spectrum of the signals that are being transmitted (see figure 6.9). In figure 6.10, it could be seen how the gain tilt control with VOA is used to compensate for the spectral tilts resulting from SRS along the transmission link. However, in most optical amplifiers, these gain tilt control systems have working speeds of several tens of milliseconds, which are very slow when compared to the time constants of power transients that occur in transmission links (several tens of microseconds).

The problem arises when large numbers of channels are dropped in a transmission link. This drop of channels will cause a large loss of the total transmitted power in the link so that the effects of SRS crosstalk are weakened. This happens because of the dependence of SRS effects on the total transmitted power in the fiber spans (see equation 6.12). As a result, the tilt in the power spectrum caused by SRS will reduce almost instantaneously.

However, because the gain tilt control has a slow speed of several tens of milliseconds, the tilt control will still remain at the old value, causing the power spectra of the transmitted signals to suffer an opposite tilt. This results in higher power transients in the transmission link. Goeger et al [35] have already shown simulation results where this problem is indicated. Their results are given in figure 9.5.

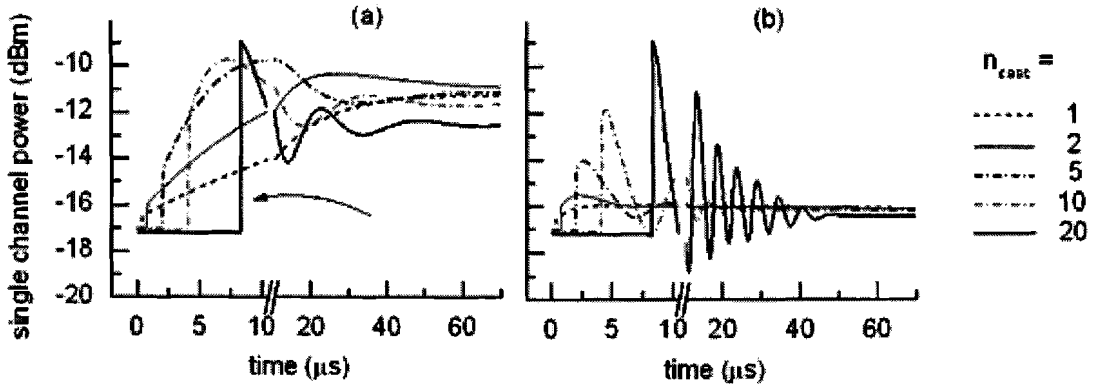

Figure 9.5: *Power transients of the 196.1 THz channel after a cascade of* n_{casc} *EDFAs* [35]. (a)*Effects of SRS after a drop of 30 out of 45 channels without fast tilt control. The arrow indicates the ultrafast SRS contribution to the transient behavior.* (b)*Same results when very fast SRS tilt control is implemented with a reaction time of 500 ns.*

Figure 9.5(a) shows the power transients at 196.1 THz after a drop of 30 out of 45 channels. In these simulation results, it is assumed that no gain tilt control mechanism is present in the EDFAs. It can be seen that the SRS effects cause high power transients with even worse behaviour when larger numbers of EDFAs are cascaded. In figure 9.5(b), it is shown that the use of a very fast gain tilt control can solve the problem.

With the simulation model presented in this thesis, similar simulations can be done to show the negative power transient effects of SRS. In this case, a simulation is done using a realistic model for the fiber spans which includes the effects of SRS. Also, another simulation with the same operating conditions is done using simple attenuation blocks to replace the fiber span models without including any SRS effects. Results are shown for the normalized channel powers at the end of a transmission link consisting of 7 fiber spans and 8 amplifiers. The simulations are done for a 76 to 5 channels drop with the surviving channels at 196.1, 194.25, 193.45, 192.75, and 191.7 THz.

Figure 9.6 shows the simulation results for the case where SRS effects are taken into account, that is, when realistic fiber span models including SRS effects are used. Figure 9.7 shows simulation results for the case where the fiber span models are replaced by simple attenuation blocks without SRS effects. From these two figures, it can clearly be seen that SRS influences the power transients in a negative manner. Figure 9.8 shows a comparison of the two power transients for the surviving channels. It can be seen that for the channel at 196.1 THz, an extra power jump of almost 3 dB occurs because of SRS.

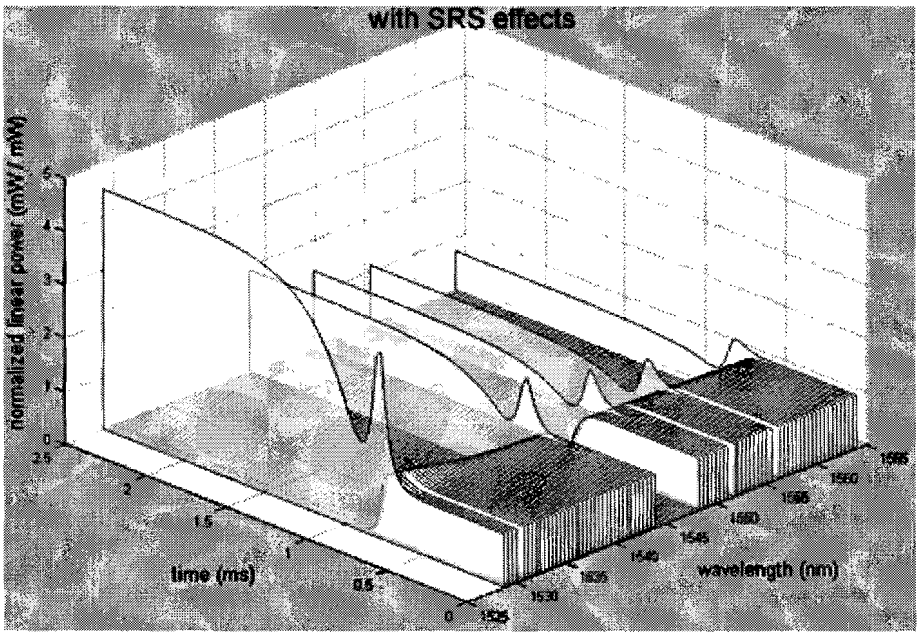

Figure 9.6: *Dynamic simulation of channel powers (normalized) at the end of a transmission link during a 76 to 5 channels drop. Realistic fiber span models which cause SRS effects are used in the simulation. Large changes in channel powers can be observed for the surviving channels.*

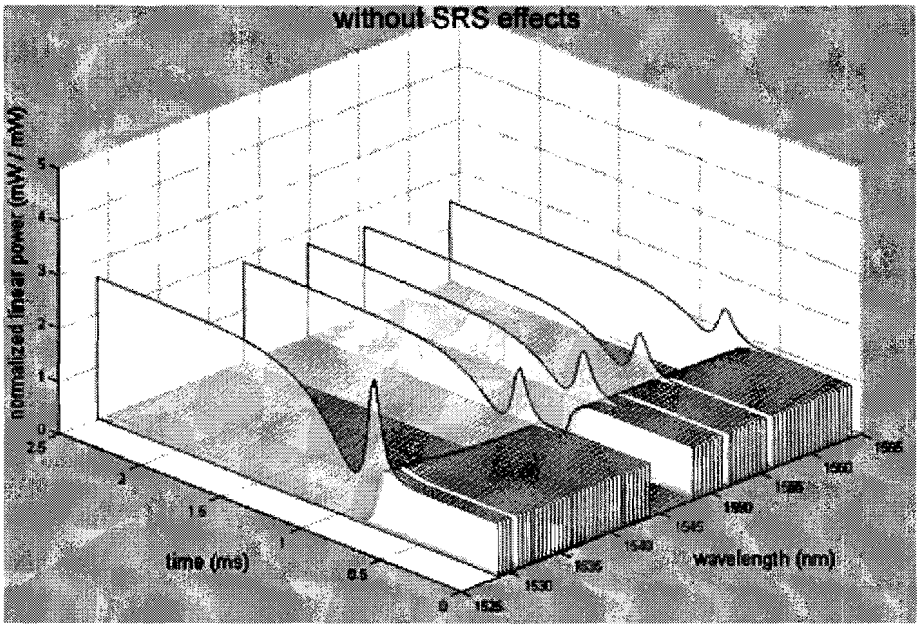

Figure 9.7: *Dynamic simulation of channel powers (normalized) at the end of a transmission link during a 76 to 5 channels drop. Simple attenuation blocks are used to simulate the loss by fiber spans yielding no SRS effects in the simulation. Smaller changes in channel powers can be observed for the surviving channels.*

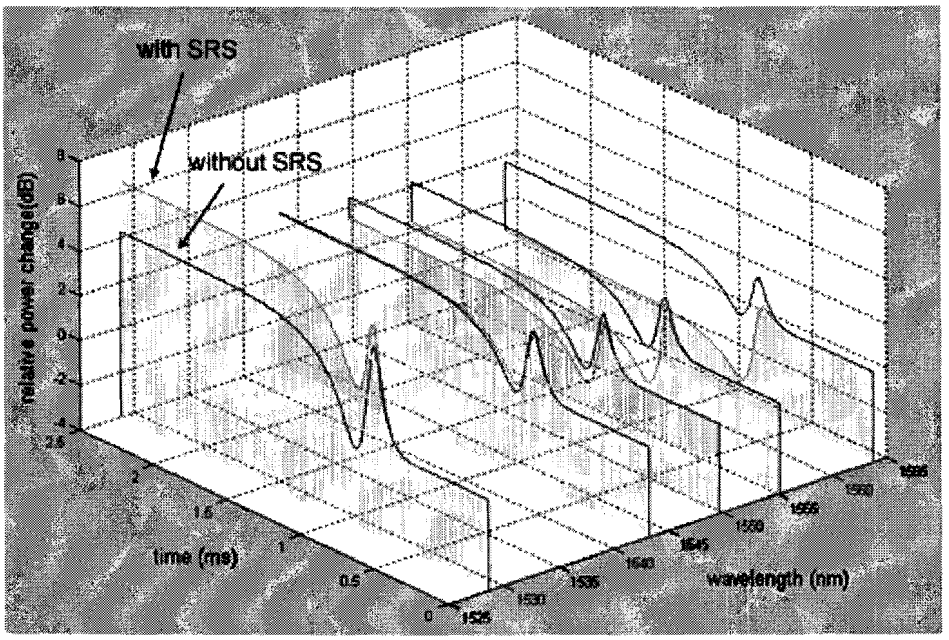

Figure 9.8: *The surviving channel power transients of figures 9.6 and 9.7 are given again and compared to each other in dB. The difference between the results with and without SRS effects can clearly be observed.*

9.3 Gain ripple

Another factor that effects the behaviour of transients is the non-flatness of the amplifier gain spectra. As shown in figure 6.2, the gain spectrum of an EDFA is not perfectly flat. With the use of gain flattening filters (GFF), these ripples in the gain spectrum can be minimized. However, because of sample and temperature dependence, it is not possible to obtain a perfectly flat gain spectrum. Therefore, small gain ripples of every optical amplifier in a transmission link can add up, thereby leading to larger gain ripples for the entire link.

This is shown in figure 9.9, where the power spectra are simulated for a transmission link with gain ripples in the amplifiers and a link without gain ripples in the amplifiers. The results are given for the end of a link consisting of 8 optical amplifiers and 20 transmitted WDM signal channels. It can be seen that for the link with gain ripples in the amplifiers, these ripples add up to give variations up to almost 3 dB in the resulting power spectrum at the end of the transmission link. As shown previously in figure 6.6, these gain ripples can cause power changes in the event of channel drops.

Figure 9.10 shows results of the power transients in the surviving channel when 19 of the 20 channels in the same transmission link simulations are dropped. The results are shown for the end of the link with the power spectra given in figure 9.9 and surviving channel at a wavelength of 1533.5 nm. It can be seen that in the case of gain ripples,

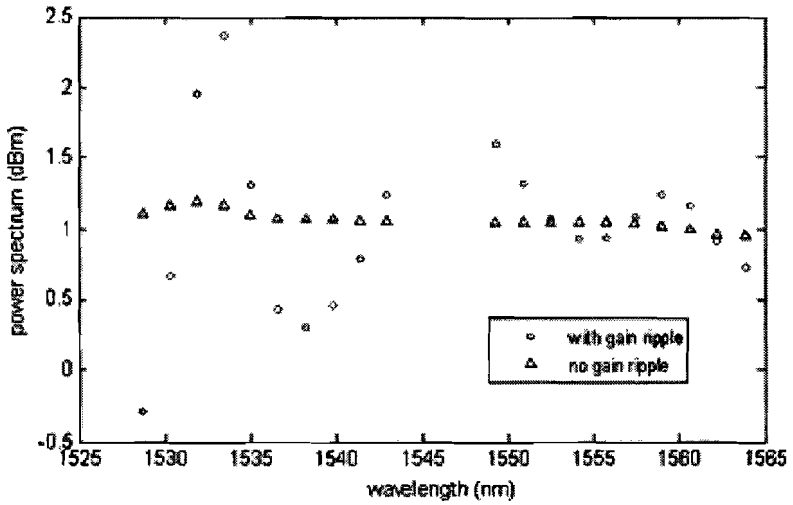

Figure 9.9: *Simulated power spectrum at the end of a transmission link consisting of 8 optical amplifiers and 20 WDM signal channels. Results are shown for a link with and without gain ripples in the optical amplifiers.*

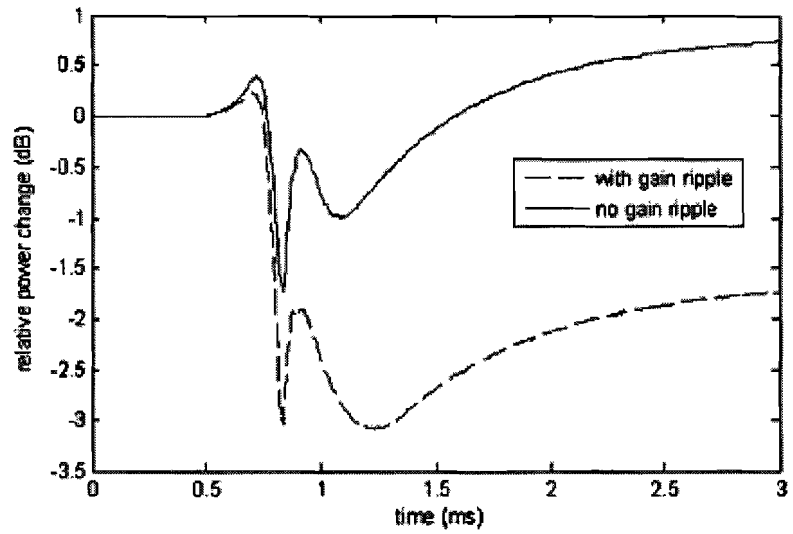

Figure 9.10: *Simulated power transients in surviving channel (1533.5 nm) of a 20 to 1 channel drop with and without gain ripple.*

the channel power jumps down 2.5 dB more compared to the case without gain ripples. When compared to its own power before the drop, the case with gain ripples suffers a jump downwards of more than 3 dB. This amount of power loss can cause eye closure at the receivers, leading to bit errors. Also, when the power falls below the receiver sensitivity, severe errors will occur.

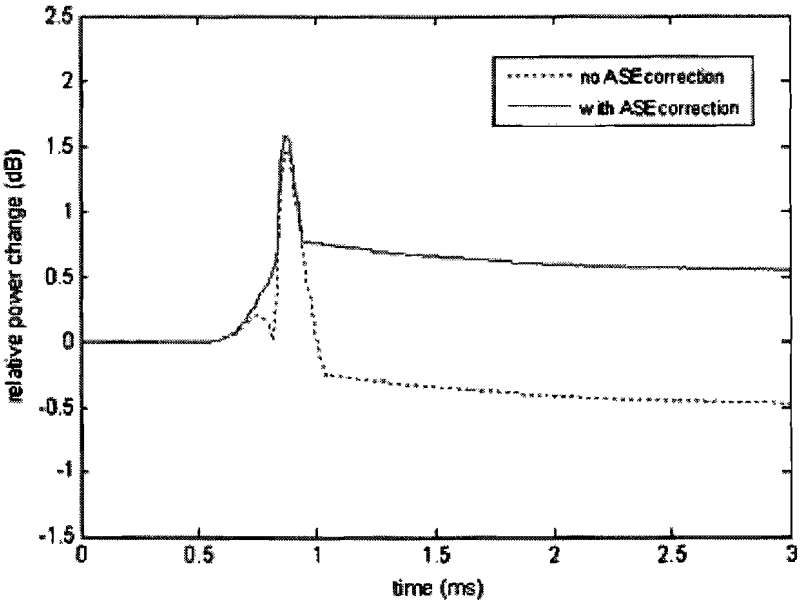

9.4 ASE correction

As discussed earlier, ASE correction is used to correct measurement errors that occur in optical powers due to ASE noise. By using ASE correction, the gain of the amplifier is set higher with an estimated factor so that the noise at the output of the amplifier is compensated. This will also influence the behaviour of the power transients when channels are added or dropped. In figure 9.4, it can be seen how ASE correction actually effects the behaviour of power transients in case of a channel drop. The figure shows simulation results for an optical amplifier in case of a channel drop from 20 to 1 channel. The surviving channel frequency is 195.5 THz.

It can be seen that ASE correction causes the steady-state value of the surviving channel power after the drop to increase by 1 dB. Depending on the parameters and values used in the ASE correction, this difference can vary from more to less. When using ASE correction, one should therefore be aware of its influence on power transients and choose appropriate parameters and values so that the power transients don't become worse.

Chapter 10

Conclusion

Nowadays, EDFAs are widely used in optical transmission networks because of their high gain over a large wavelength range, low intrinsic losses and long fluorescence times. However, issues with regard to power transients resulting from channel add/drop in optical links consisting of EDFAs still have to be solved. From simulation and measurement results obtained by others so far, these power transients occurring in EDFAs seem to be worse than had been thought.

Especially when EDFAs are cascaded in a link, power transients resulting from adding or dropping of channels can add up to several dBs and increase in speed. Therefore, fast automatic gain control is needed to control the gain of EDFAs.

From the different methods used so far, automatic gain control with electronic control seems to be one of the more promising techniques to control power transients in EDFAs. In this thesis, such an optical amplifier with fast electronic gain control is presented and discussed.

Furthermore, a simulation model is implemented to show that it is possible to simulate a state-of-the-art optical amplifier consisting of different levels of complex control mechanisms qualitatively as well as quantitatively. The comparisons with results on both a single optical amplifier and a transmission link consisting of 8 optical amplifiers and 7 fiber spans show that the simulation model can give very good corresponding results with measurement data.

For a single amplifier, static measurement results can be simulated very well with maximum errors of 0.25 dB. Dynamic measurement results can also be simulated very well when SHB effects are weak, yielding typical errors of 0.1 dB. When SHB effects are strong, larger errors up to a maximum of 0.3 dB may occur in simulation results. This is because SHB effects are not implemented in the simulation model. SHB is a complex phenomenon and is difficult to implement into the simulation model. Also, it is interesting to find out how much influence SHB has on the difference between measurement and simulation results.

For a transmission link with 8 optical amplifiers, the static simulation results showed errors of at most 1 dB. Dynamic simulation results showed errors of typically 1 dB when SHB effects are weak. When SHB effects are strong, maximum errors of 2.5 dB occur. Despite this, the simulation model gives good corresponding results with measurement data. For best results, SHB effects should be studied more deeply and implemented into the simulation model.

With the accurate simulation model, simulations can be done to replace systematic measurements so that only special cases need to be measured. Besides this, the simulation model can be used to understand the behaviour of power transients in a complex optical amplifier better and help with new design ideas. Up till now, the simulation model has proved to be of good use by helping with the solving of problems in the current optical amplifier designs. Also, the simulation model is being used for testing new designs of future versions of optical amplifiers. The use of FPGAs in the optical amplifier gain control is also currently being investigated with this simulation model.

Bibliography

[1] E. Desurvire, "Analysis of Transient Gain Saturation and Recovery in Erbium-Doped Fiber Amplifiers," *IEEE Photonics Technol. Lett.*, vol. 1, pp. 196-199, Aug. 1989.

[2] C. R. Giles, E. Desurvire, and J. R. Simpson, "Transient gain and cross talk in erbium doped fiber amplifiers," *Opt. Lett.*, vol. 14, pp. 880-882, Aug. 1989.

[3] E. Desurvire, C. R. Giles, and J. R. Simpson, "Gain dynamics of erbium-doped fiber amplifiers," *Proc. SPIE Conf. Fiber Laser Sources and Amplifiers*, vol. 1171, pp. 103-117, Sep. 1989.

[4] N. S. Bergano, J. Aspell, C. R. Davidson, P. R. Trischitta, B. M. Nyman, and F. W. Kerfoot, "Bit Error Rate measurements of 14000km 5Gbit/s fibre-amplifier transmission system using circulating loop," *Electron. Lett.*, vol. 27, pp. 1889-1890, Oct. 1991.

[5] J. L. Zyskind, Y. Sun, A. K. Srivastava, J. W. Sulhoff, A. J. Lucero, C. Wolf, and R. W. Tkach, "Fast power transients in optically amplified multiwavelength optical networks," *OFC '96*, vol. 2, pp. 451–454, Feb. 1996, San Jose, CA, PDP31.

[6] Y. Sun, A. K. Srivastava, J. L. Zyskind, J. W. Sulhoff, C. Wolf, and R. W. Tkach, "Fast power transients in WDM optical networks with cascaded EDFA's," *Electron. Lett.*, vol. 33, pp. 313-314, Feb. 1997.

[7] A. Turukhin, D. Al-Salameh, E. Gonzales, and S. Lumish, "Transient measurements of bit-error-rate ratio at 10 Gb/s in WDM 6x80 km transmission links," *ECOC '04*, vol. 1, pp. 96-97, Sep. 2004.

[8] W. S. Wong, Huan-Shang-Tsai, Chien-Jen-Chen, Hak-Kyu-Lee, and Min-Chen-Ho, "Novel time-resolved measurements of bit-error-rate and optical-signal-to-noise-ratio degradations due to EDFA gain dynamics in a WDM network," *OFC '02*, vol. 1, pp. 515-516, Mar. 2002, Anaheim, CA, ThR4.

[9] A. K. Srivastava, Y. Sun, J. L. Zyskind, and J. W. Sulhoff, "EDFA Transient Response to Channel Loss in WDM Transmission Systems," *IEEE Photonics Technol. Lett.*, vol. 9, pp. 386-388, Mar. 1997.

[10] C .R. Giles, E. Desurvire, and J. R. Simpson, "Transient gain and cross talk in erbium-doped fiber amplifiers," *Optical Letters, Optical Society of America*, vol. 14, pp. 880–882, Aug. 1989.

[11] S. Y. Park, H. K. Kim, G. Y. Lyu, S. M. Kang, and S. Y. Shin, "Dynamic gain and output power control in a gain-flattened erbium-doped fiber amplifier," *IEEE Photonics Technol. Lett.*, vol. 10, pp. 787–789, Jun. 1998.

[12] N. E. Jolley, F. Davis, and J. Mun, "Out-of-band electronic gain clamping for a variable gain and output power EDFA with low dynamic gain tilt," *OFC '97*, pp. 134–135, Feb.1997, Dallas, TX, WF7.

[13] J. Drake, A. Tipper, A. Ford, B. Flintham, and K. P. Jones, "A comparison of practical gain and transient control techniques for erbium doped fiber amplifiers," *Optical Amplifiers and Their Applications*, pp. 163–165, 1998, TuD12.

[14] N. Suzuki, K. Shimizu, T. Kogure, and J. Nakagawa, "Optical fiber amplifiers employing novel high-speed AGC and tone-signal ALC functions for WDM transmission systems," *ECOC '00*, vol. 2, pp. 179–180, Sep. 2000.

[15] N. E. Jolley, F. Davis, and J. Mun, "A Bragg grating optically gain-clamped EDFA with adjustable gain, low noise figure and low multipath interference," *OFC '98,* pp. 139–140, Feb. 1998, San Jose, CA, WG6.

[16] J. Chung, S. Y. Kim, and C. J. Chae, "All-optical gain-clamped EDFAs with different feedback wavelengths for use in multi-wavelength optical networks," *Electron. Lett.*, vol. 32, pp. 2159–2161, Nov. 1996.

[17] G. Luo, J. L. Zyskind, Y. Sun, A. K. Srivastava, J. W. Sulhoff, and M. A. Ali, "Relaxation-oscillations and spectral hole burning in laser automatic gain control of EDFAs," *OFC '97*, vol. 6, pp. 130–131, Feb. 1997, Dallas, TX, paper WeF4.

[18] H. X. Dai, J. Y. Pan, and Ch. Lin, "An optical gain control of in-line edfa for hybrid am/digital wdm systems," *OFC '97*, vol. 6, pp. 133–134, Feb. 1997, Dallas, TX, paper WeF6.

[19] E. Delevaque, T. Georges, J. F. Bayon, M. Monerie, P. Niay, and P. Bernage, "Gain control in erbium-doped fiber amplifiers by lasing at 1480 nm with photoinduced bragg gratings written on fiber ends," *Electron. Lett.*, vol. 29, pp. 1112–1114, Jun. 1993.

[20] B. Landousies, T. Georges, E. Delevaque, R. Lebref, and M. Monerie, "Low power transient in multichannel equalized and stabilized gain amplifier using passive gain control," *Electron. Lett.*, vol. 32, pp. 1912–1913, Sep. 1996.

[21] M. Zirngibl, "Gain control in erbium-doped fiber amplifiers by an all-optical feedback loop," *Electron. Lett.*, vol. 27, pp. 560–561, Mar. 1991.

[22] E. Desurvire, M. Zirngibl, H. M. Presby, and D. DiGiovanni, "Dynamic gain compensation in saturated erbium-doped fiber amplifiers," *IEEE Photonics Technol. Lett.*, vol. 3, pp. 453–455, May 1991.

[23] J. L. Zyskind, A. K. Srivastava, Y. Sun, J. C. Ellison, G. W. Newsome, R. W. Tkach, A. R. Chraplyvy, J. W. Sulhoff, T. A. Strasser, J. R. Pedrazzani, and C. Wolf, "Fast link control protection for surviving channels in multiwavelength optical networks," *ECOC '96*, vol. 5, pp. 49–52, Sep. 1996, Oslo, Norway, ThC.3.6.

[24] A. K. Srivastava, Y. Sun, J. L. Zyskind, J. W. Sulfoff, C. Wolf, and R. W. Tkach, "Fast gain control in an erbium-doped fiber amplifier," *Optical Amplifiers and Their Applications*, vol. 5, pp. 24–27, 1996, Monterey, CA, paper PDP4.

[25] A. K. Srivastava, J. L. Zyskind, Y. Sun, J. Ellson, G. Newsome, R. W. Tkach, A. R. Chraplyvy, J. W. Sulfoff, T. A. Strasser, C. Wolf, and J. R. Pedrazzani, "Fast-link control protection of surviving channels in multiwavelength optical networks," *IEEE Photonics Technol. Lett.*, vol. 9, no. 12, pp. 1667–1669, Dec. 1997.

[26] G. P. Agrawal, *Nonlinear Fiber Optics*, 2nd ed., San Diego: Academic Press, 1995, Optics and photonics.

[27] S. Bigo, S. Gauchard, A. Bertaina, and J. Hamaide, "Experimental Investigation of Stimulated Raman Scattering Limitation on WDM Transmission Over Various Types of Fiber Infrastructures," *IEEE Photonics Technol. Lett.*, vol. 6, pp. 671–673, Jun. 1999.

[28] M. Menif, L. A. Rusch, and M. Karasek, "Application of Preemphasis to Achieve Flat Output OSNR in Time-Varying Channels in Cascaded EDFAs Without Equalization," *IEEE J. Lightwave Technol.*, vol. 19, pp. 1440-1452, Oct. 2001.

[29] A. R. Chraplyvy, J. A. Nagel, and R. W. Tkach, "Equalization in Amplified WDM Lightwave Transmission Systems," *IEEE Photonics Technol. Lett.*, vol. 4, pp. 920–922, Aug. 1992.

[30] A. R. Chraplyvy, R. W. Tkach, K. C. Reichmann, P. D. Magill, and J. A. Nagel, "End-to-End Equalization Experiments in Amplified WDM Lightwave Systems," *IEEE Photonics Technol. Lett.*, vol. 4, pp. 428–429, Apr. 1993.

[31] G. Keiser, *Optical Fiber Communications*, 3rd ed., Singapore: McGraw-Hill, 2000, Communications and Signal Processing.

[32] D. M. Spirit, and M. J. O'Mahony, *High Capcity Optical Transmission Explained*, Chichester: John Wiley & Sons Ltd, 1996.

[33] M. Schilling, *Dynamik von Regelungsprozessen in transparenten optischen Netzwerken*, Leipzig, Fachhochschule Leipzig, 2002, Master Dissertation.

[34] L. Rapp, *Verstaerkungs- und Rauscheigenschaften eines erbiumdotierten Faserverstaerkers*, Stuttgart, Universitaet Stuttgart, 1994, Master Dissertation.

[35] G. Goger, and B. Lankl, "Raman transients in transparent dynamically configurable optical networks," *OFC '02*, pp. 99–100, Mar. 2002, Anaheim, CA.

[36] E. Desurvire, J. L. Zyskind, and J. R. Simpson, "Spectral Gain Hole Burning at 1.53 μm in Erbium-Doped Fiber Amplifiers," *IEEE Photonics Technol. Lett.,* vol. 2, no. 4, pp. 246-248, Apr. 1990.

[37] J. L. Zyskind, E. Desurvire, J. W. Sulhoff, and D. J. Di Giovanni, "Determination of Homogeneous Linewidth by Spectral Gain Hole Buming in an Erbium-Doped Fiber Amplifier with GeO_2:SiO_2 Core," *IEEE Photonics Technol. Lett.,* vol. 2, no. 12, pp. 869-871 Dec. 1990.

[38] A. K. Srivastava, J. L. Zyskind, J. W. Sulhoff, J. D. Evankow, Jr., and M. A. Mills, "Room temperature spectral hole-burning in erbium-doped fiber amplifiers," *OFC '96*, pp. 33-34, Feb. 1996, San Jose, CA, paper TuG7.

[39] J. W. Sulhoff, A. K. Srivastava, C. Wolf, Y. Sun, and J. L. Zyskind, "Spectral hole burning in erbium-doped silica and fluoride fibers," *IEEE Photonics Technol. Lett.*, vol. 9, no. 12, pp. 1578–1579, Dec. 1997.

[40] G. Luo, J. L. Zyskind, Y. Sun, A. K. Srivastava, J. W. Sulhoff, C. Wolf, and M.A. Ali, "Performance Degradation of All-Optical Gain-Clamped EDFA's Due to Relaxation-Oscillations and Spectral-Hole Burning in Amplified WDM Networks," *IEEE Photonics Technol. Lett.*, vol. 9, no. 10, pp. 1346–1348, Oct. 1997.

[41] W. A. Arellano, M. O. Berendt, A. A. Rieznik, Ildefonso de Faria, and H. L. Fragnito, "Observation of Spectral Hole Burning in the Amplified Spontaneous Emission Spectrum of Erbium Doped Fibers," *IX Simposio Brasileiro de Microondas e Optoeletronica*, pp. 122-124, Aug. 2000, Joao Pessoa, PB.

[42] T. Aizawa, T. Sakai, A. Wada, and R. Yamauchi, "Effect of Spectral-Hole Burning on Multi-Channel EDFA Gain Profile," *OFC '99*, vol. 2, pp. 102-104, Feb. 1999, San Diego, CA.

[43] M. J. Yadlowsky, "Pump Wavelength -Depedent Spectral-Hole Burning in EDFA's," *IEEE J. Lightwave Technol.*, vol. 17, pp. 1643-1648, Sep. 1999.

[44] M. Bolshtyansky, "Spectral Hole Burning in Erbium-Doped Fiber Amplifiers," *IEEE J. Lightwave Technol.*, vol. 21, pp. 1032-1038, Apr. 2003.

Appendix A

Spectral Hole Burning

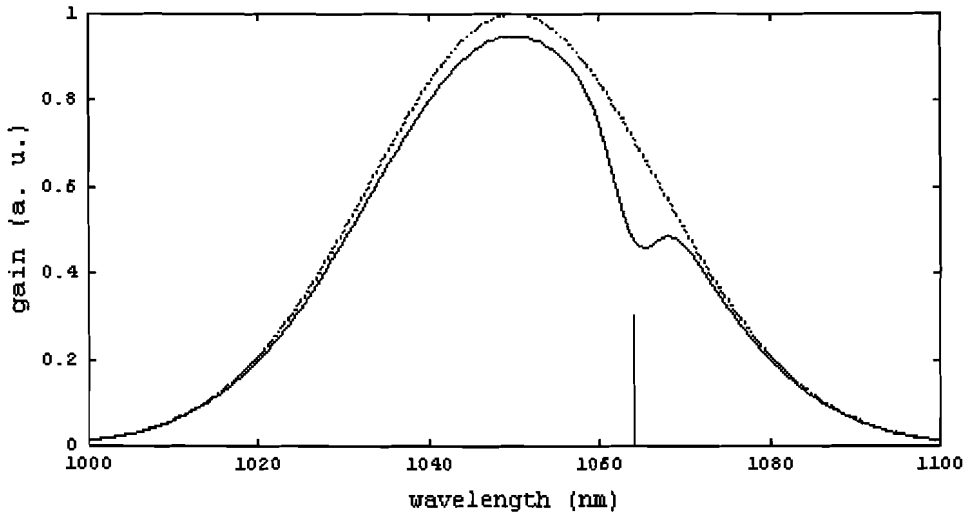

Figure A.1: *A demonstration of spectral hole burning. A laser at 1064 nm saturates the gain around 1064 nm more than the gain at other wavelengths. For comparison, the unsaturated gain (without laser power) is shown as a dotted curve.*

Spectral hole burning (SHB) in erbium-doped fiber amplifiers is a phenomenon where a hole occurs in the gain spectrum of an amplifier [36], [37], [38], [39]. This is caused by inhomogeneous broadening of the gain in the EDFs when a strong laser beam is being amplified. That is, the gain of the strong laser beam will be saturated at the corresponding frequency, leading to lower gain and output power values. Figure A.1 demonstrates this effect of SHB.

With the use of the differential gain method [38] [41], observations of SHB effects in the gain spectrum of EDFAs at room temperature can be made. Essentially, the differential method consists of subtracting two gain spectra measured with the saturating laser tuned to two different wavelengths, and with power adjusted so as to produce the

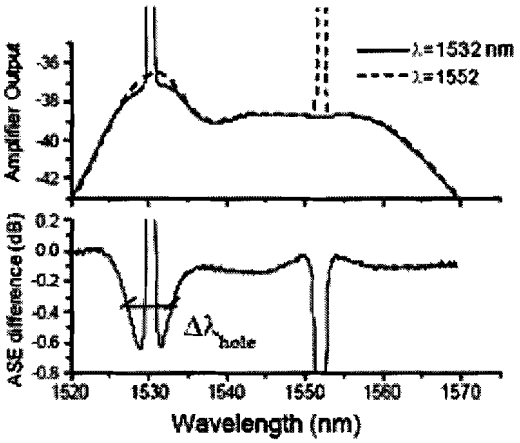

Figure A.2: *ASE spectra with saturating laser tuned to 1532 and 1552 nm (top), and the subtracted spectrum (bottom). Spectra were recorded with 0.5 nm resolution* [41].

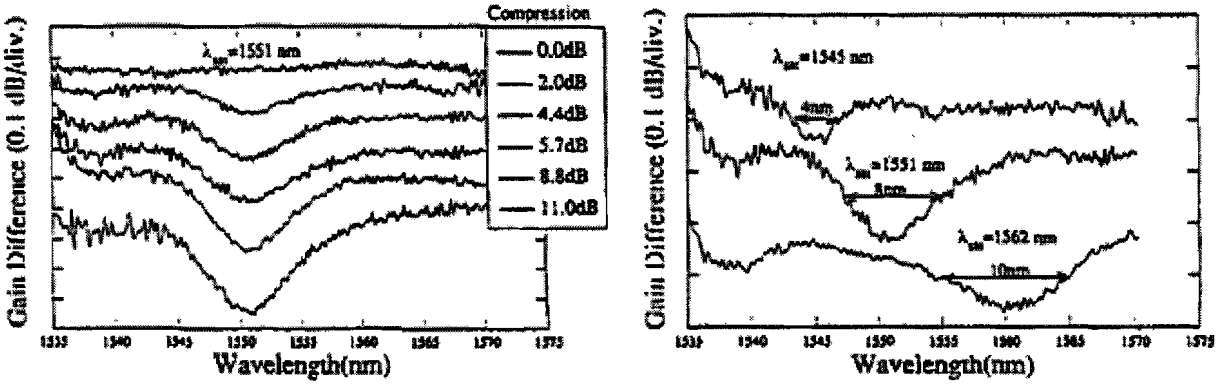

(a) (b)

Figure A.3: *SHB results obtained by Srivastava et al* [38]. (a) *Dependence of spectral hole-burning on amplifier compression for saturation at 1551 nm.* (b)*Spectral hole widths for saturation at different wavelengths.*

same amount of gain compression. This method is illustrated in figure A.2, giving the results for a typical EDFA.

Figure A.3 shows the results obtained by Srivastava et al of SHB effects for an individual EDFA at room temperature. Figure A.3(a) shows the depth and width of the hole for a saturating signal at 1551 nm depending on the compression of the amplifier. It can be seen that for a compression of 11 dB, a dip of 0.3 dB occurs in the gain spectrum of the amplifier due to SHB. As given by figure A.3(b), the shape of the spectral hole doesn't only depend on the compression, but also on the wavelength or frequency of the saturating signal. It can be seen that the width of the hole increases when the saturating wavelength is increased.

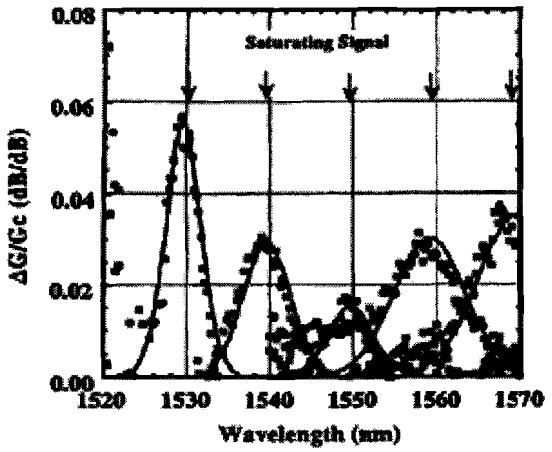

Figure A.4: *Gain reduction divided by gain, caused by SHB for one channel* [42].

Similar results have been obtained by Aizawa et al [42]. Their results are shown in figure A.4 where the normalized gain reduction as a result of SHB is measured for one single channel. It can be seen again that for signals of smaller wavelengths, the width of the hole is smaller. The interesting part is however, that for a constant gain, the depth of the hole is larger for signals with smaller wavelengths than for those with larger wavelengths. This means that SHB has a narrower but larger effect for signals of smaller wavelengths (high frequencies) compared to those with larger wavelengths.

Although the results show that SHB has small effects on the gain spectrum of an EDFA, it must be kept in mind that the cumulative effects in a cascade of EDFAs could be several dBs or more and will have a significant impact on system performance in long-haul systems.